# Přílohy

# I.

Drahota P., Kulakowski O., Culka A., **Knappová M.**, Rohovec J., Veselovský F., Racek F. (2018) Arsenic mineralogy of near-neutral soils and mining waste at the Smolotely-Líšnice historical gold district, Czech Republic. *Applied Geochemistry* **89**, 243–254.

Applied Geochemistry 89 (2018) 243–254

Contents lists available at ScienceDirect

Applied Geochemistry

journal homepage: www.elsevier.com/locate/apgeochem

# Arsenic mineralogy of near-neutral soils and mining waste at the Smolotely-Líšnice historical gold district, Czech Republic

Petr Drahota[a,*], Ondřej Kulakowski[a], Adam Culka[a], Magdaléna Knappová[a], Jan Rohovec[b], František Veselovský[c], Martin Racek[d]

[a] Institute of Geochemistry, Mineralogy and Mineral Resources, Faculty of Science, Charles University, Albertov 6, 128 43 Prague 2, Czech Republic
[b] Institute of Geology, The Czech Academy of Sciences, v.v.i., Rozvojová 269, 165 00 Prague 6, Czech Republic
[c] Czech Geological Survey, Geologická 6, 152 00 Prague 5, Czech Republic
[d] Institute of Petrology and Structural Geology, Faculty of Science, Charles University, Albertov 6, 128 43 Prague 2, Czech Republic

ARTICLE INFO

Handling Editor: Kate Marie Campbell.

*Keywords:*
Soil
Mining waste
Pharmacosiderite
Yukonite
Arseniosiderite

ABSTRACT

The mineralogical composition of mining wastes and contaminated soils is the key factor that controls the retention and release of pollutants. Herein, we used bulk analyses, selective extractions, X-ray diffraction, electron microprobe, and Raman microspectrometry to determine the distribution and speciation of As as a function of depth in four slightly acidic to near-neutral soil and mining waste profiles at the Smolotely-Líšnice historical Au district (Czech Republic). The soils there, which have developed from long-term weathering, exhibit As levels as high as 1.87 wt% in the richest area; the 80–90 year old mining waste contains up to 0.87 wt% As. In the soils and mining waste, the primary As ore (arsenopyrite) has almost completely oxidized to secondary As minerals such as arseniosiderite, bariopharmacosiderite, yukonite, and Fe (hydr)oxides (ferrihydrite, goethite, and hematite), with variable $As_2O_5$ and CaO concentrations (up to 27.5 and 3.8 wt%, respectively). Arsenic distribution and speciation were found to vary with depth and soil type. Whereas the presence of multiple As-hosting phases that occurred in the mining waste and cambisol developed over a granodiorite, bariopharmacosiderite was absent in the cambisol overlying gabbrodiorite. Poorly-crystalline phases such as yukonite and As-bearing ferrihydrite were not detected in the gleysol. These differences in the secondary As mineralogy were attributed to the different redox conditions and variations in the prevailing chemical systems in the saprolites/soils. The variable solubility of the secondary As-bearing phases influences the mobility of As in shallow soils and near-surface mining wastes.

## 1. Introduction

Arsenic is a trace metalloid element commonly associated with metallic deposits, which can be naturally enriched to levels ranging from hundreds to thousands of times above the respective average crustal abundance (1.8 mg/kg; Mason and Moore, 1982). Natural weathering of the As-mineralized bedrocks releases As into the surface environments, reaching As levels of several thousands of mg/kg in the soil (Bossy et al., 2010; Filippi et al., 2007; Morin et al., 2002; Pfeifer et al., 2004), and several hundreds of μg/L in the groundwater (Drahota et al., 2009). Furthermore, mining activity at these sites can aid As mobilization through the excavation and processing of As-rich ore. Percolating rainwater can facilitate the oxidation and dissolution of As from the mine wastes. Dissolved As can then be discharged into the environment at levels potentially toxic for the biota (Foy et al., 1978; Hogsden and Harding, 2012; Kelly, 1999; Younger et al., 2002).

The speciation of As in contaminated soil and mine wastes is the key factor that controls retention and release of this pollutant. Arsenic speciation is usually determined by means of X-ray diffraction (XRD), electron microprobe analysis, chemical extraction methods, or spectroscopic techniques. The main difficulty in determining As speciation comes from the fact that it is often at very low concentrations and occurs in a variety of chemical forms within the same sample, including different mineral phases and surface complexes. Thus, detailed *in situ* determination of As mineralogy in complex environmental samples still remains scientifically challenging. Detailed studies of the mineralogical composition of such heterogeneous media such as soil and mine waste (e.g., DeSisto et al., 2016; Drahota et al., 2009; Walker et al., 2009) document the mineralogical richness of these materials, and may not only help in understanding those factors controlling As mobility, but also in designing better remediation strategies.

Arsenopyrite (FeAsS) is the main host for As in metallic deposits,

* Corresponding author.
*E-mail address:* petr.drahota@natur.cuni.cz (P. Drahota).

https://doi.org/10.1016/j.apgeochem.2017.12.018
Received 14 September 2017; Received in revised form 14 December 2017; Accepted 18 December 2017
Available online 20 December 2017
0883-2927/ 

such as mesothermal gold deposits in the Czech Republic (Morávek et al., 1992). Other primary As minerals such as As-bearing pyrite ($FeS_2$) or löllingite ($FeAs_2$) may be present in smaller amounts. If exposed to the ambient atmosphere, the primary As minerals break down into a number of As-bearing secondary minerals and phases (Majzlan et al., 2014). Under the usual oxidizing conditions of most soils and mine wastes, As is sorbed to or co-precipitated with Fe (hydr)oxides, clay minerals, and organic matter (Stollenwerk, 2003; Wang and Mulligan, 2006). It may also be directly substituted into the crystal structure of a limited number of secondary minerals (Savage et al., 2005) and precipitated as secondary As minerals (Majzlan et al., 2014). Despite the variety of arsenate and arsenite minerals documented in the literature ($n$ = 425; IMA, 2016), only a limited number of them have been repeatedly identified in the mine wastes and soils (Drahota and Filippi, 2009). Under circumneutral conditions, arseniosiderite ($Ca_3Fe_4(OH)_6(AsO_4)_4{\cdot}3H_2O$), yukonite ($Ca_2Fe_3(AsO_4)_3(OH)_4{\cdot}4H_2O$), and minerals of the pharmacosiderite supergroup ($A_xB_4(OH)_4(AsO_4)_3{\cdot}yH_2O$) (A = K, Na, Ba, Tl, Cs, Sr, $H_3O$; x = 0.5–1; B = Fe, Al; y = 4–7) are among the most important arsenate mineral phases occurring in some gold ores, mine wastes, and As-rich soils (e.g., Bossy et al., 2010; Cancès et al., 2008; Filippi et al., 2007; Morin et al., 2002; Paktunc et al., 2004; Walker et al., 2009). The findings of these observations and the recent experimental results of Paktunc et al. (2015) suggest that arseniosiderite and yukonite are likely to form from slightly acidic to alkaline solutions rich in Ca, Fe(III), and As, which may arise from gypsum- or calcite-saturated solutions in contaminated soils and mine wastes containing ferric arsenates such as scorodite ($FeAsO_4{\cdot}2H_2O$), amorphous ferric arsenate, and minerals of the pharmacosiderite supergroup. In contrast, conditions promoting minerals of the pharmacosiderite supergroup's formation, transformation, and environmental stability are not well known (Haffert et al., 2010).

The present study site is located in the Smolotely-Líšnice Au district (Czech Republic) which is characterized by an elevated geochemical background of As in the soils (Seidl, 1991). Our primary goal was to identify the As-bearing secondary mineral phases and to determine their spatial distribution in different types of naturally contaminated soil and mining waste, in order to evaluate the fate of As following pedogenesis and long-term weathering, respectively. Two complementary approaches were employed: (i) bulk chemical analyses and selective chemical extractions were used to establish the spatial distribution of the different forms of As, and (ii) a combination of chemical microanalyses and Raman microspectrometry was used for the characterization of the mineral phases on the microscale.

## 2. Study site

The Smolotely-Líšnice ore district is located in the central part of the Czech Republic, 60 km south of Prague (Fig. 1). The ore deposits in the district are hosted by Variscan granodiorites of the Central Bohemian Plutonic Complex and regionally metamorphosed rocks formed from a Neoproteorozoic volcanic and sedimentary complex of the Jílové Belt (Morávek et al., 1992). The area between Horní Líšnice and Nepřejov contain vein-type polymetallic mineralization with Ag-bearing galena (PbS), sphalerite (ZnS), pyrite ($FeS_2$), as well as less common chalcopyrite ($CuFeS_2$), pyrrhotite ($Fe_{1-x}S$), and arsenopyrite in the quartz-carbonate gangue (Morávek et al., 1992). Probably, the later stages of hydrothermal mineralization produced the Au ores, which are accompanied by abundant arsenopyrite, minor As-bearing pyrite, and traces of Bi-Te phases, bismuth (Bi), bismuthinite ($Bi_2S_3$), kobellite ($Pb_{22}Cu_4(Bi,Sb)_{30}S_{69}$), molybdenite ($MoS_2$), and galena (Durembergová and Kratochvíl, 1977). The Au mineralization occurs as quartz veins (several cm-80 cm thick veins) with minor carbonate and impregnations in the NE endocontact zone of the granodiorites. The ore grade is highly variable, and the chemical compositions of the Au ores range from traces to 80 g/t Au (2.1–2.9 g/t average Au grade) and up to 30 wt % As (Ježek, 1929).

Exploitation of the Au mineralization in the district started during the 14th century (Valta, 1936). Discovery of Ag-rich polymetallic ores in 1808 led to a revival of the mining activities (until 1857) that also included small-scale Au mining. Probably the most intensive exploration/mining activities for Au in the district dates back to the short periods between 1924–1928 and 1934–1938 (Morávek et al., 1992). Materials from the mining waste dumps, generated at those times, were studied in this work. Other subjects of our mineralogical study were different types of naturally developed soils with high concentrations of As (Fig. 1). Detailed geochemical prospecting (more than 3000 samples) in the area of the district showed that As formed a relatively large geochemical anomaly in the soil, with As levels of > 200 mg/kg over approximately 3 $km^2$ (Seidl, 1991).

The ore district is situated in a hilly area (altitude: 350–540 m above sea level). The soils can be defined as cambisols and gleysols, and their thickness is usually very small (< 50 cm for cambisols). The annual precipitation over the past 40 years averaged between 600 and 700 mm/year, and the average annual temperature was 6–7 °C.

## 3. Materials and methods

### 3.1. Materials

Two soil types located at three sites (A, B, C) in the ore district plus the mining waste (D) were sampled in four profiles (Fig. 1). Solid samples were collected from excavation pits and composited along a profile for discrete depth intervals (5–20 cm) on the basis of morphological transitions (color, consistency). The solids were collected using a stainless steel hand trowel, stored in a sealed plastic bags, and transported to the laboratory. In the laboratory, the samples were air- or freeze-dried (Alpha 1–2 LD plus, Martin Christ, Germany) and sieved to obtain the < 2 mm fraction. For bulk chemical analyses and oxalate extractions, a split subsample was ground in an agate ball mill (Fritsch, Germany) to analytical fineness. Another part of the < 2 mm fraction was used for the mineralogical characterizations.

### 3.2. Chemical analyses

The colors of the fresh samples were determined *in situ* using a Munsell soil color chart. The pH was measured by a WTW multimeter equipped with a SenTix 41 pH electrode (WTW, Germany), in a 1:2.5 (w/v) soil-deionized water suspension after 1 h agitation (Pansu and Gautheyrou, 2006). Selected metals and metalloids (Al, Ba, Bi, Ca, Cu, Fe, K, Mg, Mn, Na, Pb, Sb, and Zn) in the soil and mining waste samples were determined after digestion in mineral acids (HF-$HClO_4$-$HNO_3$) by inductively coupled plasma optical emission spectrometry (ICP-OES; Agilent 5100, USA) and inductively coupled plasma mass spectrometry (ICP-MS; ThermoScientific Xseries$^{II}$, USA). The concentration of As was determined in the pseudo-total digests that were obtained by a standardized *aqua regia* extraction protocol according to ISO Standard 11466 (ISO 1995). The content of total sulfur, organic carbon (TOC), and total inorganic carbon (TIC) were determined using a combination of Eltra CS 530 and Eltra CS 500 TIC analyzers (combustion with infrared detection analyzer; ELTRA, Germany).

The quality of the analytical determinations of the bulk element concentrations was controlled by replicated digestions/measurements using standard reference material NIST 2710a (NIST, USA, Montana I Soil - highly elevated trace element concentrations) and NIST 2709 (NIST, USA, San Joaquin Soil) and was found to be satisfactory (Table S1). Every fourth digestion/measurement was performed in duplicate, showing a standard deviation of < 2% for all elements, except for Bi in two analyses, which each showed a standard deviation of 21%; four procedural blanks were run during digestion procedures.

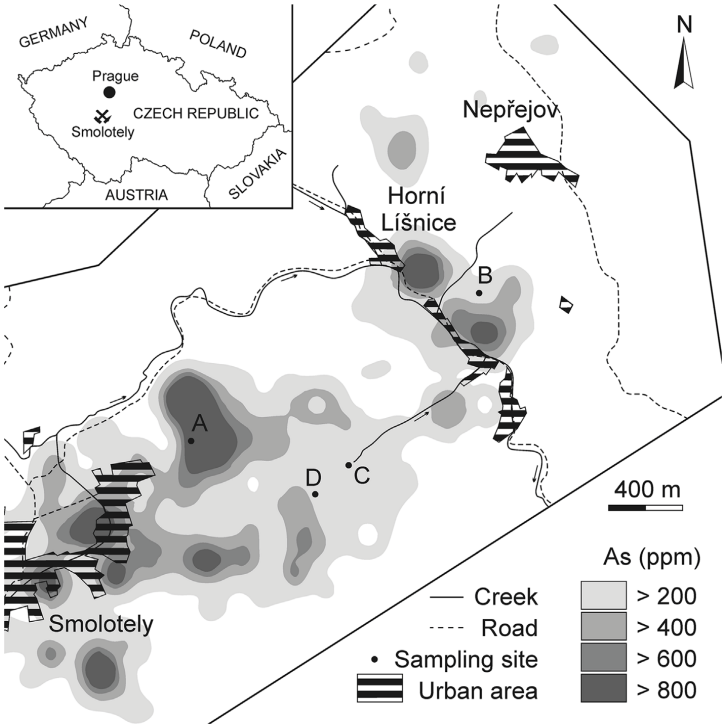


**Fig. 1.** A schematic map of the arsenic concentration in soils in the Smolotely-Líšnice ore district (after Seidl, 1991). The locations of the sampling sites (black circles) are shown. The inset shows the location of the village within central Europe.

### 3.3. Mineralogical analyses

The heavy mineral fraction was separated from selected bulk soil samples ($n = 4$). This fraction was obtained by centrifugation of the 0.05–0.5 mm size fraction of bulk samples in 1,1,2,2-tetrabromoethane diluted with 1,4-dioxane (specific gravity of 2.70 g/cm$^3$). The mineralogical compositions of bulk samples, heavy mineral fractions, and grain separates were assessed by X-ray diffraction analysis (XRD) using a PANalytical X'Pert Pro diffractometer (PANalytical, the Netherlands) equipped with a diffracted-beam monochromator and X'Celerator multichannel detector, using Cu Kα radiation (40 keV, 30 mA). Powders of the samples were scanned from 3° to 70° 2$\theta$, in steps of 0.02°, with a 200 s count time at each step. The diffraction data were analyzed using X'Pert HighScore Plus software, version 1.0d, and semiquantitative estimates of abundances of major minerals were obtained by comparing the integrated intensities of the diffraction peaks.

For the chemical and phase compositions of individual grains, polished sections ($n = 9$) were prepared from the heavy-grain concentrates as well as the bulk soil and mining waste samples. Backscattered images and compositional maps of secondary As mineral assemblages were obtained on a scanning electron microscope (SEM; TESCAN VEGA, Czech Republic) equipped with an energy dispersion spectrometer (EDS; Link X-Max 50, Oxford Instruments, UK) calibrated against the SPI set of standards (SPI supplies, USA), operating at 15 kV, with a beam current of 6 nA. The quantitative chemical analyses of representative mineral phases were measured by electron microprobe (EMPA; Cameca SX100, France) in wavelength-dispersive mode under the operating conditions of: 15 keV, 10 nA, and a beam diameter of 2 µm. For the following X-ray lines, standards and detector crystals were used for the analyzed elements: Na ($K\alpha$, jadeite, LTAP), K ($K\alpha$, sanidine, LPET), Ca ($K\alpha$, diopside, LPET), Mg ($K\alpha$, periclase, LTAP), Ba ($L\alpha$, barite, LPET), Si ($K\alpha$, quartz, TAP), Al ($K\alpha$, jadeite, TAP), S ($K\alpha$, barite, LPET), Fe ($K\alpha$, hematite, LIF), Mn ($K\alpha$, spinel, LIF), P ($K\alpha$, apatite, LPET), As ($L\beta$, GaAs, LTAP). In total, 235 spot analyses were performed using EMPA.

Raman microspectrometric (RMS) analyses were performed on the grains previously explored by SEM and EMPA (locations of RMS spot analyses in the grains were identical to the microprobe spots) using a Renishaw InVia Reflex Raman spectrometer (Renishaw plc, UK) coupled with a Leica microscope (Leica Microsystems, Germany) with a 50 × objective. Excitation was provided by the 514.5 nm line of a diode laser. The spectrum of each mineral was recorded at 5% laser power (~5 mW) to avoid thermal degradation over the spectral range of 100–1200 cm$^{-1}$. Scanning parameters were as follows: 20 s accumulation time and 15–20 scans were taken to improve the signal-to-noise ratio.

### 3.4. Selective chemical extractions

A 0.2 M $NH_4$-oxalate/oxalic acid (pH = 3) was used under dark conditions to release As associated with amorphous and reactive Fe (hydr)oxides plus Fe arsenates by dissolution of these species (Drahota et al., 2014; Schwertmann, 1964). A similar solution was used in the light and at 80 °C to release As incorporated in secondary Fe mineral phases with higher structural orders such as goethite, jarosite, and scorodite (Drahota et al., 2014). For all extractions, the solid to solution ratio was set at 0.5 g of the solid sample in 50 mL of solution. After extraction, supernatant fluids were passed through 0.2 µm nylon membrane filters and analyzed for As and Fe by ICP-OES. Extractions were performed in duplicate, showing standard deviations of less than 7% for As and 8% for Fe; several procedural blanks were run during the extraction procedures. In addition to the oxalate extractions, all

samples were analyzed for their contents of exchangeable or readily soluble As, Ba, Ca, and K using $NH_4NO_3$ extraction according to DIN 19730 (1997).

Pure pharmacosiderite, arseniosiderite, and yukonite, the common secondary arsenate phases in near-neutral As-rich soils and mine wastes (Majzlan et al., 2014), were used to test the selectivity of the pH 3 $NH_4$-oxalate solution under both extraction conditions. Arseniosiderite and yukonite were produced following the synthesis methods described by Paktunc et al. (2015) and Bohan et al. (2014), respectively. The natural pharmacosiderite sample was obtained from the greisen deposit at Krásno near the Horní Slavkov ore district (Czech Republic). Examination of the synthetic phases by XRD confirmed the identity and purity of the phases; the natural pharmacosiderite contained quartz and scorodite impurities. The As content in the phases was measured after their total dissolution in 7 M HCl. In the first dissolution experiment, the solid to solution ratio was set at 0.05 g of the pure arsenate in 100 mL oxalate solution in the dark. The resulting solutions were sampled with a syringe sampler after 10, 20, 35, 60, 120, and 240 min of reaction time, then filtered and analyzed by ICP-OES. In the second experiment, the dissolution of pure arsenates was tested in the hot oxalate solution after 180 min of reaction time. The total dissolutions were performed in triplicate; the dissolution experiments in duplicate, both showing a standard deviation of less than 5%.

## 4. Results

### 4.1. Physical and chemical characteristics

A detailed description and properties of the studied soils and mining waste are reported in Table S2. The soils, collected from different parts of the ore district, are classified as cambisols (sites A and B) and gleysol (site C). The pH of soils and mining wastes ranged from slightly acidic to near-neutral (5.0–7.0), with the exception of organic-rich topsoil horizons, which reflected lower pH in the gleysol (~4.3) and mining waste (~3.8). From the profiles studied, only damp gleysol exhibited slightly reducing conditions as demonstrated from the field Eh data (50–110 mV).

Metal(loid) concentrations reflect the compositions of the parental bedrock and ores mined; arsenic is by far the most significant metal (oid) in all samples studied (134–18670 mg/kg, $\bar{x}$: 3670 mg/kg), while other potential trace metal(oid)s such as Bi, Cu, Pb, Sb, and Zn are almost insignificant (up to 201 mg/kg), and accompany As in the soil (significant positive correlation of Sb and Zn with As: $R^2 > 0.81$, $p < .01$), or they accumulate in the gold ore (high content of Bi in the mining waste D). The distribution of As in the profiles is highly variable (Fig. 2). Its concentration decreases with depth in the cambisol A and gleysol C; it increases with depth at the cambisol B, and displays an irregular distribution pattern in profile D (mining waste). The different trends of these As concentration profiles indicate that the vertical distribution of As may be due to different factors such as: (i) plowing and annual crop off-take at agricultural site B, (ii) mobilization of As in the reducing conditions of gleysol C, and (iii) deposition of mining waste materials with initial variable proportions of arsenopyrite ore (site D). The concentration of sulfur, a major compound of sulfide minerals, is very low (< 2900 mg/kg). The highest S contents occurred in the organic-rich topsoil horizons (Table S2). Surprisingly, the lowest S contents were detected in those materials that had the highest potential contents of sulfide minerals, i.e., mining waste (48–970 mg/kg). The contents of TIC were always below 0.1 wt%.

The results of readily soluble As, Ba, Ca, and K in the soil and mining waste samples using 1M $NH_4NO_3$ are given in Table S3. The ammonium nitrate-extractable fractions generally decreased in the order: Ca > Ba ≫ K > As. Very low extractable As (less than 0.03% of the total As) was particularly found in the oxic cambisols (site A and B) and in the mining waste samples (site D). This finding can be attributed to the high ionic strength of the 1 M $NH_4NO_3$ solution, which decreases the electrostatic potential of negatively charged mineral surfaces in the soil and mining waste, and thus favours adsorption of anions such as the arsenate anion (Gryschko et al., 2005). The statistical comparison of the $NH_4NO_3$-extractable fractions of As, Ba, Ca, and K with their corresponding total contents showed a significant correlation only between both variables for Ba ($R^2 = 0.70$, $p < .01$).

### 4.2. Mineralogy

#### 4.2.1. X-ray diffraction

The bulk powder XRD patterns showed that the soils and mining waste are dominated by quartz, plagioclase, biotite, clay minerals (chlorite and minor kaolinite); and locally by amphibole (cambisol A, gleysol C, and mining waste D) or K-feldspar (cambisol A, and mining waste D). The XRD investigation of the heavy mineral fractions (> 2.70 g/cm$^3$), which were separated from the richest part of each profile with respect to As content, indicated concentrations of mineral phases of high density (biotite, amphibole, magnetite, anatase), and also identified pharmacosiderite in mining waste D.

More detailed insights into the mineralogy of As was provided by the XRD investigation of specific grains, separated from the heavy mineral fractions using a binocular optical microscope. The grains of interest displayed a brown color resembling the presence of Fe (hydr) oxides and arsenates (Filippi et al., 2007). It should be noted here that these grains were common in the mining waste D as well as in cambisols A and B. In contrast, they were very rare in gleysol C. Phase composition of the separated grains revealed the presence of several As-bearing phases. Separated grains in the cambisol A, gleysol C, and mining waste D were composed of minerals from the pharmacosiderite supergroup; but also contained a large proportion of goethite in the gleysol C, and amorphous phase in the mining waste D, resembling 2-line ferrihydrite (Fig. S1). In addition, the residual peaks in the mining waste were tentatively attributed to another arsenate mineral, arseniosiderite. These mineral phases weren't identified in the cambisol B, although the concentration of As here (~1.8 wt%) reached even higher values than in the mining waste D (~0.8 wt%). The diffraction pattern of the relatively abundant blackish-brown grains from the cambisol B strongly resembles that of arseniosiderite, but differs in its broader peaks (Fig. S1). These poorly resolved peaks have been attributed to the poorly-crystalline Ca-Fe arsenate phase, yukonite.

#### 4.2.2. Electron microprobe analyses and Raman microspectrometry

The chemical compositions of the secondary As-bearing phases in the soil ($n = 124$) and in the mining waste ($n = 111$) samples indicated that Fe (hydr)oxides, Ca-Fe arsenates, and Ba-Fe arsenates are the dominant As-bearing species, forming approximately 95% of the As-bearing mineral grains in all of the samples studied. The remaining secondary As-bearing phases, including Fe (hydroxo)sulfates (resembling chemical composition of jarosite) and Mn (hydr)oxides, occur in trace concentrations. The secondary As-bearing phases essentially occur as discrete particles displaying zoning and banding (Fig. 3b and 4a, g) or as complex agglomerations (Fig. 4c), and only rarely as replacement products of arsenopyrite (Fig. 3a and 4c). The intimate association of Fe (hydr)oxides and both chemical groups of arsenates in successive bands and zones (Figs. 3a and b and 4a, c, f, g) is suggestive of precipitation and co-precipitation at close intervals. Arsenopyrite occurs in minor to trace quantities in the mining waste D (Fig. 4c) as well as in cambisol B (identified only in one grain) as relic particles embedded in Ba-Fe arsenates (Fig. 3a).

There are apparent differences in the As mineralogy of the four profiles (Fig. 5). Cambisol A and mining waste D are characterized by an abundance of Fe (hydr)oxides, with variable levels of As and the presence of Ca-Fe and Ba-Fe arsenates. Cambisol B contains large amounts of Ca-Fe arsenates and Fe (hydr)oxides; Ba-Fe arsenates are not present here. Gleysol C contained very low amounts of As-bearing phases. Of these, only Fe (hydr)oxides with low levels of As were

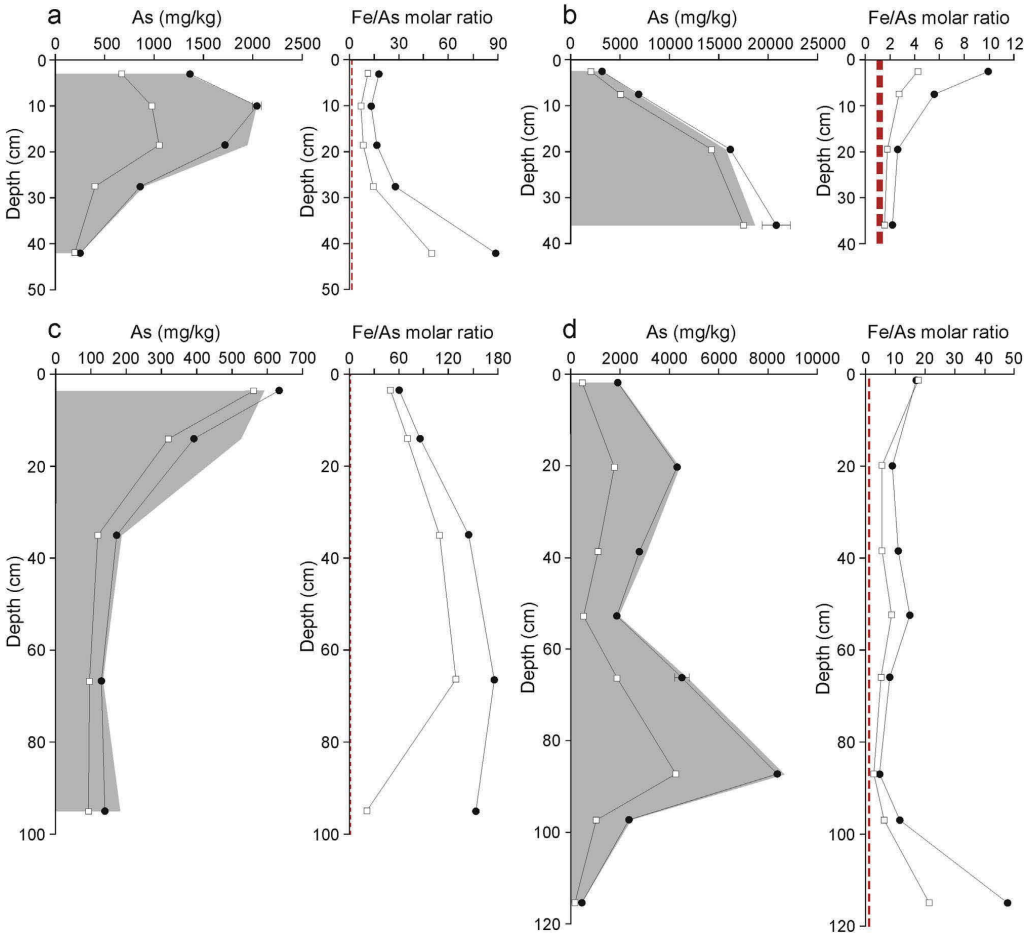


**Fig. 2.** Depth variations in the distribution of arsenic fractions in the cambisols (**a**: site A; **b**: site B), (**c**) gleysol, and (**d**) mining waste profiles: total arsenic concentrations (grey field), oxalate-extractable arsenic in the dark (open square) and light (black circle). The Fe/As molar ratio in the oxalate fractions, both in the dark (open square) and light (black circle), could be indicative of the relative proportion of As bound to Fe (hydr)oxides and Fe arsenates. Red dashed lines represent constant Fe/As molar ratio of 1.0–1.33, indicating congruent dissolution of Fe arsenates such as pharmacosiderite, arseniosiderite, and yukonite. Most error bars are obscured by symbols. (For interpretation of the references to color in this figure legend, the reader is referred to the Web version of this article.)

detected using a microprobe.

The RMS analyses were carried out on the spots of all microprobe analyses ($n = 235$), and 141 analyses were employed for mineral identification. The remaining part of the analyses (~40%) was not used for mineral identification due to high background due to fluorescence, which overwhelmed any signal that may have been present from a mineral. According to RMS, all Ba-Fe arsenates belong to the pharmacosiderite supergroup (Filippi et al., 2007; Frost and Kloprogge, 2003). All the spectra exhibit a well-resolved Raman band at 477 $cm^{-1}$, broader bands at 392 $cm^{-1}$, 789 $cm^{-1}$, and 865 $cm^{-1}$ with a shoulder at ~877 $cm^{-1}$ (Raman spectrum *R2*; Fig. 3c). The chemical composition of these minerals ($n = 44$) corresponds to almost pure bariopharmacosiderite ($\bar{x} \pm \sigma$: 9.57 ± 1.05 wt% BaO, 37.98 ± 2.82 wt% $Fe_2O_3$, 39.33 ± 2.36 wt% $As_2O_5$), with very low Na, K, and Al concentrations (< 0.06 wt%, < 0.11 wt%, and < 3.55 wt%, respectively). This average composition is almost identical to the average for the type-bariopharmacosiderite from Robinson's Reef, Clunes, Australia (Hager et al., 2010). The Raman spectra of Ca-Fe arsenates allowed for the distinguishing of two phases: arseniosiderite and yukonite. The yukonite spectra have two well-resolved Raman bands at 392 $cm^{-1}$ and 863 $cm^{-1}$ (Raman spectrum *R9*; Fig. 4h). By contrast, arseniosiderite exhibits sharper and more intense bands at these positions (Raman spectrum *R3*; Fig. 3c), and an additional band at higher wavenumbers (936 $cm^{-1}$), indicative of $HAsO_4^{2-}$ units as observed in the infrared spectra (Gomez et al., 2010; Myneni et al., 1998). Electron microprobe analyses indicate that the arseniosiderite particles were chemically homogeneous. The average composition of the arseniosiderite is 13.74 ± 0.37 wt% CaO, 31.26 ± 1.18 wt% $Fe_2O_3$, 41.75 ± 0.85 wt% $As_2O_5$, 0.93 ± 0.69 wt% $SiO_2$, and 0.57 ± 0.50 wt% $Al_2O_3$ ($\bar{x} \pm \sigma$), based on 18 spot microanalyses. This composition is comparable to the average of those for arseniosiderites from the Ketza River mine (Paktunc et al., 2004), naturally contaminated soil at Mokrsko (Filippi et al., 2007), and to the nominal arseniosiderite composition. In contrast, yukonite has a relatively variable composition with

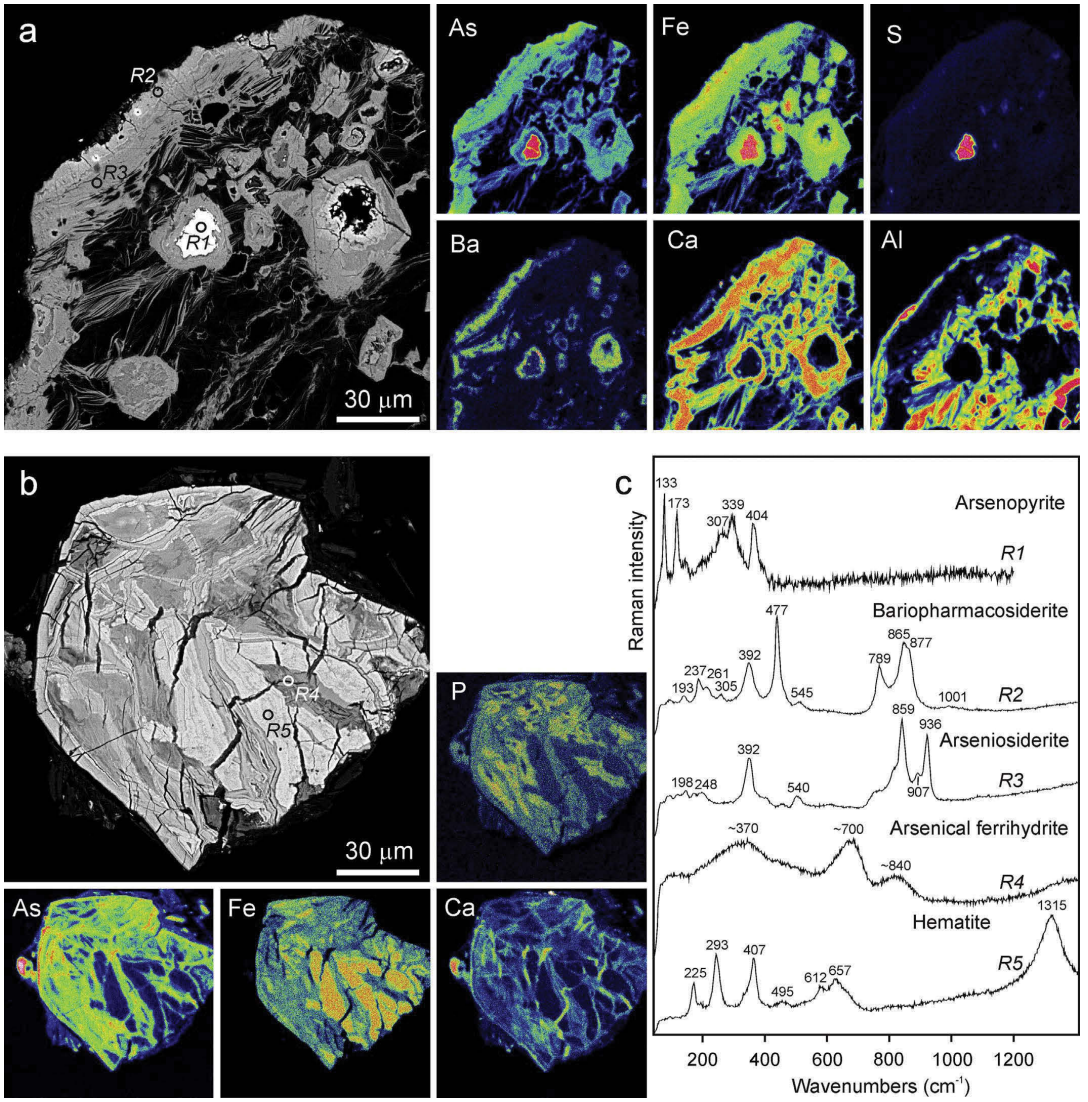


**Fig. 3.** Back-scattered electron images and quantitative As*Lα*, Fe*Kα*, S*Kα*, Ba*Kα*, Ca*Kα*, Al*Kα*, and P*Kα* X-ray maps showing (**a**) progressive replacement of arsenopyrite (light grain) by bariopharmacosiderite and arseniosiderite and (**b**) replacement of arsenical ferrihydrite (~17 wt% $As_2O_5$) by hematite (~3 wt% $As_2O_5$). (**c**) Raman spectra obtained from locations *R1-R5*. Microprobe analyses of *R2-R5* spots are given in Table S4.

11.01 ± 1.73 wt% CaO, 36.04 ± 5.31 wt% $Fe_2O_3$, 36.50 ± 3.97 wt% $As_2O_5$, 2.21 ± 0.68 wt% $SiO_2$, 0.84 ± 0.77 wt% $P_2O_5$, and 0.76 ± 0.64 wt% BaO ($\bar{x} \pm \sigma$), based on 18 spot analyses (Fig. 5). This average composition is similar to those of the yukonite specimens reported by Dunn (1982) and Paktunc et al. (2015) from the type-localities in Yukon, Canada. Yukonites from the Grotta Della Monaca cave in Italy (Garavelli et al., 2009), Sterling Hill deposit in New Jersey, U.S.A. (Dunn, 1982), and Rędziny deposit in Poland (Pieczka et al., 1998) appear to be more deficient in Fe.

The RMS results show that the As-bearing Fe (hydr)oxides are represented by three mineral species: ferrihydrite, goethite, and hematite. Iron-rich Fe (hydr)oxides ($\bar{x} \pm \sigma$: 86.06 ± 0.91 wt% $Fe_2O_3$) with relatively low As concentrations ($\bar{x} \pm \sigma$: 2.29 ± 0.56 wt% $As_2O_5$) exhibit sharp Raman bands at 225 $cm^{-1}$, 293 $cm^{-1}$, and 407 $cm^{-1}$ (based on 9 spot analyses), indicative of hematite (Raman spectrum *R5*; Fig. 3c). Goethite has a more variable composition with 81.24 ± 5.33 wt% $Fe_2O_3$ and 3.54 ± 4.35 wt% $As_2O_5$ ($\bar{x} \pm \sigma$), based on 14 spot microanalyses. In accordance with previously published data (e.g., de Faria et al., 1997; Müller et al., 2010; Das and Hendry, 2011), our goethite spectra have three well-resolved bands at 300 $cm^{-1}$, 388 $cm^{-1}$, and ~551 $cm^{-1}$ (Raman spectrum *R6*; Fig. 4h). The spectra of hematite and goethite also exhibit broad features of moderate intensity located at

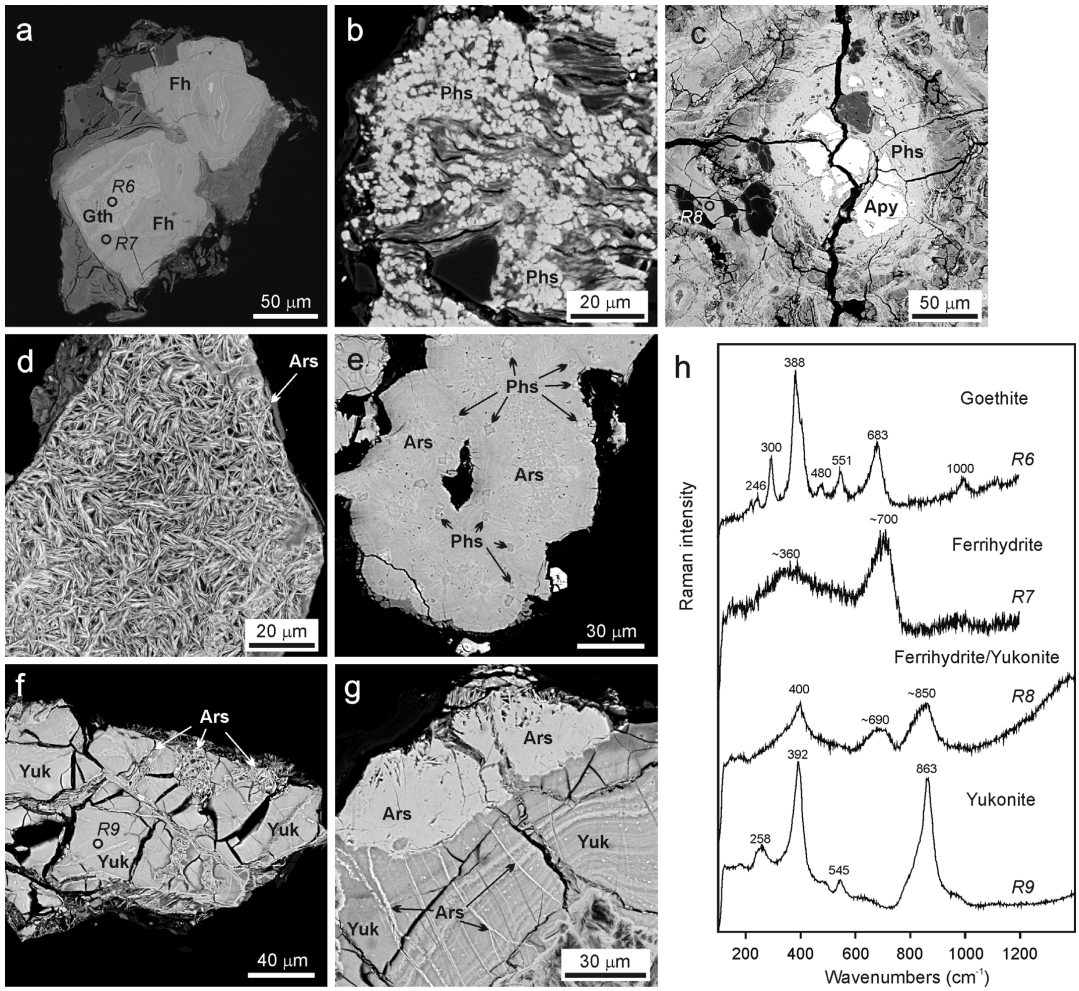


**Fig. 4.** Back-scattered electron images showing typical habit of (**a**) As-bearing goethite (~2 wt% $As_2O_5$) and ferrihydrite (~3 wt% $As_2O_5$), (**b**, **c**) bariopharmacosiderite, (**d**, **e**) arseniosiderite, and (**f**, **g**) yukonite. (**c**) Bariopharmacosiderite pseudomorph after arsenopyrite, (**e**) radiaxial arseniosiderite as a replacement after cubic crystals of bariopharmacosiderite, and (**f**, **g**) pervasive veins and fractures of arseniosiderite filling in yukonite. The mineral identification is based on Raman spectrometry and microprobe analyses (Table S4). Open circles *R6-R9* represent locations of Raman microspectrometry analyses shown in **h**. Apy – arsenopyrite; Ars – arseniosiderite; Fh – ferrihydrite; Gth – goethite, Phs – bariopharmacosiderite; Yuk – yukonite.

about 657 $cm^{-1}$ and 683 $cm^{-1}$, respectively (which were attributed to structural disorder). The intensive hematite feature at ~1315 $cm^{-1}$ is assigned to a two-magnon scattering (de Faria et al., 1997). In contrast, the As(V)-O stretching band at 826 $cm^{-1}$ (Das et al., 2014) or 866 $cm^{-1}$ (Müller et al., 2010), previously documented in As-loaded hematite, is not noticeable in our spectra. The ferrihydrite spectra show two broad Raman features located at about ~370 $cm^{-1}$ and ~700 $cm^{-1}$ (Raman spectrum *R7*; Fig. 4h). The band in the most As-rich ferrihydrite spectra located at ~840 $cm^{-1}$ (Raman spectrum *R4*; Fig. 3c) most likely can be attributed to the As-O stretching vibration of the bidentate-complexed arsenate on the surface of ferrihydrite (Jia et al., 2006; Müller et al., 2010; Das and Hendry, 2011). Ferrihydrite has a relatively variable composition with 68.91 ± 5.28 wt% $Fe_2O_3$, 14.60 ± 6.82 wt% $As_2O_5$, and 1.52 ± 0.69 wt% CaO ($\bar{x}$ ± $\sigma$), based on 34 spot microanalyses. An interesting correlation in the microprobe analyses of ferrihydrite is the distribution of Ca and As. The correlation coefficient of the ferrihydrite grouping (with 34 analyses) is 0.58, and the average Ca/As molar ratio is 0.24. The highest Ca/As molar ratio is 0.57, which corresponds to that of yukonite ($\bar{x}$: 0.60, $n$ = 18), and approaches that of arseniosiderite ($\bar{x}$: 0.67, $n$ = 18).

### 4.3. Oxalate extractions

#### 4.3.1. Pure arsenates

The dissolution reaction for yukonite was complete after 20 min contact time with pH 3 $NH_4$-oxalate in the dark, whereas the dissolution of well-crystalline arseniosiderite and pharmacosiderite was much slower (Fig. S2). After 120 min in this leachate, ~75% of the arseniosiderite and ~12% of the pharmacosiderite were dissolved. In contrast, complete dissolution of arseniosiderite and pharmacosiderite was

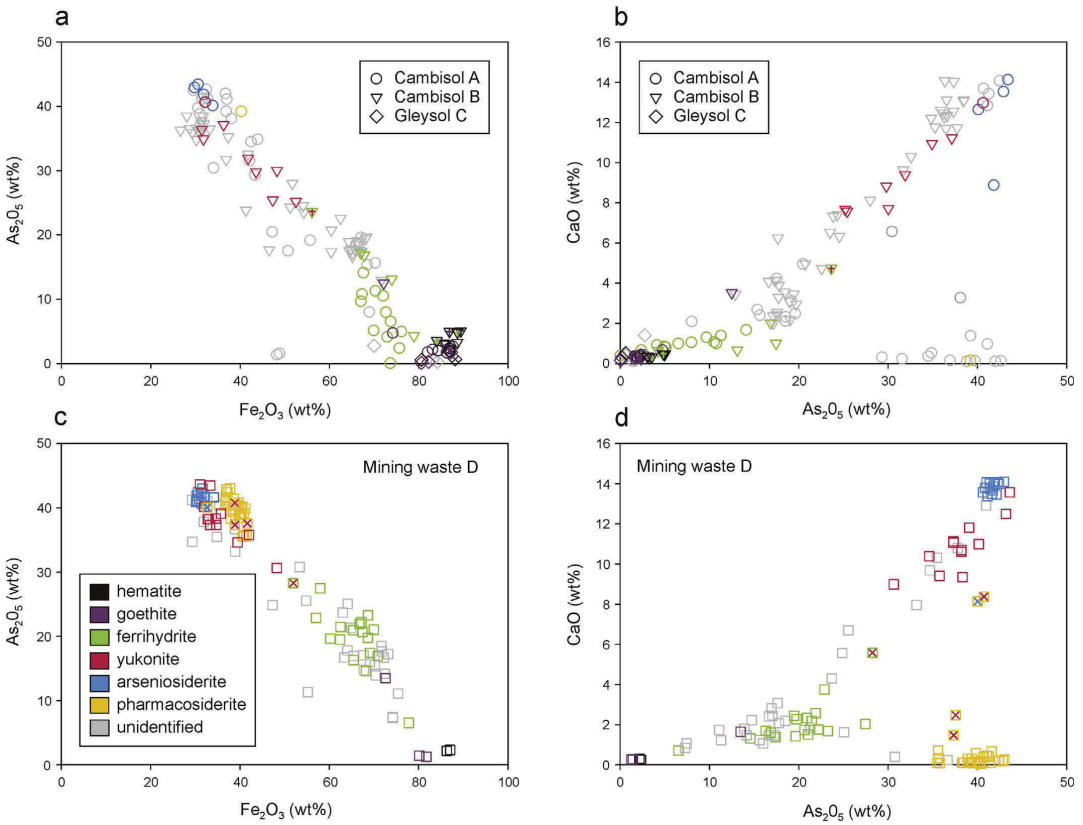


**Fig. 5.** Variation of $As_2O_5$ as a function of $Fe_2O_3$ (**a**, **c**) and CaO (**b**, **d**) in secondary arsenic-bearing minerals from Smolotely soils (**a**, **b**) and mining waste (**c**, **d**) identified by Raman microspectrometry. Two colors in one symbol correspond to a mixture of mineral phases identified in the spot Raman analysis. (For interpretation of the references to color in this figure legend, the reader is referred to the Web version of this article.)

obtained within 3 h in the light in hot pH 3 $NH_4$-oxalate (data not shown). Constant Fe/As molar ratios during the extractions of the arsenate phases in oxalate solutions (in both the dark and light) indicated congruent dissolution of the phases and an absence of re-adsorption of As that has been observed during the oxalate extractions of As-bearing Fe (hydr)oxides (Drahota et al., 2014). These findings indicate that pH 3 $NH_4$-oxalate in the dark is fairly specific for poorly-crystalline yukonite, and can be applied for its discrimination from pharmacosiderite or other well-crystalline As-bearing phases such as scorodite and goethite (Drahota et al., 2014; Schwertmann, 1964). In contrast, arseniosiderite, which in natural samples usually occurs in a complex assemblage with yukonite, pharmacosiderite, and As-bearing Fe (hydr)oxides (Majzlan et al., 2014; Paktunc et al., 2015), was substantially released in both oxalate extractions, which is indicative that it is difficult to selectively extract arseniosiderite using this selective extraction approach.

### 4.3.2. Soil and mining waste

The results of single oxalate extractions of As from soil and mining waste profiles are given in Fig. 2 and Table S5. The proportion of As extractable by oxalate in the dark (targeting ferrihydrite, yukonite, and a major part of arseniosiderite) varies from one site to another, and also changes with the profile depths. The highest proportion of extracted As ($\bar{x}$: ~90% of the total As) occurred in cambisol B, while the lowest proportion of extractable As ($\bar{x}$: ~40% of the total As) was found in the mining waste D; the other two profiles (cambisol A and gleysol C) displayed a similar As-extractable proportion of approximately 60%. For most of the samples, the amount of As extracted by hot oxalate in the light (75%–108% of the total As) corresponded to the total As (Fig. 2). These findings suggest that As in the soils and mining waste samples is almost exclusively associated with Fe (hydr)oxides and arsenates, from which poorly-crystalline and oxalate-reactive forms (ferrihydrite, yukonite, arseniosiderite) dominate in the soils (especially at site B); whereas well-crystalline and less-reactive forms (hematite, goethite, pharmacosiderite) predominate in the mining waste D.

Theoretical Fe/As molar ratios for the identified arsenate phases (arseniosiderite, pharmacosiderite, yukonite) are between 1 and 1.33; whereas these ratios for As-bearing Fe (hydr)oxides in the heavy mineral fractions of soils and mining waste were always higher than 3.0 (calculated from microprobe analyses). If the oxalate-promoted dissolution of these phases in complex soil and mining waste samples congruently releases Fe and As, then their molar ratios may roughly estimate the relative proportion of As bound to arsenates and Fe (hydr)oxides. The Fe/As ratio in the oxalate extractions varied from 1.6 to 175, with up to twice higher ratios in the hot oxalate in the light (Fig. 2 and Table S5). The lowest ratios were observed in the deeper horizons of As-rich cambisol at site B (1.6 and 1.8) and As-rich layer in the mining waste at site D (2.8). These values correspond to almost exclusive dissolution of amorphous and poorly-crystalline arsenates such

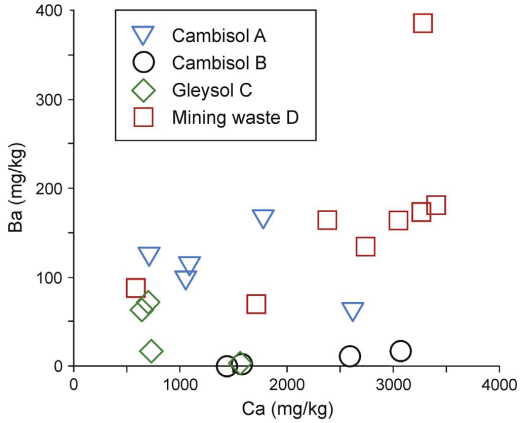


**Fig. 6.** Relationship between readily soluble ($NH_4NO_3$-extractable) Ba and Ca in soil and mining waste samples.

as yukonite, with a relatively low proportion of poorly-ordered Fe (hydr)oxides such as ferrihydrite. In contrast, very high Fe/As molar ratios in the gleysol ( > 20) correspond instead to the dominant association of As with Fe (hydr)oxides.

## 5. Discussion

### 5.1. Mineralogical evolution

Powder XRD, RMS, SEM-EDS, and electron microprobe data reveal that As and Fe, released via arsenopyrite weathering, is held in the soils and mining waste as secondary arsenates (arseniosiderite, bariopharmacosiderite, and yukonite) as well as As-bearing Fe (hydr) oxides (ferrihydrite, goethite, and hematite). These minerals generally occur as secondary phases after As sulfide alteration in near-neutral mine wastes (Paktunc et al., 2004; Cancès et al., 2008; Walker et al., 2009; Haffert et al., 2010; Foster et al., 2011; Ollson et al., 2016) as well as in naturally oxidized zones of hydrothermal ores. In contrast, low concentrations of S and trace amount of secondary (hydroxo)sulfates (rare jarosite) in the bulk soil samples indicate high mobility of this element during weathering of arsenopyrite and other sulfides at this site. Pharmacosiderite aggregates and As-bearing Fe (hydr)oxides fill dissolution cavities, likely inherited from arsenopyrite in the soil overlying the granodiorite with low-sulfide quartz veins at the Saint-Yrieix-la-Perche gold district (France) (Bossy et al., 2010), or with Li, Be, Nb, Ta, Sn, and W mineralization at the Echassières geochemical anomaly (France) (Morin et al., 2002). In the Mokrsko gold district (Czech Republic), the mineralogical assemblage of pharmacosiderite, arseniosiderite, As-bearing Fe (hydr)oxides, and probably yukonite occurs after arsenopyrite in the saprolite and overlying cambisols (Filippi et al., 2007; Drahota et al., 2009). Quantitative mineralogical analyses have shown that the proportion of As hosted by the pharmacosiderite (Morin et al., 2002; Drahota et al., 2009; Bossy et al., 2010) or arseniosiderite (Cancès et al., 2008) systematically decreases from the saprolite to the topsoil, implying that these arsenate minerals are the initial products of arsenopyrite weathering, and that an increasing Fe/As ratio and/or decreasing Fe and As concentrations during pedogenesis destabilizes pharmacosiderite or arseniosiderite, driving their transformation into As-bearing Fe (hydr)oxides (Majzlan et al., 2014).

At the Smoletely-Líšnice ore district, there are no primary sulfides in most samples. If present, only arsenopyrite occurs as relic particles embedded in secondary arsenate phases (Figs. 3a and 4c), where they are protected from further oxidative dissolution by limiting the reaction to diffusion of reactants and/or products. In addition to the presence of arsenopyrite as a minor primary ore mineral in the 80–90 year old mining waste, naturally developed soils contain very rare arsenopyrite suggesting an extremely low weathering rate of the enclosed arsenopyrite fragments. The electron microprobe analyses indicated that bariopharmacosiderite was the first crystalline product of arsenopyrite alteration in cambisol A and mining waste D (Figs. 3a and 4c). As indicated in other natural As-rich geochemical anomalies (Morin et al., 2002; Drahota et al., 2009; Bossy et al., 2010), these observations imply that minerals of the pharmacosiderite supergroup form in deep saprolite, where persistent highly dissolved As, Fe, as well as large cations (K, Ba, or Na) are maintained due to the slow groundwater flow. This is probably not valid for site B, where minerals of the pharmacosiderite supergroup were not detected. In cambisol B, yukonite is likely the initial secondary arsenate phase, forming as a product of the complete replacement of arsenopyrite and/or precipitated from solutions that have circulated through the saprolite/soil. The absence of bariopharmacosiderite in the cambisol B indicates that the chemical environment of this soil differs from that in the cambisol A as well as in the mining waste D. The conditions required for formation of bariopharmacosiderite are not known, but one could expect that a high Ba activity is required for its precipitation. The total chemical analyses revealed a significantly lower content of Ba in cambisol B than in both cambisol A and mining waste D (Table S2). The most likely source of the Ba in these sites is the K-feldspar that is the major mineral in the granodiorite underlying the cambisol A, and constituting the waste rock at site D. However, cambisol B and its gabbrodiorite bedrock do not contain K-feldspar as shown by the XRD analyses. Concentrations of readily available large cations (Ca, K and Ba), which can be controlled by and involved in the precipitation of Ca-Fe arsenates or minerals of the pharmacosiderite supergroup, show nearly identical concentrations of Ca in all of the studied profiles; however, the concentrations of available Ba in the cambisol B is significantly lower than in the other profiles (Fig. 6; Table S3). These findings indicate that bariumpharmacosiderite did not form in cambisol B due to the limited Ba concentration in the saprolite/soil system. Although the concentrations of available K are relatively high in cambisol B, these values are apparently low for pharmacosiderite formation (Table S3).

Yukonite is a nanocrystalline and Ca-deficient precursor of arseniosiderite (Gomez et al., 2010; Paktunc et al., 2015). Electron probe microanalyses of yukonite in the soils and mining waste clearly indicate a Ca deficiency with respect to the arseniosiderite specimens as well as the nominal arseniosiderite formula (Fig. 5). This deficiency probably reflects lower site occupancies in the interlayer components of yukonite (Paktunc et al., 2015). Development of the interlayer components that lead to the formation of arseniosiderite is kinetically controlled, with faster development at neutral to slightly acidic pH, and slower kinetics under alkaline conditions. The slower kinetics of yukonite transformation and its persistence at alkaline pH has been attributed to thermodynamic limitations on the activity of Ca, connecting the interlayer components (Paktunc et al., 2015). However, this finding cannot explain the obviously long-term persistence of yukonite in the soils and mining waste at the Smolotely site, which display slightly acidic to near-neutral conditions (Table S2). We presume that the lowering of Ca activity in these materials may instead be due to pedogenetic processes: (i) calcite, a source of high Ca in the initial stage of ore weathering, has been completely dissolved during pedogenesis and is not currently present in the soil (TIC < 0.1 wt%.); (ii) unsaturated conditions of shallow soils and mining waste minimize the contact time of yukonite with readily available (dissolved) Ca.

Arseniosiderite occurs as leaf-like or flaky aggregates (Fig. 4d), as well as massive replacement products of bariopharmacosiderite (Figs. 3a and 4e) or yukonite (Fig. 4f and g). Similar textural features exhibiting the replacement of pharmacosiderite by arseniosiderite are common in the naturally As-rich soil at the Mokrsko geochemical anomaly (Drahota et al., 2009). That study also found that as

pedogenesis proceeds the ratio of arseniosiderite to pharmacosiderite in the soil profiles increases from the saprolite upward. These findings suggest that the interaction of Ca-rich solutions with saprolite and soil-containing minerals of the pharmacosiderite supergroup would promote formation of arseniosiderite. This hypothesis cannot be tested by thermodynamic calculations since, to our knowledge, no solubility data for the minerals of the pharmacosiderite supergroup are available in the literature (Nordstrom et al., 2014). However, recent thermodynamic data show that arseniosiderite is a stable arsenate between pH 4 and 6 in solutions saturated with respect to scorodite, and soluble Ca minerals such as calcite and anorthite (Paktunc et al., 2015). Higher Ca activity is required for the transformation of yukonite and minerals of the pharmacosiderite supergroup to arseniosiderite. Otherwise, Fe (hydr) oxides such as goethite would form at the expense of pharmacosiderite (Morin et al., 2002).

Iron (hydr)oxides are abundant in almost all samples. Grains exhibiting complex textures and mixtures of two Fe (hydr)oxides or arsenate phases occur extensively among this group. Ferrihydrite or ferrihydrite-goethite mixtures are most commonly observed (Fig. 4a), but hematite and hematite-ferrihydrite mixtures have also been identified (Fig. 3b). Most of these Fe (hydr)oxides contain elevated concentrations of As. Lower abundances of Fe (hydr)oxides and arsenates as well as the absence of ferrihydrite and yukonite in the gleysol C are indicative of the reductive dissolution of these phases, with preferential dissolution of poorly-crystalline phases, and the resultant As releases into the groundwater. The relatively high proportion of As released in the oxalate extraction in the dark (Fig. 2c) from the gleysol are indicative of the As association with poorly-crystalline phases, but they were not detected by RMS and EMPA. This may indicate that highly oxalate-extractable As instead represents an artifact of post-collection oxidation of reduced As species.

The association of As and Ca, two of the most abundant elements in the Fe (hydr)oxides, is generally unclear. Enhanced co-adsorption of Ca and As on Fe (hydr)oxide was described by Paktunc et al. (2004), Drahota et al. (2009), Corriveau et al. (2011), and Majzlan et al. (2011). Wilkie and Hering (1996) attributed the enhancement of arsenate adsorption in the presence of Ca to favorable electrostatic effects arising from the adsorption of Ca. Paktunc et al. (2004) published an extended X-ray absorption fine structure (EXAFS) study on As- and Ca-rich mine waste, with similar As mineral associations. They considered that the presence of Ca atoms around As in Fe (hydr)oxides, as indicated by micro-EXAFS spectroscopy as well as Ca-As interatomic distances similar to arseniosiderite and yukonite model specimens, suggest the co-precipitation of Ca-Fe arsenate nanoparticles with Fe (hydr)oxide. In the present study, the presence of Ca-Fe arsenate co-precipitate would likely also explain the high Ca/As molar ratio, strong Ca-As correlations as well as too high concentrations of As in Fe (hydr)oxides (Fig. 5). This assumption is supported by two microprobe analyses (Table S4) and Raman spectra (Fig. 5) that identified a mixture of yukonite and ferrihydrite in the homogeneous grains (Raman spectrum *R8*; Fig. 4c, h).

### 5.2. Mineralogical control on As stability and solubility

The predominance of bariopharmacosiderite, Ca-Fe arsenates, and Fe (hydr)oxides in the mining waste and soil samples examined implies there is strong attenuation of As during the weathering of these arsenopyrite-bearing materials. Understanding the long-term stability and solubility of these phases is critical for predicting the mobility of As under near-surface conditions. In recent years, the solubility and stability of Ca-Fe arsenates in comparison to minerals of the pharmacosiderite supergroup have been the subject of research, driven by the abundance of Ca-Fe arsenates in mine wastes, which result from the processing of some Au and base metal ores, and the neutralization of mine effluents (Paktunc et al., 2004; Bluteau et al., 2009; Walker et al., 2009; Foster et al., 2011). In contrast, minerals of the pharmacosiderite supergroup are phases for which no thermodynamic data are available, most likely due to the unsuccessful synthesis of these phases (Mutter et al., 1984). Many observations suggest that bariopharmacosiderite is less soluble than scorodite under oxidizing and near-neutral conditions (Haffert et al., 2010), but arseniosiderite had formed (at least locally) instead of bariopharmacosiderite in cambisol A over decades under the conditions found in the mining waste. Arseniosiderite is stable under oxidizing conditions at near-neutral pH; exhibiting a relatively low solubility ($< 0.2$ mg/L) between pH 5 and 9.5 (Paktunc et al., 2015). These findings are in agreement with our extractability data that show very low As mobility ($\leq 0.55$ mg As/kg) in the samples dominated by the assemblage of bariopharmacosiderite and arseniosiderite (cambisol A and mining waste D; Table S3). In contrast, higher As mobility under oxidizing conditions was observed in cambisol B ($\leq 4.5$ mg As/kg), within which yukonite was identified as the dominant arsenate phase. A solubility study of synthetic yukonite specimens showed their solubility minimum at pH ~7 (Bohan et al., 2014), with As concentrations 1-2 orders higher than those predicted for arseniosiderite (Paktunc et al., 2015). The higher mobility of As in this oxic soil can thus be attributed to the higher solubility of the abundant yukonite.

The highest As mobility was found in gleysol C. Despite the fact that the absolute levels of $NH_4NO_3$-extractable As were almost the same as those in mining waste D; the fractions of mobile As were approximately an order of magnitude higher than those in the oxidizing conditions of the mining waste and soils (Table S3). This is not surprising, since under water-saturated or permanently damp soil conditions, arsenate phases such as arseniosiderite, pharmacosiderite, scorodite, and yukonite are subjected to biotically-generated reducing conditions, and may undergo reductive dissolution (Rochette et al., 1998; Weisener et al., 2011; Drahota et al., 2013). The higher solubility of the poorly-crystalline phases and their recrystallization into more highly-crystalline phases, induced by the appearance of $Fe^{2+}$ under reducing condition, may explain the higher proportion of crystalline Fe (hydr)oxides in the gleysol C (Pedersen et al., 2006). Nevertheless, the amount of As-bearing crystalline phases with relatively low levels of As ($\leq 2.7$ wt% $As_2O_5$) is surprisingly low with respect to total As content in the soil. This may indicate that As is also sequestered by phases that were missed by the standard mineralogical methods used in this study. These phases may include secondary As-hosted sulfides that have recently been identified in different subsurface environments such as naturally As-enriched minerothropic peatland at Gola di Lago (canton Ticino, Switzerland) (Langner et al., 2012), and a gleysol at the Mokrsko geochemical anomaly (Czech Republic) (Drahota et al., 2017); however, additional *in situ* study of arsenic speciation in the gleysol of this geochemical anomaly is needed in order to prove this hypothesis.

## 6. Conclusion

Results of the mineralogical analyses (XRD, SEM-EDS, EMPA, Raman microspectrometry) and selective chemical extractions showed that As occurs in several secondary forms (arseniosiderite, bariopharmacosiderite, yukonite; and that As is associated with ferrihydrite, goethite, and hematite) in the soils and mining waste studied. The relative proportions and assemblages of these species change with the studied profiles, and with the disappearance of: (i) bariopharmacosiderite in the soil overlying bedrock with low Ba, and (ii) poorly-crystalline As phases such as ferrihydrite and yukonite in the reducing conditions of the gleysol. In light of the detailed mineralogical analyses, the geochemical behavior of As in the soil and mining waste at this site can be explained by a series of reactions beginning within the deep saprolite or unaltered mining waste material, respectively. Under the oxic condition of these environments, the arsenopyrite is not stable, and its oxidative dissolution leads to precipitation of bariopharmacosiderite or yukonite, likely depending on the activity of Ba and Ca. These initial secondary phases are not stable and transform into arseniosiderite, but the transformation kinetics are probably very low due to insufficient activity of Ca in the unsaturated soils and mining

waste. As a result of this kinetic barrier, yukonite surprisingly is the dominant arsenate phase in the cambisol B. Whereas crystalline arseniosiderite, bariopharmacosiderite, and Fe (hydr)oxides may be considered relatively stable over the long term, depending on the environmental conditions, the predominance of highly soluble yukonite and relatively unstable As-rich ferrihydrite in the natural systems suggest that As will be relatively mobile. These less stable and more soluble components of the soils and mining wastes are also more likely to be bioavailable (Meunier et al., 2010), and they may pose a human health risk to those living near or on contaminated soils and mining wastes.

## Acknowledgements

This study was supported by the Czech Science Foundation (GACR 16-09352S) and Center for Geosphere Dynamics (UNCE/SCI/006). We are grateful to Lenka Jílková, Jaroslava Jabůrková, Marie Fayadová, Martin Štrba, and Noemi Meszárosová for assistance with sample analyses. Peter Lemkin is thanked for reviewing the English. Reviews of three anonymous reviewers helped to improve the original version of the manuscript.

## Appendix A. Supplementary data

Supplementary data related to this article can be found at http://dx.doi.org/10.1016/j.apgeochem.2017.12.018.

## References

Bluteau, M.C., Becze, L., Demopoulos, G.P., 2009. The dissolution of scorodite in gypsum-saturated waters: evidence of Ca-Fe-$AsO_4$ mineral formation and its impact on arsenic retention. Hydrometallurgy 97, 221–227.
Bohan, M.T., Mahoney, J.J., Demopoulos, G.P., 2014. The synthesis and stability of yukonite: implications in solid arsenical waste storage. In: Neelameggham, N.R., Alam, S., Oosterhof, H., Jha, A., Wang, S. (Eds.), Rare Metal Technology 2014. The Minerals, Metals & Materials Society. John Wiley & Sons, New Jersey, pp. 9–11.
Bossy, A., Grosbois, C., Beauchemin, S., Courtin-Nomade, A., Hendershot, W., Bril, H., 2010. Alteration of As-bearing phases in a small watershed located on a high grade arsenic-geochemical anomaly (French Massif Central). Appl. Geochem. 25, 1889–1901.
Cancès, B., Juillot, F., Morin, G., Laperche, V., Polya, D., Vaughan, D.J., Hazemann, J.L., Proux, O., Brown, G.E., Calas, G., 2008. Changes in arsenic speciation through a contaminated soil profile: a XAS based study. Sci. Total Environ. 397, 178–189.
Corriveau, M.C., Jamieson, H.E., Parsons, M.B., Hall, G.E.M., 2011. Mineralogical characterization of arsenic in gold mine tailings from three sites in Nova Scotia. Geochemistry: exploration, Environment. Analysis 11, 179–192.
Das, S., Hendry, M.J., 2011. Application of Raman spectroscopy to identify iron minerals to commonly found in mine wastes. Chem. Geol. 290, 101–108.
Das, S., Essilfie-Dughan, J., Hendry, M.J., 2014. Arsenate adsorption onto hematite nanoparticles under alkaline conditions: effect of aging. J. Nanoparticle Res. 16 (2490). https://doi.org/10.1007/s11051-014-2490-3.
de Faria, D.L.A., Silva, S.V., de Oliveira, M.T., 1997. Raman microspectroscopy of some iron oxides and oxyhydroxides. J. Raman Spectrosc. 28, 873–878.
DeSisto, S.L., Jamieson, H.E., Parsons, M.B., 2016. Subsurface variations in arsenic mineralogy and geochemistry following long-term weathering of gold mine tailings. Appl. Geochem. 73, 81–97.
DIN 19730, 1997. Bodenbeschaffenheit – Extraktion von Spurenelementen mit Ammoniumnitratlösung, Ausgabe Juni. Deutches Institut für Normung e. V., Berlin.
Drahota, P., Filippi, M., 2009. Secondary arsenic minerals in the environment: a review. Environ. Int. 35, 1243–1255.
Drahota, P., Rohovec, J., Filippi, M., Mihaljevič, M., Rychlovský, P., Červený, V., Pertold, Z., 2009. Mineralogical and geochemical controls of arsenic speciation and mobility under different redox conditions in soil, sediment and water at the Mokrsko-West gold deposit, Czech Republic. Sci. Total Environ. 407, 3372–3384.
Drahota, P., Falteisek, L., Redlich, A., Rohovec, J., Matoušek, T., Čepička, I., 2013. Microbial effects on the release and attenuation of arsenic in the shallow subsurface of a natural geochemical anomaly. Environ. Pollut. 180, 84–91.
Drahota, P., Grösslová, Z., Kindlová, H., 2014. Selectivity assessment of an arsenic sequential extraction procedure for evaluating mobility in mine wastes. Anal. Chim. Acta 839, 34–43.
Drahota, P., Mikutta, C., Falteisek, L., Duchoslav, V., Klementová, M., 2017. Biologically induced formation of realgar deposits in soil. Geochem. Cosmochim. Acta 218, 237–256.
Dunn, P.J., 1982. New data for pitticite and a second occurrence of yukonite at Sterling Hill, New Jersey. Mineral. Mag. 46, 261–264.
Durembergová, D., Kratochvíl, F., 1977. Minerály vizmutu a teluru ze Smolotel u Příbrami. Časopis pro Mineral. a Geol. 22, 407–410.
Filippi, M., Doušová, B., Machovič, V., 2007. Mineralogical speciation of arsenic in soils above the Mokrsko-west gold deposit, Czech Republic. Geoderma 139, 154–170.
Foster, A.L., Ashley, R.P., Rytuba, J.J., 2011. Arsenic species in weathering mine tailings and biogenic solids at the Lava Cap mine superfund site, Nevada city, CA. Geochem. Trans. 12, 1–21.
Foy, C.D., Chaney, R.L., White, M.C., 1978. The physiology of metal toxicity in plants. Annu. Rev. Plant Physiol. 29, 511–566.
Frost, R.L., Kloprogge, J.T., 2003. Raman spectroscopy of some complex arsenate minerals–implications for soil remediation. Spectrochim. Acta Part A 59, 2797–2804.
Garavelli, A., Pinto, D., Vurro, F., Mellini, M., Viti, C., Balić-Žunić, T., Ventura, G.D., 2009. Yukonite from the Grotta Della Monaca cave, Sant' Agata di Esaro, Italy: characterization and comparison with cotype material from the Daulton mine, Yukon, Canada. Can. Mineral. 47, 533–556.
Gomez, M.A., Becze, L., Blyth, R.I.R., Cutler, J.N., Demopoulos, G.P., 2010. Molecular and structural investigation of yukonite (synthetic & natural) and its relation to arseniosiderite. Geochem. Cosmochim. Acta 74, 5835–5851.
Gryschko, R., Kuhnle, R., Terytze, K., Breuer, J., Stahr, K., 2005. Soil extraction of readily soluble heavy metals and as with 1 M $NH_4NO_3$-solution – evaluation of DIN 19730. J. Soils Sediments 5, 101–106.
Haffert, L., Craw, D., Pope, J., 2010. Climatic and compositional controls on secondary arsenic mineral formation in high-arsenic mine wastes, South Island, New Zealand. N. Z. J. Geol. Geophys. 53, 91–101.
Hager, S.L., Leverett, P., Williams, P.A., Mills, S.J., Hibbs, D.E., Raudsepp, M., Kampf, A.R., Birch, W.D., 2010. The single-crystal X-ray structures of bariopharmacosiderite-C, bariopharmacosiderite-Q and natropharmacosiderite. Can. Mineral. 48, 1477–1485.
Hogsden, K.L., Harding, J.S., 2012. Consequences of acid mine drainage for the structure and function of benthic stream communities. Freshw. Sci. 31, 108–120.
IMA, 2016. The new IMA list of minerals – a work in progress. Updated : September 2016. http://nrmima.nrm.se//IMA_Master_List_%282016-09%29.pdf.
International Organization for Standardization, 1995. ISO Standard 11466, Soil Quality: Extraction of Trace Elements Soluble *Aqua Regia*. International Organization for Standardization, Geneva, Switzerland.
Ježek, B., 1929. O výskytu arsenopyritu a arsenu u Smolotel a Líšnice. Hornické a hutnické listy 11, 30.
Jia, Y., Xu, L., Fang, Z., Demopoulos, G.P., 2006. Observation of surface precipitation of arsenate on ferrihydrite. Environ. Sci. Technol. 40, 3248–3253.
Kelly, M.G., 1999. Effects of heavy metals on the aquatic biota. In: Plumlee, G.S., Logsdon, M.J. (Eds.), The Environmental Geochemistry of Mineral Deposits. Part a: Processes, Techniques and Health Issues. Reviews in Economic Geology 6A. Society of Economic Geologists, Inc., pp. 363–371.
Langner, P., Mikutta, C., Kretzschmar, R., 2012. Arsenic sequestration by organic sulphur in peat. Nat. Geosci. 5, 66–73.
Majzlan, J., Lalinská, B., Chovan, M., Bläß, U., Brecht, B., Göttlicher, J., Steininger, R., Hug, K., Ziegler, S., Gescher, J., 2011. A mineralogical, geochemical, and microbiological assessment of the antimony- and arsenic-rich neutral mine drainage tailings near Pezinok, Slovakia. Am. Mineral. 96, 1–13.
Majzlan, J., Drahota, P., Filippi, M., 2014. Parageneses and crystal chemistry of arsenic minerals. Rev. Mineral. Geochem. 79, 17–184.
Mason, B., Moore, C.B., 1982. Principles of Geochemistry. John Wiley and Sons, New York.
Meunier, L., Walker, S.R., Wragg, J., Parsons, M.B., Koch, I., Jamieson, H.E., Reimer, K.J., 2010. Effect of soil composition and mineralogy on the bioaccessibility of arsenic from tailings and soil in gold mine district of Nova Scotia. Environ. Sci. Technol. 44, 2667–2674.
Morávek, P., Pouba, Z., Janatka, J., Malec, J., Novák, F., Litochleb, J., Váňa, T., Veselý, J., Vaněček, M., Kalenda, Z., Aichler, J., Hauk, J., Skácel, J., Punčochář, M., Mrázek, I., Tásler, R., Klomínský, J., Duda, J., Ďurišová, J., Sztacho, P., Pudilová, M., Soukup, B., Šponar, P., Doškář, Z., Květoň, P., 1992. Zlato v Českém masívu. Česká geologická služba, Praha.
Morin, G., Lecocq, D., Juillot, F., Calas, G., Ildefonse, P., Belin, S., Briois, V., Dillmann, P., Chevallier, P., Gauthier, C., Sole, A., Petit, P.E., Borensztajn, S., 2002. EXAFS evidence of sorbed arsenic(V) and pharmacosiderite in a soil overlying the Echassières geochemical anomaly, Allier, France. Bull. Soc. Geol. Fr. 173, 281–291.
Müller, K., Ciminelli, V.S.T., Dantas, M.S.S., Willscher, D., 2010. A comparative study of As(III) and As(V) in aqueous solutions and adsorbed on iron oxy-hydroxides by Raman spectroscopy. Water Res. 44, 5660–5672.
Mutter, G., Eysel, W., Greis, O., Schmetzer, K., 1984. Crystal chemistry of natural and ion-exchanged pharmacosiderites. Neues Jahrbuch Mineral. Monatsh. 4, 183–192.
Myneni, S.C.B., Traina, S.J., Waychunas, G.A., Logan, T.J., 1998. Experimental and theoretical vibrational spectroscopic evaluation of arsenate coordination in aqueous solutions, solids and at mineral–water interface. Geochem. Cosmochim. Acta 62, 3285–3300.
Nordstrom, D.K., Majzlan, J., Königsberger, E., 2014. Thermodynamic properties for arsenic minerals and aqueous species. Rev. Mineral. Geochem. 79, 217–255.
Ollson, C.J., Smith, E., Sheckel, K.G., Betts, A.R., Juhasz, A.L., 2016. Assessment of arsenic speciation and bioaccessibility in mine-impacted materials. J. Hazard Mater. 313, 130–137.
Paktunc, D., Foster, A., Heald, S., Laflamme, G., 2004. Speciation and characterization of arsenic in gold ores and cyanidation tailings using X-ray absorption spectroscopy. Geochem. Cosmochim. Acta 68, 969–983.
Paktunc, D., Majzlan, J., Huang, A., Thibault, Y., Johnson, M.B., White, M.A., 2015. Synthesis, characterization, and thermodynamics of arsenates forming in the Ca-Fe (III)-As(V)-$NO_3$ system: implications for the stability of Ca-Fe arsenates. Am. Mineral. 100, 1803–1820.
Pansu, M., Gautheyrou, J., 2006. Handbook of Soil Analysis-mineralogical, Organic and Inorganic Methods. Springer-Verlag, Berlin, Heidelberg.

Pedersen, H.D., Postma, D., Jakobsen, R., 2006. Release of arsenic associated with the reduction and transformation of iron oxides. Geochem. Cosmochim. Acta 70, 4116–4129.
Pfeifer, H.R., Gueye-Girardet, A., Reymond, D., Schlegel, C., Temgoua, E., Hesterberg, D.L., Chou, J.W., 2004. Dispersion of natural arsenic in the Malcantone watershed, Southern Switzerland: field evidence for repeated sorption–desorption and oxidation–reduction processes. Geoderma 122, 205–234.
Pieczka, A., Gołębiowska, B., Franus, W., 1998. Yukonite, a rare Ca-Fe arsenate, from Rędziny (Sudetes, Poland). Eur. J. Mineral 10, 1367–1370.
Rochette, E.A., Li, G.C., Fendorf, S.E., 1998. Stability of arsenate minerals in soil under biotically generated reducing conditions. Soil Sci. Soc. Am. J. 62, 1530–1537.
Savage, K.S., Bird, D.K., O'Day, P.A., 2005. Arsenic speciation in synthetic jarosite. Chem. Geol. 215, 473–498.
Schwertmann, U., 1964. Differenzierung der eisenoxide des bodens durch extraktion mit ammoniumoxalat-lösung. Zeitschrift für Pflanzenernährung. Düngung und Bodenkunde 105, 194–202.
Seidl, K., 1991. Jílovské pásmo – dílčí úkol Smolotelský. Technical Report, Geofond (FZ 6371), Prague.
Stollenwerk, K.G., 2003. Geochemical processes controlling transport of arsenic in groundwater: a review of adsorption. In: Welch, A.H., Stollenwerk, K.G. (Eds.), Arsenic in Groundwater: Geochemistry and Occurrence. Kluwer Academic Publisher, Boston, pp. 67–100.
Valta, K., 1936. Po stopách utrpení a slávy hornictva na Příbramsku, Nákladem zaměstnanců St. báňského ředitelství v Příbrami, Příbram.
Walker, S.R., Parsons, M.B., Jamieson, H.E., Lanzirotti, A., 2009. Arsenic mineralogy of near-surface tailings and soils: influences on arsenic mobility and bioavailability in the Nova Scotia gold mining districts. Can. Mineral. 47, 533–556.
Wang, S., Mulligan, C.N., 2006. Natural attenuation processes for remediation of arsenic contaminated soils and groundwater. J. Hazard Mater. B138, 459–470.
Weisener, C.G., Guthrie, J.W., Smeaton, C.M., Paktunc, D., Fryer, B.J., 2011. The effect of Ca-Fe-As coatings on microbial leaching of metals in arsenic bearing mine waste. J. Geochem. Explor. 110, 23–30.
Wilkie, J.A., Hering, J.G., 1996. Adsorption of arsenic onto hydrous ferric oxide: effects of adsorbate/adsorbent ratios and co-occurring solutes. Colloid. Surface. Physicochem. Eng. Aspect. 107, 97–110.
Younger, P.L., Banwart, S.A., Hedin, R.S., 2002. Mine Water – Hydrology, Pollution, Remediation. Kluwer Academic Publishers, Dordrecht, Boston, London.

# II.

**Knappová M.**, Drahota P., Falteisek L., Culka A., Penížek V., Trubač J., Mihaljevič M., Matoušek T. (2019) Microbial sulfidogenesis of arsenic in naturally contaminated wetland soil. *Geochimica et Cosmochimica Acta* **267**, 33–50.

Available online at www.sciencedirect.com

ScienceDirect

Geochimica et Cosmochimica Acta 267 (2019) 33–50

Geochimica et Cosmochimica Acta

www.elsevier.com/locate/gca

# Microbial sulfidogenesis of arsenic in naturally contaminated wetland soil

Magdaléna Knappová [a], Petr Drahota [a,*], Lukáš Falteisek [b], Adam Culka [a], Vít Penížek [c], Jakub Trubač [a], Martin Mihaljevič [a], Tomáš Matoušek [d]

[a] Institute of Geochemistry, Mineralogy and Mineral Resources, Faculty of Science, Charles University, Albertov 6, 128 43 Prague 2, Czech Republic

[b] Department of Ecology, Faculty of Science, Charles University, Viničná 7, 128 43 Prague 2, Czech Republic

[c] Department of Soil Science and Soil Protection, Faculty of Agrobiology, Food and Natural Resources, Czech University of Life Sciences Prague, Kamýcká 129, 165 21 Prague 6, Suchdol, Czech Republic

[d] Institute of Analytical Chemistry, Czech Academy of Sciences, Veveří 97, 602 00 Brno, Czech Republic

Received 22 January 2019; accepted in revised form 10 September 2019; available online 18 September 2019

**Abstract**

Microbial sulfidogenesis plays a potentially important role in As biogeochemistry within wetland soils, sediments, and aquifers. This study investigated the effects of microbial sulfidogenesis on As mineralogy in the As-enriched wetland soil found at the natural geochemical anomaly of the Smolotely-Líšnice (Czech Republic) historical gold district. The distribution and speciation of As as a function of soil depth, and the metabolic properties of microbial communities in different sulfidogenic domains were examined by bulk soil as well as pore water analyses, selective chemical extractions, S isotopes, and DNA extractions. Total solid-phase analyses and selective extractions of the soil samples below ~40 cm showed that As (up to 1.16 g $kg^{-1}$) and Fe(II) are coupled to S and TOC, and had accumulated to a considerable extent in the exterior parts of NOM fragments (up to 19 wt.% As). Microscale imaging and Raman spectroscopy revealed that As speciation in the NOM exteriors is a combination of realgar ($\alpha$-$As_4S_4$), bonazziite ($\beta$-$As_4S_4$) and arsenian Fe sulfides, primarily greigite ($Fe_3S_4$) and framboidal pyrite ($FeS_2$). The sulfide phases were depleted in the $^{34}S$ isotope by 6.3–29.4‰ relative to pore water $SO_4^{2-}$; thus implying their biologically induced formation. Microbial communities associated with sulfidogenic environments in NOM and bulk soil had variable compositions, although the dissimilative $SO_4^{2-}$ reduction was usually the main metabolic trait. Relatively low isotopic fractionation in sulfide-rich NOM fragments (6.3–11.6‰) compared to bulk soil (down to −26.1‰) revealed a reservoir effect that developed probably at mm-scales. This indicates formation of sulfide phases in highly localized environments depleted in aqueous $SO_4^{2-}$ due to strong microbial sulfidogenesis when compared to the transfer rate of the solutes. The very high proportion of fermenting microorganisms in sulfide-rich NOM fragments provided further evidence of strongly reducing conditions, which are a prerequisite for sulfide phase precipitation. We have shown that by the development of suitable conditions for sulfidogenesis, NOM fragments play an active role in As immobilization in an As-enriched wetland soil. Regarding the effectiveness of As sulfidogenesis in shallow wetland soils to remediate groundwater, our findings imply that As contamination may either be limited by the low content of labile organic matter or by the fast transfer of solutes (groundwater flow).



*Keywords:* Wetland soil; Natural organic matter (NOM); Arsenic; Sulfidogenesis; Realgar; Bonazziite; Fe sulfides

* Corresponding author. Fax: +420 221 951 496.
*E-mail address:* petr.drahota@natur.cuni.cz (P. Drahota).

https://doi.org/10.1016/j.gca.2019.09.021
0016-7037/

## 1. INTRODUCTION

Wetland soils, by virtue of their periodic or permanent water saturation (Mitsch and Gosselink, 2007), are characterized by steep gradients in soil redox conditions that sustain a complex pattern of biogeochemical cycling of redox-sensitive, potentially hazardous metal(loid)s such as As (Fendorf and Kocar, 2009; Lizama et al., 2011; Zhang et al., 2017). The effect of changing redox conditions on the mobility of As in wetland soils has been addressed in a number of field and laboratory studies, showing that the fate of As is primarily linked to the biogeochemical cycling of Fe and S, as well as their relative abundances (La Force et al., 2000; Roberts et al., 2011; Burton et al., 2014; Drahota et al., 2017). Under well-aerated (oxic) soil conditions, As primarily exists in its As(V) oxidation state as the arsenate oxyanions. The high affinity of As(V) for metal (oxyhydr)oxides, in particular those of Fe(III), often leads to very low As concentrations in the aqueous phase at comparatively high solid phase concentrations (Drahota et al., 2012). In $O_2$ depleted soils, microbial decomposition of natural organic matter (NOM) drives the reductive dissolution of metal-(oxyhydr)oxides and thus the release of associated As(V) and its redox transformation into more mobile As(III) (Nickson et al., 2000; Islam et al., 2004). Arsenic behavior in anoxic soils may also be affected by microbial $SO_4^{2-}$ reduction. Microbially produced $H_2S$ can reduce both As(V) and Fe(III), which thereby drives As release into the aqueous phase (Rochette et al., 2000; Poulton et al., 2004). Alternatively, in low As(V) and Fe (III) environments, sulfide can immobilize As by facilitating its binding to sulfhydryl groups of NOM (Hoffmann et al., 2012; Langner et al., 2012) or by precipitation of As sulfide and Fe sulfide minerals (Belzile and Lebel, 1986; Rittle et al., 1995; O'Day et al., 2004; Lowers et al., 2007; Langner et al., 2013; Drahota et al., 2017). Most contaminated reducing wetland aquifers usually contain elevated Fe (II) (Smedley and Kinniburgh, 2002), reflecting the role of Fe(III) (oxyhydr)oxides in the development of high-As groundwater. Sulfate reduction in these environments sequesters Fe by facilitating the precipitation of Fe sulfide minerals, including mackinawite (FeS), greigite ($Fe_3S_4$), and pyrite ($FeS_2$) (Wilkin and Ford, 2006; Rickard and Luther, 2007). Sequestration of As by co-precipitation with, or adsorption onto these Fe sulfides is often of minor importance (Kirk et al., 2010; Kocar et al., 2010; Burton et al., 2011), except for high As loading and slightly acidic pH (Gallegos et al., 2008; Burton et al., 2014). In environments where dissolved Fe(II) is primarily low or transformed to Fe sulfides, free $H_2S$ is available for As complexation, allowing for the formation of thiolated As species and/or the precipitation of As minerals such as orpiment ($As_2S_3$), realgar ($\alpha$-$As_4S_4$), and bonazziite ($\beta$-$As_4S_4$) (Rittle et al., 1995; O'Day et al., 2004; Couture and Van Cappellen, 2011; Langner et al., 2012; Falteisek et al., 2019). Indeed, the *in situ* formation of realgar, orpiment, as well as arsenopyrite (FeAsS) and arsenian pyrite in the shallow subsurface has been observed in aquifer sediment from: a former pesticide manufacturing facility near San Francisco Bay (California, USA) (O'Day et al., 2004; Root et al., 2009), a naturally As-enriched minerothropic peatland at Gola di Lago (Switzerland) (Langner et al., 2012, 2013), a naturally As-enriched wetland soil at the Mokrsko geochemical anomaly (Czech Republic) (Drahota et al., 2013, 2017), and in abandoned As-rich mine wastes in southern New Zealand (Kerr et al., 2018). These sulfide minerals coexisted with As(III/V)-bearing Fe (III) (oxyhydr)oxides in the samples, suggesting an authigenic formation of the sulfide minerals in highly localized environments (microenvironments), characterized by strongly reducing conditions (Langner et al., 2013; Drahota et al., 2017; Kerr et al., 2018). In our previous study (Drahota et al., 2017), we found that these soil microenvironments are strictly anaerobic domains associated with NOM and dominated by sulfate-reducing and fermenting metabolisms. Based on the $^{34}S$ depletion of realgar relative to aqueous $SO_4^{2-}$, we postulated that formation of realgar deposits in the wetland soil is a consequence of dissimilatory sulfate-reducing activity (Drahota et al., 2017).

Although microbial sulfidogenesis has been recognized as a prominent process in the immobilization of As under different sulfate-reducing conditions in laboratory experiments (Kirk et al., 2010; Battaglia-Brunet et al., 2012; Omoregie et al., 2013; Burton et al., 2014; Rodriguez-Freire et al., 2014, 2015; Le Pape et al., 2017; Falteisek et al., 2019), an understanding of As sulfidation in natural soils, sediments, and mine wastes in the presence of complex mineralogical assemblages, as well as the heterogeneous distribution of NOM is still in its infancy. Herein, we examine the sulfidation of As and Fe in a naturally As-enriched wetland soil located at Smolotely (Czech Republic). In a previous study (Drahota et al., 2018), we identified an interesting assemblage of As-hosted phases in oxic soils at this site; however, dominant As solid-speciation in the slightly-reducing wetland soil remains unrevealed to us. Here, we seek to: (1) provide information on the distribution and speciation of As in the wetland soil, (2) elucidate the role of NOM and soil microorganisms in Fe–As–S mineral formation, and (3) assess the retention and reactivity of As-bearing sulfides in soil environments under changing redox conditions.

## 2. MATERIALS AND METHODS

### 2.1. Sampling and sample processing

In a preceding study, we sampled wetland soil at location C close to a spring of an unnamed stream in the naturally As-enriched geochemical anomaly ($\leq$1.87 wt.% As) of the Smolotely-Líšnice historical gold district (Fig. S1), and we observed that As was predominantly sequestered by Fe (III) (oxyhydr)oxides (Drahota et al., 2018). In September 2017, we collected soil samples from two additional soil pits (locations A and B) located approximately 3 m from each other as well as from the initial sampling location C (Drahota et al., 2018). The pits were excavated to a depth of 100 cm (A) and 110 cm (B). The samples were collected at 10 cm intervals ($n = 21$) and split into two subsamples. The subsamples intended for pH and Eh measurements were transferred into a 50 mL screw-cap centrifuge vial,

completely filled (no bubbles or headspace) by a minimum of deoxygenated deionized water, and sealed in a plastic bag under an atmosphere of Ar. The subsamples intended for geochemical and mineralogical characterization were immediately placed in Ar-purged zip-lock plastic bags and stored at 4 °C and in anoxic conditions until their return to our laboratory. The soil material was freeze-dried (Vargas et al., 2015), processed (sieving < 2 mm and milling < 50 μm) in an anoxic glove box ($pO_2 < 1$ ppm), and kept anoxic until the analyses. To concentrate the As-bearing mineral phases from the soil, heavy minerals were separated from samples situated at three different depths (10–20 cm, 40–50 cm, 90–100 cm) of profile A. Heavy minerals were obtained by centrifugation of the 0.05–0.5 mm size fraction of bulk soil samples in 1,1,2,2-tetrabromoethane diluted with 1,4-dioxane (specific gravity of 2.80 g $cm^{-3}$). After centrifugation and other manipulations of the samples (<12 h), the heavy mineral concentrates were returned to anoxic conditions in the glove box.

Soil samples were described (i.e., Munsell color, soil group, mottling, accumulations of NOM), and several particles of NOM (decomposing tree roots) with a massive yellow powdery accumulations in their subsurface were collected from a depth of 70–100 cm in the soil profiles, rinsed in deoxygenated deionized water to remove any loose soil and retained in anoxic conditions in 50 mL centrifuge tubes under Ar atmosphere. Mineralogical and geochemical analyses of the yellow powdery accumulations were determined in two composite samples (R1 and R2) that were scraped from the exterior parts of the NOM fragments. In addition, NOM particles ($n = 5$) with yellow powdery accumulations and the surrounding soil with visible signs of yellow sulfide impregnations ($n = 3$) were collected into sterile 15 mL tubes for DNA extraction. In the laboratory, DNA was carefully extracted from the yellow sulfide-rich exterior parts of the NOM particles, avoiding coarse contamination from loose soil on the surface of the NOM particles.

Pore-water samples ($n = 6$) were collected by a tension lysimeter (SPE 20 with a double 0.2 μm nylon membrane) that was installed between the excavation pits A and B (Fig. S1) to monitor the chemical pore water composition of the wetland soil. The lysimeter was installed at a depth of ~100 cm and allowed to equilibrate with the pore water for 2 months before the first sampling.

### 2.2. Solid-phase methods

Particle size distribution was determined by the hydrometer method (Gee and Bauder, 1979). The soil pH and Eh were determined using a WTW multimeter (within 4 h of sample collection) by direct insertion of calibrated electrodes into the soil sample under the Ar atmosphere in the glove box.

Homogenized soil samples were analyzed for total element concentrations by energy-dispersive X-ray fluorescence (XRF) spectrometry (ARL 9400 $XP^+$, Thermo ARL). The accuracy for elements was within 7%, based on the analysis of standard reference materials (NIST 2710a: Montana I Soil - Highly Elevated Trace Element Concentrations; NIST 2711: Montana II Soil - Moderately Elevated Trace Element Concentrations), except for Al (≤33%) and P (≤20%). Near-total Fe and trace element (As, Bi, Cu, Mo, Pb, Sb, Zn) contents were determined in triplicate by Lefort *aqua regia* digestion (3:1, $HNO_3$:HCl) on a hot plate and recovered 73% ± 4% and 95% ± 6% of total Fe and As concentrations, as determined by XRF. Triplicate digestion of certified reference soils (NIST 2710a and NIST 2711) yielded precision within 9% for all elements, except for Cr (≤29%) and Sb (≤32%). The recoveries of As, Cr, Cu, Fe, Pb, and Zn were within 90% of the confidence limits of the certified values. In contrast, the recoveries of Co, Ni, Mn, Sb, and V were significantly lower (53–84%). As a further quality assurance measure, the precision of triplicate digestions were usually within 8% (except for Bi, Cr, Mo, Sb, and Se, which were within 31%).

The reactive solid-phase Fe(II) was extracted from 0.5 g of soil with a 15 mL solution of deoxygenated 1 M HCl by shaking for 1 h (Kostka and Luther, 1994). This procedure extracts Fe(II) mainly from nanocrystalline mackinawite and siderite, as well as a small fraction of greigite and pyrite (Wallmann et al., 1993; Rickard and Morse, 2005). The concentration of Fe(II) was quantified *via* the 1,0-phenanthroline method using a Hach Lange DR3900 spectrophotometer. Duplicate extractions showed that precision was within 15%. Exchangeable As was determined in duplicate (precision within 15%) by extracting samples in deoxygenated 0.1 M $NaH_2PO_4$ buffered to pH 5.5 for 16 h (Keon et al., 2001; Paul et al., 2009). Arsenic bound to poorly crystalline Fe (oxyhydr)oxides was targeted by a 0.2 M $NH_4$-oxalate extract (2 h in darkness) (Keon et al., 2001; Drahota et al., 2014). Duplicate extractions had a precision within 9% for all elements (As, Fe, Mn). After centrifugation and filtration (0.2-μm nylon pore filter), all extractants and digests were analyzed using either inductively coupled plasma optical emission spectrometry (ICP-OES; Agilent 5100) or quadrupole-based inductively coupled plasma mass spectrometry (ICP-MS; Thermo Scientific $X^{II}$series). All extractions were conducted under an atmosphere of Ar. It should be noted that the selectivity of HCl, oxalate, and phosphate extractions was tested on two As sulfides: orpiment (synthetic $As_2S_3$; 99.9%, Alfa Aesar) and realgar (Baia Sprie mine; from collection of the Mineral Museum of the Faculty of Sciences, Charles University, Prague). Negligible amounts of As recovered from poorly crystalline orpiment (0.041% ± 0.001% in HCl, 0.021% ± 0.016% in oxalate, and 0.25% ± 0.01% in phosphate) as well as crystalline realgar (0.056% ± 0.017% in HCl, 0.054% ± 0.014% in oxalate, and 0.48 ± 0.05% in phosphate) are in accord with the results of Paul et al. (2009) and are due to the low solubility of As sulfides at an acidic pH (Wilkin and Ford, 2002).

Total C, N, S, and inorganic C (TIC) were determined in duplicate (precision within 7%) using elemental analyzers (Thermo Flash 2000, Eltra SC 500, and CS-530). Total organic carbon (TOC) was determined by subtracting the TIC from the total C. Soluble and adsorbed inorganic $SO_4^{2-}$ was determined in duplicate (precision within 9%) by shaking the samples under an atmosphere of Ar in deoxygenated 15 mM $NaH_2PO_4$ for an hour (Johnson

and Henderson, 1979), and then centrifuging the sample for 10 min. After centrifugation, the supernatant solution was passed through a 0.2-μm nylon pore filter and analyzed for $SO_4^{2-}$ by ion chromatography.

The mineralogical compositions of the bulk soil samples, heavy mineral concentrates, and separated yellow powdery accumulations were assessed by X-ray powder diffraction (XRD) analysis. The dried samples were exposed to air for <5 min prior to commencement of XRD in order to minimize potential oxidation-induced changes in mineralogy. X-ray diffractograms were obtained for randomly oriented powder using a PANalytical X'Pert Pro diffractometer equipped with a diffracted-beam monochromator and X'Celerator multichannel detector, using Cu Kα radiation (40 keV, 30 mA). Samples were step scanned from 5 to 80° 2θ using a 0.02° 2θ step and 200–500 s count times. The diffraction data were analyzed using X´Pert HighScore Plus software, version 1.0d., and semiquantitative estimates of the abundances of major minerals were obtained by comparing the integrated intensities of the diffraction peaks. Samples for examination by scanning electron microscopy (SEM) were mounted on aluminum stubs, coated with carbon, and the elemental composition and morphology of selected specimens were determined using a JEOL JXA-8530F electron microprobe analyzer (EMPA) equipped with a field emission gun source (FEG) for SEM imaging and energy dispersive spectrometry (EDS) analysis (JEOL JED-2300F spectrometer). The X-ray maps and quantitative microanalyses of selected elements in the polished sections of NOM particles as well as heavy mineral concentrates were acquired using (1) the same EMPA instrument or (2) a TESCAN VEGA SEM instrument equipped with an X-Max 50 EDS (Oxford Instruments). The operating conditions of the SEM were 15 kV, with a beam current of 1.5 nA for quantitative point analysis, and 7 nA for compositional mapping. The EMPA was operated under a 15 kV accelerating voltage and beam current of 20 nA in focused beam mode for quantitative analyses; compositional maps were acquired under 20 kV and 50 nA, except those maps including sulfide phases that were acquired with 10 kV and 15 nA (due to the instability of realgar under higher probe current). For both EDS and EMPA analysis, the following standards and X-ray lines were used for detection and quantification: $SiO_2$ (Si, Kα), anhydrite (S, Kα), magnetite (Fe, Kα), and GaAs (As, Lα).

Raman microspectrometric (RMS) analyses were performed on the grains previously explored by EDS or EMPA (locations of RMS spot analyses in the grains were almost identical to the microprobe spots) using a Renishaw InVia Reflex Raman spectrometer (Renishaw plc) coupled with a Leica microscope (Leica Microsystems, Germany) with a 50× objective. Excitation was provided by either the 514.5 nm or 785 nm line of a diode laser for nonsulfide and sulfide phases, respectively. The spectrum of each phase was recorded at 0.1–5% laser power to avoid thermal degradation over the spectral range of 100–1200 $cm^{-1}$. Scanning parameters were as follows: 20 s accumulation time, and 15–20 scans were taken to improve the signal-to-noise ratio.

### 2.3. Sulfur isotope analysis

Total S for $\delta^{34}S$ determination was extracted from the soil ($n = 21$) and NOM exterior ($n = 2$) samples by Eschka's procedure in the form of $BaSO_4$ (Novák et al., 1994). Pore water samples for sulfur isotopes analyses ($n = 3$), collected during November and December 2018, were filtered (<0.2 μm nylon membrane filter), acidified (pH 3), and brought to the laboratory. After $CO_2$ removal from a hot water sample (90 °C), aqueous $SO_4^{2-}$ was precipitated as $BaSO_4$. All $BaSO_4$ precipitates were analyzed measuring the $^{34}S/^{32}S$ ratio following online combustion with a Thermo Delta V Plus coupled with a Thermo Flash 2000 Elemental Analyzer at the Laboratories of Mass Spectrometry of the Faculty of Science, Charles University. Randomly selected soil samples ($n = 9$) and two samples of primary arsenopyrite ore from the Smolotely-Líšnice gold district were also analyzed for S isotope ratios using a MAT 253 stable isotope ratio mass spectrometer coupled with a Costech ECS 4010 elemental analyzer at the Queen's University Facility for Isotope Research (Queen's University, Canada). All results were expressed as a ‰ deviation of the $^{34}S/^{32}S$ ratio in the sample from the Vienna Canyon Diablo Troilite, with an analytical error of <0.3‰. The isotope data obtained from the same samples in two laboratories indicated good agreement ($R^2 = 0.986$, $n = 9$), with a variability of ±1.8‰.

### 2.4. Pore-water analyses

Pore waters were sampled in the period between November 2017 and May 2018 using a suction lysimeter installed at a depth of ~100 cm, coinciding with increased TOC and S in the soil profiles.

Samples were immediately analyzed in the field for temperature, Eh, pH, and dissolved $H_2S$, Fe(II), and total Fe using a portable WTW multimeter and DR3900 spectrophotometer (Hach Lange). The concentration of dissolved $H_2S$ was analyzed by the methylene blue method (Hach method 8131). An aliquot of pore water was added to 1,10-phenanthroline solutions for $Fe^{2+}$ determination. Total aqueous Fe was also determined using this method, following pre-reduction of $Fe^{3+}$ by ascorbic acid. Samples for major cation and trace element analyses were acidified with trace-metal-grade $HNO_3$ (Merck); a sample aliquot for aqueous As speciation analysis was preserved by adding 0.1 M EDTA-$Na_2$ solution to a concentration of 1 mM (Bednar et al., 2002).

Concentrations of major and minor cations as well as trace elements were analyzed by ICP-OES (Agilent 5100) and ICP-MS (Thermo Scientific Xseries$^{II}$). The major anions were analyzed by high-performance liquid chromatography (HPLC; Dionex ICS-2000). Bicarbonate was calculated from the alkalinity, measured by microtitration (Schott TitroLine Easy automatic titrator) with 0.05 M HCl. The measured concentrations of elements in the certified standards NIST 1640 (trace elements in natural water) and NIST 1643d (trace elements in water) were generally within ±5% of their certified values. The analyses of aque-

ous arsenite and arsenate were performed by anion exchange HPLC-ICP-MS (Agilent 1200 Series HPLC isocratic pump, and Agilent 7700x mass spectrometer). The limit of detection was 0.1 μg As $L^{-1}$, and the intra-assay coefficient of variation was better than 5% for all species.

### 2.5. Molecular biology methods

The fragments containing the V4 region of the 16S rDNA of bacteria and archaea were amplified by PCR in triplicate using universal primers U515F and U806R, following the procedure outlined in Caporaso et al. (2012). Unique sequence tags were placed at the 5' end of the primers, enabling multiplex sequencing. The amplicons were sequenced on the MiSeq platform (Illumina) at the Laboratory of Environmental Microbiology, Institute of Microbiology of the Academy of Science of the Czech Republic (Prague).

Sequence data were analyzed by the pipeline SEED v. 2.0.4 (Větrovský and Baldrian, 2013). Paired ends were joined by fastq-join (Aronesty, 2011). All of the sequences with mismatches in tags were removed from the dataset. All sequences were clustered into operational taxonomic units (OTUs), and chimeras were deleted using UPARSE implementation in USEARCH 8.1.1861 (Edgar, 2013) with a 97% similarity threshold. The consensus from each OTU was constructed from a MAFFT alignment (Katoh et al., 2009), based on the most abundant nucleotide at each position. The OTUs were identified, and their environmental requirements were assessed by megaBLAST and BLASTn algorithms against the GenBank nt/nr database. A phylogenetic tree was constructed using non-singleton bacterial and archaeal 16S rDNA sequences under the GTRCAT model in RAxML (Stamatakis, 2014). The tree was used in phylogenetic dissimilarity calculations performed in Mothur (Schloss et al., 2009). Affiliation of microbial communities to soil process domains was tested by AMOVA based on UniFrac distances with 10,000 Monte Carlo generations.

Selected sequences representing OTUs with abundances over 1% were deposited in GenBank under accession numbers MK703883 - MK703934.

## 3. RESULTS

### 3.1. Chemistry and mineralogy of soil

The wetland soils collected from two sites were classified as Dystric Stagnic Gleysols (IUSS Working Group WRB, 2006). Analyses of the soil samples ($n = 21$) revealed a near neutral environment ($\bar{x} \pm \sigma$: pH $6.59 \pm 0.29$) with vertical and lateral variations in the pedological and geochemical characteristics between sites A and B (Fig. 1, Tables S1, S2). Results of grain-size analysis showed that site A was dominated by sand (≥60%). Site A also had an organic-rich (~4.4% TOC) layer at 30–40 cm depth that probably resulted in the relatively sharp transition from oxic to reducing conditions as demonstrated from the Eh drop from + 549 to −38 mV between the A25 and A35 samples (Fig. 1). In contrast, site B reflected a gradual decrease of Eh with depth. Here, an accumulation of organic matter occurred at the depth of 70–100 cm, and it coincided with the Eh minimum as well as a finer texture (≤42% of sand) (Fig. 1).

Near-total As concentrations in the bulk soils ranged from 0.11 to 4.63 g $kg^{-1}$ ($\bar{x} \pm \sigma$: $0.58 \pm 0.75$ g $kg^{-1}$). The highest As concentrations were detected in the uppermost horizons (especially B5; most likely due to anthropogenic contamination), but As also concentrated in the deeper soil layers characterized by an abundance of NOM fragments (especially A95 at a depth of 90–100 cm). Distribution of As below ~40 cm at both sites A and B resembles the distribution of S and TOC (Fig. 1), suggesting a possible connection between all three elements in the reducing soil environment. The exchangeable fraction of As ($As_{PO4}$) was in the range of 5.5–16.6% ($\bar{x} \pm \sigma$: $11.2 \pm 3.3\%$) of the total As, with the highest fractions generally observed in the deeper parts of the soil profiles (Fig. 1; Table S3). The fraction of As bound to poorly-crystalline Fe (oxyhydr)oxides ($As_{OX}$) is relatively high ($\bar{x} \pm \sigma$: $50 \pm 22\%$), and either decreases with depth (from 76% in the topsoil to 8% at the bottom of profile A) or varies in accordance with the Eh values (site B) (Fig. 1).

Most of the labile Fe ($\bar{x} \pm \sigma$: $27.8 \pm 9.7\%$) was in the form of (oxyhydr)oxides ($Fe_{OX}$), with the maxima approaching 37.8% and 61.4% of the near-total Fe in the A and B topsoil samples, respectively (Fig. 1; Table S3). Labile Fe(II) ($Fe(II)_{HCl}$) was frequently less than 5% of the near-total Fe, and its proportion generally increased with depth. However, this excludes the notable exception at site B where the deepest soil samples (≥85 cm) contained a lower TOC and displayed a coarser texture as well as a higher Eh, consistent with less reducing conditions (Fig. 1; Tables S1, S3).

The characterization of the bulk soil samples as well as the heavy mineral concentrates by XRD indicated a similar mineralogy as a function of depth (Fig. S2). These consisted mostly of quartz and plagioclase with lesser amounts of amphibole and phyllosilicate minerals (chlorite and muscovite/illite) in the bulk soil samples; and amphibole with minor amounts of magnetite, quartz, plagioclase, and chlorite in the heavy mineral concentrates. Examination by SEM and EDS or EMPA of the As-bearing phases in the heavy mineral concentrates showed that the uppermost soil sample (10–20 cm) contains abundant Fe (oxyhydr)oxides with highly variable As concentrations ($\bar{x} \pm \sigma$: $3.28 \pm 3.39$ wt.% As). The examination of these Fe (oxyhydr)oxides by the combination of RMS and EMPA showed that the highest As concentrations occurred in ferrihydrite (4.8–10.0 wt.%), while the crystalline Fe (oxyhydr)oxides identified by RMS (as goethite and hematite) contained significantly lower amounts of As (≤1.2 wt.% As) (Figs. 2, 3, S3). Arsenic-bearing Fe (oxyhydr)oxides were also detected in the heavy mineral fractions concentrated from the reducing samples in the deeper parts of the soil profile (≤40 cm), but they were always present in significantly lower amounts, and contained a lower concentration of As (≤0.6 wt.% As) comparing to the uppermost sample (Fig. 3). It should be noted that RMS characterization of Fe (oxyhydr)oxides from the deeper parts of the soil profile

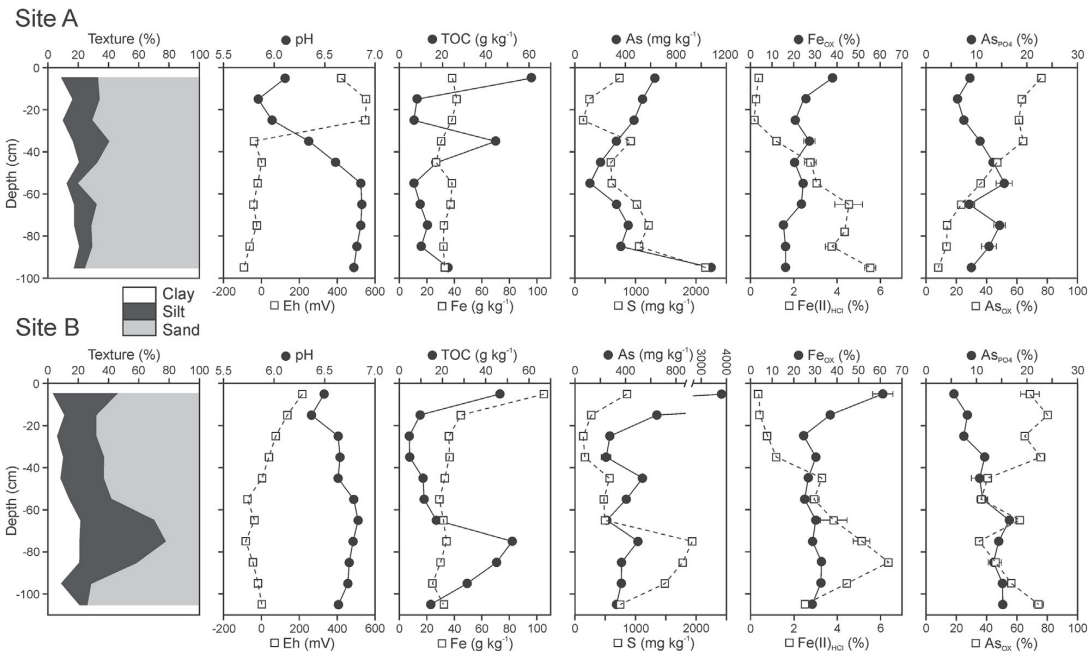


Fig. 1. Soil properties at sites A and B (median grain size analysis; organic carbon (TOC), Fe, As, and S distribution; Fe fraction in 0.2 M oxalate extracts; Fe(II) fraction in 1 M HCl extracts; As fractions in 0.1 M $NaH_2PO_4$ ($As_{PO4}$) and 0.2 M oxalate ($As_{OX}$) extracts).

led to the identification of only crystalline species such as goethite and magnetite. Moreover, these phases often displayed different alteration features (Fig. 2), suggesting the impact of reductive dissolution processes.

### 3.2. Chemistry and mineralogy of NOM fragments

NOM fragments with yellow subsurface accumulations (Fig. S4) occurred in the bottom of the Gleysol profiles (≥70 cm). Analyses of these fragments revealed very high concentrations of TOC (R1: 27.7 wt.%; R2: 38.8 wt.%), S (R1: 13.0 wt.%; R2: 4.9 wt.%), As (R1: 19.3 wt.%; R2: 4.5 wt.%), and Fe (R1: 4.7 wt.%; R2: 2.7 wt.%) as well as enrichment in most trace elements compared to the soil matrix (Table S4). Enrichment factors (EFs) calculated as the ratio of trace element concentration in the NOM exterior to that in the surrounding soil matrix, exhibited particularly high values (EFs > 10) for Cr, Mo, Sb, and Se; and slightly lower (EFs > 2) values for Co, Cu, Ni, V, and U. The other trace elements analyzed (Ba, Bi, Pb, Th) were not enriched, nor revealed depletion with respect to the surrounding soil.

XRD results for two NOM fragments rich in yellow powdery accumulations indicated realgar ($\alpha$-$As_4S_4$) and bonazziite ($\beta$-$As_4S_4$) as the major phases (>80%) (Fig. S2). Quartz and pyrite occurred in minor amounts. Despite the fact that XRD confirmed realgar and bonazziite as the sole AsS phases (Fig. S2), RMS revealed an association of these phases with pararealgar (Fig. S5a). The formation of pararealgar might be attributed to light-induced alteration of realgar and bonazziite (Douglass et al., 1992; Bonazzi et al., 1996), which took place between the collection and mineralogical analyses of the samples. Examination of NOM fragments with SEM and EDS showed that realgar and bonazziite occur in the form of feather-like aggregates or small dispersed particles (Fig. 4; S6a, b), and also frequently exhibits as filamentous shapes such as nanowires (Fig. S6c, d) and tubes with a diameter of approximately 1–4 μm (Fig. 4b, S6e). Raman microspectra of AsS phases often showed a shift of the realgar bands to the frequencies characteristic for bonazziite (Muniz-Miranda et al., 1996; Bindi et al., 2015) and *vice versa* (Fig. S5a), indicating a mixture of $As_4S_4$ polymorphs at the micrometer scale (area of analyzed sample ~5 $\mu m^2$). EDS analyses showed that nearly equimolar AsS contained no detectable (≤0.1 wt.%) trace elements such as Al, Co, Cr, Cu, Fe, Mo, Ni, Se, Si, or Sb. Realgar and bonaziite are often associated with Fe sulfides and disulfides, which usually occur in minor amounts. The combination of SEM/EDS and RMS allowed us to distinguish three different FeS phases: pyrite, greigite, and an unidentified FeS phase (Fig. S5b). The pyrite always occurred as framboids, which ranged in diameter from 5 to 40 μm, with an average diameter of ~15 μm (Fig. 4). Crystallites, either spherical or octahedral, comprising individual framboids differed in size (0.2–5 μm), averaging 1 μm in diameter. The average As content of eight pyrite framboids is 0.44 wt.% with an observed range from 0.31 to 0.66 wt.%. Most nonframboidal FeS grains displayed both Fe:S ratios and Raman spectra consistent with the mineral greigite, which typically

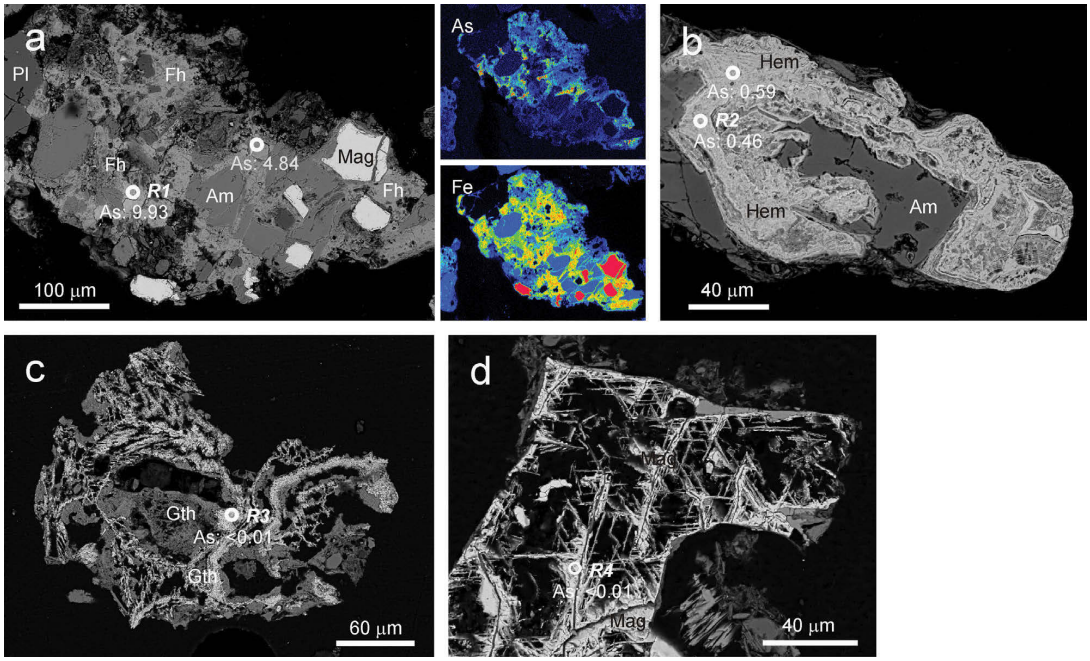


Fig. 2. Back-scattered electron images and X-ray elemental mapping showing typical habit of Fe (oxyhydr)oxides from the (a, b) uppermost (HF-A15: 10–20 cm), and (c, d) the deepest sample (HF-A95: 90–100 cm). Arsenic concentrations are expressed in wt.%. Raman spectra obtained from locations *R1-R4* are given in (Fig. S3). Am - amphibole; Fh - ferrihydrite; Gth - goethite; Hem - hematite; Mag - magnetite; Pl - plagioclase.

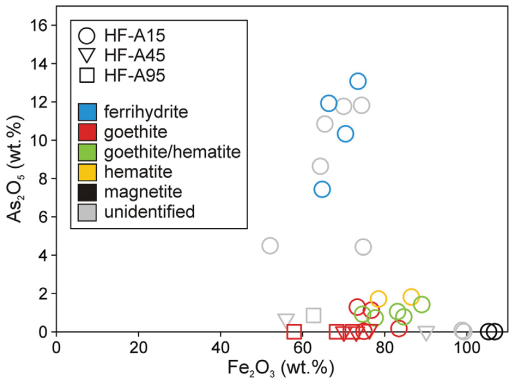


Fig. 3. Variation of $As_2O_5$ as a function of $Fe_2O_3$ in secondary Fe (oxyhydr)oxides from Smolotely gleysol identified by Raman microspectrometry. The sample notation indicates the mean sampling depth in centimeters (HF-A15: 10–20 cm; HF-A45: 40–50 cm; HF-A95: 90–100 cm). (For interpretation of the references to color in this figure legend, the reader is referred to the Web version of this article.)

occurs as ~2–8 μm spherical grains filling wood cells of NOM (Fig. 4d, e). All nine greigite grains we examined had As, Co, and Ni contents above the level of detection, averaging 1.69 wt.% As (0.99–2.27 wt.%), 0.51 wt.% Co (0.23–0.86 wt.%), and 0.17 wt.% Ni (≤0.33 wt.%). Within the wood cells, we also identified rare FeS grains with a Fe:S ratio consistent with a stoichiometry between $Fe_5S_6$ and $Fe_7S_8$. Raman spectra of these phases (bands at 318, 335, and 380 $cm^{-1}$; Fig. S5b) are not indicative of metastable mackinawite or any other known Fe monosulfide mineral (Bourdoiseau et al., 2008), but are almost consistent with spinel-structured violarite ($FeNi_2S_4$) (R060846; Lafuente et al., 2015). The As (0.70–1.50 wt.%) and Co (0.25–1.39 wt.%) contents in this metastable FeS generally overlap with As and Co in greigite, but the metastable FeS phases have considerably higher concentrations of Ni (0.68–1.62 wt.%) than greigite. However, these concentrations of Ni are still far from the stoichiometry of violarite. We assume that our unidentified Ni-rich FeS phase is very suggestive of a metastable Fe monosulfide phase, which Wang et al. (2015) and Weber et al. (2017) associated with the alteration of pyrrhotite and troilite, respectively. Concentrations of other trace elements such as Cr, Cu, Mo, Se, and Sb in Fe sulfides and disulfides were below the EDS detection limit.

### 3.3. Pore-water chemistry

Concentrations of dissolved As species and other constituents in pore water sampled from the site monitoring lysimeter are reported in Table S5. It should be noted that

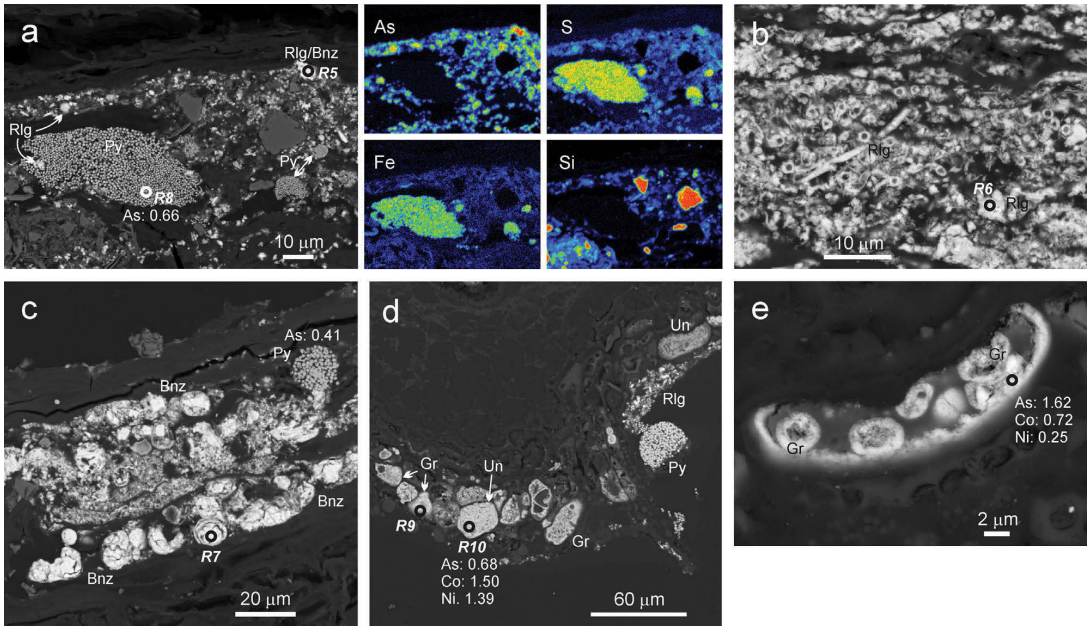


Fig. 4. Back-scattered electron images and X-ray elemental mapping showing sulfide phases on the fragments of buried natural organic matter (NOM) in the wetland soil. (a) Framboid texture of As-bearing pyrite with finely dispersed particles of realgar and bonazziite. (b) Filamentous aggregate composed of realgar tubes (~1 µm in diameter). (c) Relatively massive aggregates of bonazziite with framboidal pyrite. (d) Association of realgar, greigite, framboidal pyrite, and unidentified metastable FeS phase in wood cells of NOM. (e) Magnified image of the wood cell with greigite. Elemental concentrations are expressed in wt.%. Raman spectra obtained from locations *R5-R10* are given in (Fig. S4). Bnz - bonazziite; Gr - greigite; Py - pyrite; Rlg - realgar; Un - unidentified FeS phase.

direct information on pore water chemistry was restricted to the screened soil depth of ~ 100 cm, which was below the water table. Pore-water pH ranged from 6.90 to 7.27, and field Eh data demonstrated slightly reducing conditions (Eh: 87–145 mV). Total dissolved As concentrations were generally high, ranging from 316 to 634 µg $L^{-1}$, and included both As(III) (63–99%) and As(V) (≤37%) species. The pore water concentrations of Fe(II) were always higher than 94% of the total Fe ( $\bar{x} \pm \sigma$: 20.5 ± 3.5 mg $L^{-1}$), indicating that Fe(III) was negligible compared to Fe(II). Similarly, the pore water $H_2S$ concentrations ($\bar{x} \pm \sigma$: 0.040 ± 0.017 mg $L^{-1}$) were negligible compared to dissolved $SO_4^{2-}$ ($\bar{x} \pm \sigma$: 131 ± 14.9 mg $L^{-1}$). The dominance of Ca, Fe(II), $SO_4^{2-}$, and $HCO_3^-$ in the pore water is consistent with the dissolution of carbonate and sulfide minerals associated with the ore accumulations in the bedrock as well as with iron-reducing conditions in the saturated zone of the soil. The concentrations of trace metals and metalloids such as Al, Co, Cr, Cu, Mo, Sb, Se, U, and Zn were always very low (<3 µg $L^{-1}$, except for Zn).

### 3.4. Sulfur isotope analyses

The $\delta^{34}S$ values generally decreased from primary ore, to pore-water, and to sulfide-rich NOM fragments, and also decreased down soil profile A (Table S6). Isotopic data of primary arsenopyrite-rich ore from the Smolotely-Líšnice gold deposits (+4.0 and +4.2‰) correspond to the $\delta^{34}S$ values of primary sulfides from the nearby Mokrsko gold deposit (+3.0 ± 1.5‰, $n = 10$) as well as the other Variscan Au-bearing quartz vein deposits (+5.2 ± 2.3‰, $n = 30$) in the central part of the Bohemian Massif (Zachariáš et al., 2013). The $\delta^{34}S$ values of $SO_4^{2-}$ in the pore water (+2.6 ± 0.9‰) were slightly depleted in comparison to the values formed by mixing of S isotope signatures of bedrock sulfides and atmospheric deposition (e.g., 5.4 ± 0.3‰; Novák et al., 2005). Thus, changes in the isotopic signature from lithogenic and atmospheric sources to soil pore water are due to isotope fractionation processes within the soil such as S mineralization (Fuller et al., 1986; Alewell and Gehre, 1999) or oxidation of secondary sulfide phases. The latter possibility may be due to the drop of groundwater level that was registered during the sampling period. The isotopic composition of the sulfide-rich NOM (−8.3 and −4.7‰) was significantly lower than that of primary sulfides in the bedrock as well as $SO_4^{2-}$ in the pore water (Table S6).

The range of $\delta^{34}S$ values in the total soil S was between −26.1 and +5.8‰. Surprisingly, the total soil S at site A was significantly depleted in $^{34}S$ (with the range of $\delta^{34}S$ of samples ≥30 cm between −26.1 and −13.3‰) compared to soil at the nearby site B (with the range of $\delta^{34}S$ of samples ≥30 cm between −7.3 and +5.8‰), and even with respect to the secondary sulfides measured in the NOM

fragments. The decrease of $\delta^{34}S$ with increasing depth in profile A was ascribed to dissimilatory microbial $SO_4^{2-}$ reduction, a process known to discriminate against the heavier $^{34}S$. The decreasing $\delta^{34}S$ ratio coincided with a build-up in the S concentration from 30 to 100 cm below the soil surface (Fig. 5). The negative $\delta^{34}S$ values at depths $\geq$70 cm of profile B could also be ascribed to dissimilatory $SO_4^{2-}$ reduction; however, the depth dependent increase in the soil layer at depths of 40–70 cm indicate that aerobic metabolism (assimilatory $SO_4^{2-}$ reduction and S mineralization) contributed to the positive $\delta^{34}S$ signal in this soil (Fuller et al., 1986; Novák et al., 1996).

### 3.5. Microbial community patterns

A total of 2957 non-singleton OTUs at the 97% similarity level were determined among 46,043 16S rDNA sequences from 8 samples of sulfide-rich NOM fragments and surrounding soil. The communities were dominated by sulfate-reducing *Deltaproteobacteria*, both fermentative and sulfate-reducing *Firmicutes*, and *Chloroflexi* that usually belong to anaerobic groups capable of dehalorespiration (Table S7). Interestingly, the communities of individual samples were dominated by members of distinct microbial phyla despite the fact that they originated from seemingly identical microhabitats.

Thorough characterization of 53 OTUs, representing at least 1% of at least one sample, revealed heterotrophic $SO_4^{2-}$ reduction as the most abundant type of energy metabolism (Table 1). The metabolic traits of microbial communities from the sulfide-rich NOM and surrounding sulfide-bearing soil were highly similar to the metabolism of microbial communities detected at corresponding habitats at the realgar-precipitating wetland soil in Mokrsko, as previously described (Drahota et al., 2017). The communities from Smolotely differed by their higher aerobicity and decreased proportion of fermentation, hydrogenotrophy, and methanogenesis (Table 1). This corresponds well with several physico-chemical parameters (higher Eh of pore water, higher hydraulic conductivity, and lower TOC in Smolotely compared to Mokrsko), indicating less reducing conditions in the Smolotely wetland soil comparing to the Mokrsko wetland soil.

The high similarity to Mokrsko soil was also evident from the relatively great proportion of shared microbial genotypes. Among the 53 most abundant OTUs from Smolotely, 28 OTUs (53%) had a similarly abundant counterpart with a sequence identity over 95% at Mokrsko. Comparison of the Smolotely samples with microbial communities from various soil process domains from Mokrsko, by weighted UniFrac metrics, revealed that Smolotely communities cluster with the reduced realgar-bearing domains from Mokrsko, but differ from the oxidized topsoil horizons ($p < 0.0001$).

## 4. DISCUSSION

Arsenic speciation within the Smolotely wetland soil varies with depth. In the upper parts of the soil profiles (depth $\leq$ 30 cm in profile A), defined by oxic conditions (Fig. 1), As is predominantly bound to Fe (oxyhydr)oxides (ferrihydrite, goethite, and hematite). These results are consistent with our previous study (Drahota et al., 2018), which recognized that As above the water table at location C is bound to crystalline Fe (oxyhydr)oxides (goethite and hematite), and rarely to bariopharmacosiderite [$Ba_{0.5}Fe_4(AsO_4)_3(OH)_4{\cdot}5H_2O$]. With increasing depth, arsenic sorbed to Fe (oxyhydr)oxides persist with decreasing abundances and concentrations (Figs. 1 and 3). Ferric (oxyhydr) oxides are of lesser importance as an As residence below ~40 cm, especially at site A. Arsenic sulfides (realgar and bonazziite) as well as minor pyrite and greigite apparently account for the majority of As in the deeper ($\geq$40 cm) water-saturated soil (Fig. 4). Drahota et al. (2017) similarly recognized that more than 71% of the total As in the naturally contaminated Mokrsko wetland soil at depths

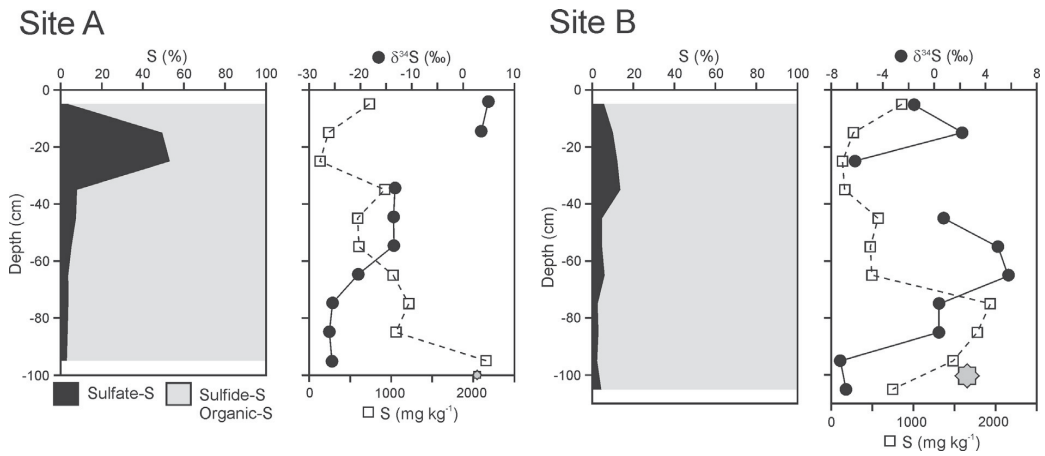


Fig. 5. Vertical distribution of sulfur species and sulfur isotopes in the soil profiles. The gray asterisk corresponds to the $\delta^{34}S$ value of $SO_4^{2-}$ in the pore water collected by lysimeter.

Table 1
Main metabolic and ecological traits of microbial OTUs with abundance over 1% in at least one sample of sulfide-rich NOM (NOM) and surrounding sulfide-enriched soil (Soil) from sites A and B (Smolotely). Abundance values are in % and represent $\bar{x} \pm \sigma$ (minimum-maximum). Similar domains (Soil and NOM) from realgar-bearing gleysols at Mokrsko are given for comparison (data by Drahota et al., 2017). Values from both sites within a similarity in the 50% range are highlighted in gray color. Abundances of the analyzed OTUs were recalculated to a 100% sum for each sample.

| | | Smolotely | | Mokrsko | | Mokrsko/Smolotely | |
|---|---|---|---|---|---|---|---|
| | | Soil ($n$ = 3) | NOM ($n$ = 5) | Soil ($n$ = 8) | NOM ($n$ = 10) | Soil | NOM |
| Trophy | A+F | 11.2±8.8 (2.8-23.3) | 6.9±4.2 (0.5-12.7) | 11.1±10.7 (1.4-33.1) | 7.6±4.4 (0.9-13.8) | ***0.99*** | ***1.10*** |
| | H | 88.8±8.8 (76.7-97.2) | 93.1±4.2 (87.3-99.5) | 88.9±10.7 (66.9-98.6) | 92.4±4.4 (86.2-99.1) | ***1.00*** | ***0.99*** |
| O | A+M | 25.1±9.1 (14.5-36.8) | 5.6±3.3 (2.1-11.1) | 7.0±7.4 (2.0-23.2) | 7.7±6.9 (1.3-24.2) | 0.28 | ***1.37*** |
| | F | 12.1±0.9 (11.1-13.2) | 11.3±8.7 (1.4-23.4) | 7.3±5.3 (2.5-18.3) | 4.3±3.9 (0.7-12.1) | ***0.60*** | 0.38 |
| | N | 62.7±9.6 (51.0-74.4) | 83.1±10.9 (65.5-96.5) | 85.3±10.1 (65.3-95.0) | 88.0±8.1 (68.7-96.2) | ***1.36*** | ***1.06*** |
| S | O | 4.9±3.9 (1.9-10.4) | 2.3±1.9 (0.1-4.6) | 2.2±2.4 (0.3-7.9) | 1.3±1.2 (0.1-3.3) | 0.45 | ***0.58*** |
| | R | 44.8±1.5 (43.7-46.9) | 31.6±3.8 (15.9-56.7) | 57.9±16.3 (37.9-86.0) | 31.3±14.5 (3.9-52.1) | ***1.29*** | ***0.99*** |
| Fe | O | 4.2±2.9 (1.9-8.2) | 1.7±1.2 (0.1-3.5) | 3.1±6.7 (0.0-19.5) | 1.2±1.6 (0.0-4.3) | ***0.74*** | ***0.70*** |
| | R | 5.2±1.1 (3.9-6.6) | 4.3±2.4 (1.0-7-3) | 7.4±6.2 (0.0-20.7) | 4.8±3.6 (0.2-9.6) | ***1.41*** | ***1.12*** |
| N | O | 3.3±1.8 (0.9-5.2) | 1.7±1.1 (0.4-3.3) | 1.8±2.3 (0.0-5.6) | 1.6±1.9 (0.0-4.7) | ***0.54*** | ***0.97*** |
| | R | 29.5±12.1 (12.7-40.2) | 7.1±4.1 (2.3-14.4) | 17.7±28.0 (3.2-86.0) | 5.2±3.7 (1.6-12.5) | ***0.60*** | ***0.74*** |
| H | O | 6.2±1.1 (4.7-7.2) | 4.5±2.3 (1.0-7.9) | 13.3±6.9 (5.1-25.9) | 10.3±5.1 (2.8-19.1) | 2.14 | 2.28 |
| | R | 4.8±2.0 (2.3-7.4) | 5.6±3.0 (2.2-10.6) | 10.0±5.9 (0.1-20.6) | 21.9±19.4 (3.8-57.6) | 2.06 | 3.94 |
| Metabolism | F | 5.3±1.0 (4.2-6.6) | 25.0±18.0 (4.3-55.7) | 24.1±14.7 (3.5-48.9) | 45.1±22.5 (14.5-86.4) | 4.51 | ***1.81*** |
| | R | 94.3±1.6 (92.4-96.2) | 72.5±20.2 (37.8-93.8) | 68.5±14.2 (42.6-91.8) | 41.0±14.1 (13.2-56.3) | ***0.73*** | ***0.56*** |
| | M | 0.2±0.1 (0.1-0.3) | 1.6 ±2.5 (0.0-6.5) | 0.7±1.7 (0.0-4.9) | 5.3±11.5 (0.0-33.4) | 3.56 | 3.31 |
| | Rdhr | 12.1±7.4 (3.5-21.6) | 25.6±12.2 (10.1-41.2) | 9.3±4.9 (0.0-15.9) | 19.0±21.1 (0.4-59.7) | ***0.77*** | ***0.74*** |
| | Rmt | 20.6±12.4 (3.6-32.7) | 4.5±1.5 (2.9-7.3) | 11.2±5.7 (0.0-19.3) | 3.0±3.4 (0.1-10.7) | ***0.55*** | ***0.65*** |

| | | |
|---|---|---|
| Trophy | A | autotrophic |
| | F | facultatively autotrophic |
| | H | heterotrophic incl. facultative phototrophs |
| O | A+M | aerobic and microaerophilic |
| | F | facultatively anaerobic |
| | N | anaerobic |
| S, N, Fe, H | O | oxidize |
| | R | reduce |
| Metabolism | F | fermentative |
| | R | respirative |
| | M | methanogenesis |
| Specialized respiration | Rdhr | dehalorespiration |
| | Rmt | methylotrophy |

of ≥60 cm is incorporated in newly-formed realgar, with the remaining portion in As(V)- and As(III)-containing Fe (oxyhydr)oxides. Although already recognized as important, the details of sulfidation of As and Fe in highly heterogeneous and complex natural systems, such as soil, have only been described very generally.

### 4.1. Sulfate-reducing activity in soil

The main pathway of sulfide phase formation in soil and NOM fragments was dissimilatory bacterial reduction of aqueous $SO_4^{2-}$ in the pore water. This is clearly indicated by the low $\delta^{34}S$ values (down to −26.1‰ for total S in soil), which indicate a maximum fractionation of almost 30‰ and 12‰ in sulfide-bearing soil and sulfide-rich NOM exteriors, respectively (Fig. 5, Table S6), when compared to aqueous $SO_4^{2-}$. These figures are within the typical range of fractionation due to bacterial $SO_4^{2-}$ reduction of freshwater $SO_4^{2-}$ (Novák et al., 1994; Novák et al., 1996). Highly variable S isotopic fractionation values associated with sulfide formation in bulk soil at a depth ≥ 40 cm at site A (between 14.9 and 29.4‰), and NOM exteriors (between 6.3 and 11.6‰) indicate some variability in the biological and environmental controls on isotopic fractionation. Relatively low isotopic fractionations, such as those observed in the sulfide-rich NOM exterior in this study are consistent with levels of S fractionation in realgar-rich NOM (between 9.5 and 12.5‰) in Mokrsko wetland soil (Drahota et al., 2017) as well as pyrite- and greigite-bearing NOM fragments (between 1.4 and 10.7‰) buried in the wetland soil at Gerolfingen, Germany (Stanjek et al., 1994). We propose that these low isotopic fractionations are due to reservoir

effects in a transport-limited system characterized by the unlimited availability and lability of the organic substrate (Canfield, 2001; Bradley et al., 2016). In this scenario, a combination of low $SO_4^{2-}$ concentrations and high microbial sulfate-reduction rates lead to reservoir effects whereby $SO_4^{2-}$ concentrations are drawn down, leading to the enrichment of the residual $SO_4^{2-}$ pool in $^{34}S$ (Gomes and Hurtgen, 2013; Gomes and Hurtgen, 2015). These reservoir effects are typically thought to develop at the basin-scale, where the restriction of water movements limits the re-supply of $SO_4^{2-}$, but similar reservoir effects may also develop at highly localized environments such as sulfate-reducing cells or microbial biofilms (Raven et al., 2016; Louca and Crowe, 2017). Pore-scale mass transfer limitations of microbially mediated reactions in organic-rich wetland soil are expected to be fairly common, because soil microorganisms preferentially reside in exterior parts of NOM fragments (Cleveland et al., 2004), which in wetland soils tend to be associated with the immobile region of the porous structure (Rezanezhad et al., 2016). If we consider that combination of the slow transfer of solutes into or out of the system of NOM fragments and a high specific rate of $SO_4^{2-}$ reduction (rate per cell) due to abundant organic matter (Canfield, 2001) results in the consumption of a relatively large fraction of the local $SO_4^{2-}$ reservoir, then newly-precipitating sulfide phases will have relatively high $\delta^{34}S$ values, and will display low isotopic fractionation, such as that in the exterior parts of NOM fragments at Smolotely (between 6.3 and 11.6‰). However, if sulfide minerals are formed in soil regions characterized by higher solute exchange (by advection) or lower organic matter content (slower specific rate of $SO_4^{2-}$ reduction), such as those in bulk soil at a depth $\geq$40 cm at site A (between 14.9 and 29.4‰), then the fractionation values will be higher because neither the $SO_4^{2-}$ or the $H_2S$ reservoirs have evolved to higher values because the fraction of the $SO_4^{2-}$ reservoir that has been consumed by microbial reduction is low at this location (Sim et al., 2011). It should be noted that the positive $\delta^{34}S$ signal in the soil layer at 40–70 cm depth in profile B was ascribed to isotopically selective mineralization of organic S. While the resulting isotopically light S was solubilized and lost (Alewell et al., 1999), the residual isotopically heavier organic S remained *in situ* (Novák et al., 1994; Mitchell et al., 2001). Regardless of which S isotope redistribution mechanism prevailed, the evidence of mineralization and microbial $SO_4^{2-}$ reduction in one soil profile reflected spatial inhomogeneities in the intensity of processes of isotope fractionation in wetland soil.

Microbial communities associated with sulfide-precipitating environments (NOM and surrounding anoxic soil) had variable compositions (Table S7); nevertheless, the dissimilative $SO_4^{2-}$ reduction was usually the main metabolic trait (Table 1). Sulfate reducers were significantly enriched in soils compared to sulfide-rich NOM fragments at both the Smolotely and Mokrsko wetlands (Drahota et al., 2017). Thus the NOM fragments mineralized by sulfide phases did not appear as the hot spots of $SO_4^{2-}$ reduction in soils. In contrast, they were substantially enriched by fermentative microorganisms compared to surrounding soils (Table 1). These findings are consistent with Falteisek et al. (2019), who reported formation of realgar and bonazziite in batch experiments characterized by a significant proportion of fermenters (up to 95%) and highly variable proportion of sulfate reducers (between 2% and 84%). Moreover, the fermenters in realgar-rich NOM fragments in the Mokrsko wetland soil were enriched with respect to nearby NOM fragments free of sulfides (Drahota et al., 2017). These findings strongly support the hypothesis that has arisen from the variable isotopic S fractionation associated with sulfide formation in bulk soil and NOM fragments, which indicates mass-transfer limitation on $SO_4^{2-}$ transport in the sulfide-rich exterior parts of NOM fragments. It seems that the slow diffusional transfer of solutes in combination with fast microbial reduction in the NOM exteriors resulted in the development of steep redox gradients at the mm scale. These highly localized environments are characterized by the high activity of fermenting microorganisms, producing evidence of highly reducing conditions in the NOM exteriors, in contrast to only slightly reduced conditions in bulk soil (Fig. 1). Highly reducing conditions are a prerequisite for As sulfide and Fe sulfide precipitation (O'Day et al., 2004) and these highly localized and reducing environments associated with NOM were evidently suitable for the precipitation of different sulfide phases in variable low-temperature environmental systems (Stanjek et al., 1994; Yoon et al., 2012; Langner et al., 2013; Stuckey et al., 2015; Drahota et al., 2017; Kerr et al., 2018). In contrast, pore water collected from bulk soil fell within the regions where aqueous As(III), As(V), and either the Fe(II,III) phases (shown as green rust) or the Fe(III) phases (shown as ferrihydrite) were the predominant species, based on pH and Eh measurements (Fig. S7). None of the pore water samples fell within the calculated stability fields where As sulfides or Fe sulfides are predicted to be predominant, but this is not surprising since the contribution of aqueous species from the highly reducing conditions of NOM to bulk pore water is negligible (Masue-Slowey et al., 2011; Rezanezhad et al., 2016; Drahota et al., 2017).

### 4.2. Sulfide mineral formation and arsenic sequestration in soil

Chemical analyses and selective extractions from the soil samples below ~40 cm showed that As and Fe(II) are coupled to S and TOC, and they substantially accumulated in the exterior parts of the NOM fragments (up to 19 wt.% As and 4.7 wt.% Fe). Microscale imaging and spectroscopy reveals that As speciation in these domains is a combination of $As_4S_4$ polymorphs, realgar, and bonazziite as well as arsenian Fe sulfides, primarily greigite, and framboidal pyrite. It should be noted that to date this is the first report published on the precipitation of bonazziite in a shallow subsurface environment at low temperatures. Bonazziite has recently been characterized and approved as a new mineral species (Bindi et al., 2015), and was currently been identified in an incubation experiment with microcosms isolated from the Mokrsko wetland (Falteisek et al., 2019).

The results demonstrate that greigite and pyrite were important Fe sulfidation products within the NOM exteriors. In all samples, pyrites are only present as sub-micron equidimensional and equimorphic crystals, often aggregated into framboids (Fig. 4). Although pyrite framboids have been shown to form abiotically at elevated temperatures (60–350 °C) (Sweeney and Kaplan, 1973; Graham and Ohmoto, 1994), no laboratory studies have yet generated framboids abiotically at lower temperatures (Ohfuji and Rickard, 2005). Recent work by MacLean et al. (2008) provides evidence for the formation of framboidal pyrite on organic templates within microbial biofilms. Many studies consider the formation of pyrite and greigite from Fe monosulfide minerals (e.g., mackinawite) (Benning et al., 2000; Rickard and Morse, 2005; Rickard and Luther, 2007). Pyrite forms via the reaction of Fe monosulfide with $H_2S$ or zerovalent sulfur (Rickard and Luther, 2007), while greigite forms by a solid-state transformation of mackinawite following partial oxidation of structural Fe(II) (Boursiquot et al., 2001). There is currently no experimental evidence demonstrating that greigite can precipitate directly from solution (Rickard and Luther, 2007). As such, the presence of greigite in the NOM exteriors examined here implicates the solid-state oxidative transformation of mackinawite as an important Fe sulfidation pathway.

Under reducing conditions, mackinawite is the first precipitate to form following reaction between dissolved $Fe^{2+}$ and $H_2S$ during the initial stages of Fe sulfide formation (Benning et al., 2000; Rickard and Morse, 2005; Rickard and Luther, 2007). Although mackinawite was not identified in our samples by mineralogical methods, its presence in the water-saturated zone of the soil is highly probable, as it is the precursor to pyrite and greigite. It appears that this assumption is supported by the increasing concentration of non-sulfate S (estimated by subtracting the sulfate-S from the total S) and HCl-extractable Fe(II) with increasing depth of soils (Fig. 1). However, the fraction of mackinawite in the water-saturated soils, whose maximum amounts can theoretically be linked to HCl-extractable Fe (II) (between 2.8% and 6.4% of the total Fe), is much lower than the fraction of oxalate-extractable Fe ($\bar{x} \pm \sigma$: $19 \pm 4\%$ and $29 \pm 3\%$ of total Fe at sites A and B, respectively; Table S3), which is a proxy for amorphous Fe(III) (oxyhydr)oxides (Schwertmann, 1964). The chemical prediction of poorly-crystalline Fe(III) (oxyhydr)oxides in the water-saturated zone of soils is in accordance with equilibrium modeling showing that almost all pore water samples fell within the calculated stability field of ferrihydrite (Fig. S7). As demonstrated by oxalate-extractable As, poorly-crystalline Fe(III) (oxyhydr)oxides in the water-saturated soils sequester a high fraction of As ($\bar{x} \pm \sigma$: $24 \pm 14\%$ and $50 \pm 14\%$ of total As at sites A and B, respectively; Table S3). These data demonstrate a much higher fraction of oxalate-extractable Fe and As in water-saturated soil at site B compared to site A. Higher amounts of As-bearing Fe (oxyhydr)oxides at site B are broadly consistent with the detection of intensive aerobic metabolism, which contributed to the positive $\delta^{34}S$ signal in this soil (Fig. 5). In view of the facts that the sorptive affinity of As(III) and As(V) for ferrihydrite is 3–6 orders of magnitude greater than mackinawite (Dixit and Hering, 2003; Wolthers et al., 2005; Couture et al., 2013), and that phosphate has no effect on the sorption of As species to mackinawite (Niazi and Burton, 2016), the high fraction of phosphate-extractable As below ~40 cm (9–13% and 11–17% of total As at sites A and B, respectively; Table S3), which often additionally increases with depth (Fig. 1), can be attributed to adsorption of As to poorly-crystalline Fe (oxyhydr)oxides. All of these facts imply an important role of poorly-crystalline Fe (oxyhydr)oxides in the sequestration of As, and possibly controlling As mobility in the oxic and even in the water-saturated zone of wetland soils. As transportation and laboratory conditions in our study were strictly anoxic, the occurrence of Fe oxyhydroxides and/or greigite in the soil samples are not an artifact of post-collection oxidation. This has been proven by similar results of As and Fe partitioning in water-saturated soil samples that (i) have been similarly prepared as mentioned in the methodology above (freeze-drying, storage, and preparation under Ar atmosphere), and (ii) have been immediately analyzed in both their fresh and wet form.

Yet there is scant evidence showing an association between As and greigite (Wilkin and Ford, 2006). In contrast, more conclusive data show the occurrence of As in pyrite, where it may be incorporated by adsorption (Farquhar et al., 2002) as well as by chemical substitution (Savage et al., 2000). The As content of the pyrite ($0.44 \pm 0.09$ wt.%) was within the range of values reported for low-temperature pyrite in both laboratory and field studies. For example, Lowers et al. (2007) examined authigenic pyrite in the Bengal Basin, and found the As content ranging up to 1.1 wt.% in framboidal pyrite, with an average concentration of 0.27 wt.%. Our results indicate that pyrite sequestered considerably less As than greigite ($1.69 \pm 0.47$ wt.%). Moreover, greigite also serves as a host for Ni ($0.17 \pm 0.13$ wt.%) and Co ($0.51 \pm 0.26$ wt.%); whereas these elements were often below the EDS detection limit (cca. 0.1 wt.%) in framboidal pyrite. The ability of biogenic mackinawite and greigite to efficiently trap Ni, Co, and many other trace elements has been previously documented by many studies (e.g., Morse and Arakaki, 1993; Huerta-Diaz et al., 1998; Farquhar et al., 2002; Ikogou et al., 2017). It should also be noted that sulfide phases may be slightly enriched in other trace elements (Cr, Cu, Mo, Sb, Se, V, U), because these elements were significantly accumulated in sulfide-rich NOM exteriors compared to the surrounding soil (Table S4), and generally tend to accumulate in Fe sulfides and disulfides (Kolker, 2012; Veeramani et al., 2013). Our findings suggest that Co and Ni as well as a portion of the As sequestered in greigite are mobilized during the greigite transformation to pyrite. It is also possible that the way in which trace elements are associated with greigite could impact the stability of greigite by slowing down (or inhibiting) its transformation to pyrite (Wilkin and Ford, 2006). Therefore, the *in situ* rates of greigite replacement by pyrite may need to be considered when predicting the long-term behavior of As and some trace metals in sulfidogenic environments.

The lower solubility of Fe monosulfide compared to As sulfides at circumneutral pH suggests that Fe monosulfide is

more likely to form than realgar, bonazziite, and orpiment in most naturally contaminated environments with elevated Fe(II) in solutions. Therefore, the availability of Fe(II) would generally allow Fe sulfide formation to limit $H_2S$ activity to levels below that necessary for saturation of As sulfides. If As sulfides form in these environments, their occurrence is likely restricted to zones with a relatively low Fe(II) concentration. The first *in situ* formation of realgar in low-temperatures environments was documented in a shallow aquifer sediment approx. 15 years ago (O'Day et al., 2004). Since that time, authigenic realgar formation has been evidenced in many sites and variable environmental systems such as peatland (Langner et al., 2012, 2013), wetland soil (Gao and Schulze, 2010; Drahota et al., 2013; Drahota et al., 2017) and lake sediment (Demergasso et al., 2007; Bentz and Peterson, 2017; Schuh et al., 2018); contaminated from natural or anthropogenic sources, as well as mine waste (Kerr et al., 2018). Reaction path modeling indicated that realgar precipitation is favored under strongly reducing and nearly neutral pH conditions, in which the $H_2S$ activity is buffered by the coexistence of Fe(II/III) (oxyhydr)oxides and Fe sulfides (O'Day et al., 2004; Root et al., 2009). Under such conditions, As(III) can be reduced by Fe monosulfides, leading to the formation of realgar and greigite, or alternatively green rust (Gallegos et al., 2008; Han et al., 2011; Root et al., 2013). In this model, it is expected that As sulfide formation is limited by the activity of dissolved As(III), and inhibited by excess $H_2S$ or low pH conditions that have been reported to favor either formation of soluble thioarsenite complexes or precipitation of orpiment (Bostick et al., 2005; Couture and Van Cappellen, 2011). This hypothesis is consistent with the co-association of greigite and both $As_4S_4$ polymorphs observed in the NOM exterior (Fig. 4d); however, assemblages of As sulfides and Fe sulfides or green rust in other sites have been lacking (O'Day et al., 2004; Langner et al., 2013; Drahota et al., 2017; Kerr et al., 2018). It should be noted that scant evidence of nanometer-sized Fe sulfides or green rust in natural soils or sediments may be explained by their nanocrystalline nature or very fast sulfide oxidation (Burton et al., 2009). Another proposed mechanism of realgar and bonazziite formation involves reduction of an amorphous orpiment precursor driven by $H_2S$ (Le Pape et al., 2017). Their hypothesis is mainly based on microcosm experiments showing an increase in the proportion of realgar compared to orpiment with incubation time (Lee et al., 2007; Rodriguez-Freire et al., 2015; Le Pape et al., 2017). In this model, one might expect the co-association of $As_4S_4$ polymorphs with older orpiment, at least in some samples; but orpiment was not detected in most sites (Demergasso et al., 2007; Langner et al., 2013; Bentz and Peterson, 2017; Drahota et al., 2017; Kerr et al., 2018; Schuh et al., 2018) including in the Smolotely wetland soil. All these findings suggest another mechanism of $As_4S_4$ precipitation, or alternatively enable more precipitation pathways. Formation of realgar and bonazziite in association with fermenting microorganisms in organic-rich soil domains suggests that reduction of As(III) may be due to reducing products of microbial fermentative metabolism (e.g., hydrogen, formate). Another mechanism of As(III) reduction that may be theoretically suggested includes respirative electron transfer to an extracellular acceptor. A number of extracellular electron transfer mechanisms using redox-active membrane proteins, conductive pili, and soluble electron shuttles (e.g., quinones, flavines, ferredoxins) have recently been documented (Lovley, 2012). The reductive potential of the electron shuttles is generally sufficient for realgar and bonazziite biogenesis, since it usually reaches values deeply below −300 mV in strict anaerobes including clostridia (Stams and Plugge, 2009), which were abundant in the $As_4S_4$-bearing NOM fragments.

### 4.3. Arsenic retention and reactivity

Arsenic, Fe, and S enrichment in NOM exteriors suggests supply through an aqueous source with precipitation on the NOM fragments. The Fe and As supply likely came from reductive dissolution of As-bearing Fe (oxyhydr)oxides and secondary arsenate phases (Drahota et al., 2018) as well as the weathering of primary silicate minerals (e.g., amphibole; Fig. S2). The reduction of Fe (oxyhydr) oxides as a major mechanism for As mobilization in the groundwater is consistent with proportion of dissolved Fe (II) ($20.0 \pm 3.4$ mg $L^{-1}$; $97.3 \pm 1.8\%$ of aqueous $Fe_{tot}$) and As(III) ($340 \pm 168$ µg $L^{-1}$; $76.2 \pm 14.7\%$ of aqueous $As_{tot}$) with respect to their total concentrations in the pore water (Table S5). This is further supported by distinct dissolution features of crystalline Fe (oxyhydr)oxides (Fig. 2c, d) surviving in very low amounts in the bottom of the soil profile. Although the authigenic As sulfides and arsenian Fe sulfide phases host appreciable As within the water-saturated zone of the soil (≤40 cm), and microbial reduction has been proposed as the prominent mobilization pathway for As and Fe in water-saturated soil, a substantial fraction of the As is hosted by poorly-crystalline Fe (oxyhydr)oxides. Moreover, it should be noted that poorly-crystalline Fe(III) (oxyhydr)oxides are more susceptible for reductive dissolution than crystalline Fe (oxyhydr)oxides (Larsen and Postma, 2001; Bonneville et al., 2004). These seemingly contradictory findings point to dynamic redox-cycling in the shallow wetland soils, which allow simultaneous (i) formation of Fe and As sulfide phases as a result of microbial $SO_4^{2-}$ reduction, (ii) microbial reduction of Fe(III) (oxyhydr)oxides, and (iii) precipitation of poorly-crystalline Fe(III) (oxyhydr)oxide in spatially close soil domains. Lateral variations in As and Fe speciation has been demonstrated between the examined soil profiles (i.e., variable amounts of oxalate-extractable Fe and As at sites A and B); but the spatial redox variability in the soil domains obviously occurs at significantly smaller scales (µm to cm), as has been suggested by the different proportions of the main metabolic traits of microbial communities in NOM exteriors and the surrounding soil (Table 1). A similar close proximity of reduced and oxidized Fe and As species has been directly observed in mining waste by Kerr et al. (2018), who found an intimate association of authigenic realgar with As(III) trioxide and Fe(III) (oxyhydr)oxides on the scale of a few tens of microns.

Realgar and bonazziite appear as the most efficient host sulfide phase for As scavenging since these phases contain approximately a two order greater concentration of As than Fe sulfides. The greigite and pyrite sequestered little As, containing on average 1.69 and 0.44 wt.%, respectively. Realgar and probably bonazziite also appear as the most efficient host phase for As scavenging since they are less sensitive to oxidative dissolution than Fe monosulfides and disulfides (Lenkge et al., 2009). At near-neutral pH and an $O_2$ partial pressure of ~0.2 atm, the half-life of authigenic realgar from the Gola di Lago wetland was 215 days, and a nearly complete oxidation was expected within 4–7 years (Langner et al., 2014). Under similar conditions, mackinawite was found to oxidize rapidly, with a half-life from 29 to 60 min (Di Toro et al., 1996; Burton et al., 2009). Greigite and pyrite are expected to be more stable at lower pH values in more oxygenated environments (Rickard and Luther, 2007). Recently, Moon et al. (2017) demonstrated that there was little correlation between the pH and the amount of oxidized greigite. They found that after 4 days, across a pH range of 3.5–6.5, 20–85% of greigite oxidized to Fe (oxyhydr)oxides and native S. Taken as a whole, short-term falls of the water table in a wetland soil will probably not cause oxidation of As sulfides, but can potentially cause an oxidation-induced loss of As from Fe monosulfides. While our findings imply that a relatively large fraction of As is sequestered by poorly-crystalline Fe (oxyhydr)oxides, the efficiency of pre-existing and freshly formed Fe (oxyhydr)oxides to sequester As can be limited, partly because of the reduced accessibility of Fe (oxyhydr)oxide surfaces for As in undisturbed soil, which may cause As solution concentrations to locally and temporarily rise above the common background levels.

Our results show that effective sequestration of As in sulfide phases in the wetland soil is limited by the small proportion and spotty distribution of environments suitable for As sulfidation (i.e., exterior parts of NOM fragments). These results further indicate that precipitation of As-bearing sulfides in complex and heterogeneous environments such as soils in the Smolotely or Mokrsko natural wetlands (Drahota et al., 2017) do not control dissolved As concentrations in pore waters, and thus have a relatively low potential for remediating As-bearing waters in natural wetland systems. This finding is in contrast with laboratory experiments, which have confirmed that As bioprecipitation as a sulfide mineral phase removes almost all dissolved As in anaerobic bioreactors (Rodriguez-Freire et al., 2015; Le Pape et al., 2017). We assume that lowering of the redox conditions in soil environments by the addition of labile organic matter and/or deceleration of groundwater flow (diffusion of solutes slow down) leads to more effective sequestration of As *via* formation of As sulfide phases.

## 5. CONCLUSIONS

We identified extensive precipitation of realgar, bonazziite, and arsenian Fe sulfides in a naturally As-enriched wetland soil. Arsenic released during weathering of the granodiorite bedrock leads to precipitation of secondary arsenate phases and As-bearing Fe (oxyhydr)oxides in the overlying oxic soils (Drahota et al., 2018). The As supply in the wetland soil results from reductive dissolution of the oxidized secondary As phases around the time of changes in the redox conditions of water-saturated soil due to water table fluctuations.

Microbiological and S isotope results indicate that sulfide phases were generated by *in situ* microbial reduction of oxidized forms of S in the deeper (≥40 cm), water-saturated soil. Sulfidation of As is mainly associated with buried NOM fragments at varying stages of decomposition. These NOM fragments were primarily characterized by macroscopic yellow accumulations in their exterior parts that were composed of realgar, bonazziite, and two minor and distinct mineral forms of arsenian Fe sulfides: greigite and framboidal pyrite. In the bulk soil, the sulfide phases were more diffusely and sporadically distributed, and were associated with As-bearing Fe(III) (oxyhydr)oxides displaying reductive dissolution textures and containing lower As concentrations when compared to the Fe (oxyhydr)oxides in the uppermost samples (≤40 cm). Microbiological and S isotope results indicate that buried NOM fragments in the wetland soil represents highly localized environments with mass-transfer limitations on solute transport, where microbial sulfidogenesis leads to $SO_4^{2-}$ depletion and an enrichment in isotopically heavy $SO_4^{2-}$, which in turn mutes the fractionation associated with sulfide formation. It should be noted that the buried NOM fragments are not the hotspots of $SO_4^{2-}$ reduction in the wetland soil, because they are depleted in $SO_4^{2-}$ reducers with respect to the surrounding bulk soil. Substantial enrichment of fermenting microorganisms in sulfide-rich NOM fragments strongly indicates development of highly localized strongly reducing conditions, which are suitable for the formation and long-term persistence of sulfide phases. This study demonstrated the intricate link between the geochemistry and hydrologic dynamics as well as the microbial community in wetland soils by providing a more sound understanding of As sulfidation processes, and may potentially lead the way for developing more effective remediation strategies in constructed wetlands.

## ACKNOWLEDGEMENTS

This study was supported by the Czech Science Foundation (GACR 16-09352S) and the Center for Geosphere Dynamics (UNCE/SCI/006). The contribution of T.M. was supported by the Czech Academy of Sciences, Institute of Analytical Chemistry (Institutional Research Plan no. RVO: 68081715). Part of the laboratory equipment for this study was purchased from the Operational Programme Prague - Competitiveness (Project CZ.2.16/3.1.00/21516). A number of colleagues helped with sample processing and analyses: Martin Štrba and František Veselovský (separation of heavy minerals); Věra Vonásková and Lenka Jílková (sample digestions and analyses); Lenka Vondrovicová (isotope analyses); Martin Racek (SEM, EMPA); František Laufek (interpretation of XRD data). We also wish to thank Peter Lemkin for editing the English manuscript.

## APPENDIX A. SUPPLEMENTARY MATERIAL

Supplementary data to this article can be found online at https://doi.org/10.1016/j.gca.2019.09.021.

## REFERENCES


Alewell C. and Gehre M. (1999) Patterns of stable S isotopes in a forested catchment as indicators for biological S turnover. *Biogeochemistry* **47**, 310–333.

Alewell C., Mitchell M. J., Likens G. E. and Krouse H. R. (1999) Sources of stream sulfate at the Hubbard Brook Experimental Forest: Long-term analyses using stable isotopes. *Biogeochemistry* **44**, 281–299.

Aronesty E. (2011) Command-line tools for processing biological sequencing data Available from: http://code.google.com/p/ea-utils, .

Battaglia-Brunet F., Crouzet C., Burnol A., Coulon S., Morin D. and Joulian C. (2012) Precipitation of arsenic sulphide from acidic water in a fixed-film bioreactor. *Water Res.* **46**, 3923–3933.

Bednar A. J., Garbarino J. R., Ranville J. F. and Wildeman T. R. (2002) Preserving the distributions of inorganic arsenic species in groundwater and acid mine drainage samples. *Environ. Sci. Technol.* **36**, 2213–2218.

Belzile N. and Lebel J. (1986) Capture of arsenic by pyrite in near-shore marine-sediments. *Chem. Geol.* **54**, 279–281.

Benning L. G., Wilkin R. T. and Barnes H. L. (2000) Reaction pathways in the Fe-S system below 100°C. *Chem. Geol.* **167**, 25–51.

Bentz J. L. and Peterson R. C. (2017) Realgar and hörnesite precipitation in an iron-poor, sulfate-rich mudflat, Laguna Chiar Khota, Bolivia. *Can. Mineral.* **55**, 1009–1025.

Bindi L., Pratesi G., Muniz-Miranda M., Zoppi M., Chelazzi L., Lepore G. O. and Menchetti S. (2015) From ancient pigments to modern optoelectronic applications of arsenic sulfides: bonazziite, the natural analogue of $\beta$-$As_4S_4$ from Khaidarkan deposit, Kyrgyzstan. *Mineral. Mag.* **79**, 121–131.

Bonneville S., Van Cappellen P. and Behrends T. (2004) Microbial reduction of iron(III) oxyhydroxides: effects of mineral solubility and availability. *Chem. Geol.* **212**, 255–268.

Bonazzi P., Menchetti S., Pratesi G., Muniz-Miranda M. and Sbrana G. (1996) Light-induced variations in realgar and $\beta$-$As_4S_4$: X-ray diffraction and Raman studies. *Am. Miner.* **81**, 874–880.

Bostick B. C., Fendorf S. and Brown G. E. (2005) In situ analysis of thioarsenite complexes in neutral to alkaline arsenic sulphide solutions. *Mineral. Mag.* **5**, 781–795.

Bourdoiseau J. A., Jeannin M., Sabot R., Rémazeilles C. and Refait Ph. (2008) Characterization of mackinawite by Raman spectroscopy: effects of crystallization, drying and oxidation. *Corrosion Sci.* **50**, 3247–3255.

Boursiquot S., Mullet M., Abdelmoula M., Genin J. M. and Ehrhardt J. J. (2001) The dry oxidation of tetragonal FeS, mackinawite. *Phys. Chem. Mineral.* **28**, 600–611.

Bradley A. S., Leavitt W. D., Schmidt M., Knoll A. H., Girguis P. R. and Johnston D. T. (2016) Patterns of sulfur isotope fractionation during microbial sulfate reduction. *Geobiology* **14**, 91–101.

Burton E. D., Bush R. T., Sullivan L. A., Hocking R. K., Johnston S. G., Fitzpatrick R. W., Raven M., McClure S. and Jang L. Y. (2009) Iron-monosulfide oxidation in natural sediments: Resolving microbially mediated S transformations using XANES, electron microscopy, and selective extractions. *Environ. Sci. Technol.* **43**, 3128–3134.

Burton E. D., Johnston S. G. and Bush R. T. (2011) Microbial sulfidogenesis in ferrihydrite-rich environments: effects on iron mineralogy and arsenic mobility. *Geochim. Cosmochim. Acta* **75**, 3072–3087.

Burton E. D., Johnston S. G. and Kocar B. D. (2014) Arsenic mobility during flooding of contaminated soil: the effect of microbial sulfate reduction. *Environ. Sci. Technol.* **48**, 13660–13667.

Canfield D. E. (2001) Isotope fractionation by natural populations of sulfate-reducing bacteria. *Geochim. Cosmochim. Acta* **65**, 1117–1124.

Caporaso J. G., Lauber C. L., Walters W. A., Berg-Lyons D., Huntley J., Fierer N., Owens S. M., Betley J., Fraser L., Bauer M., Gormley N., Gilbert J. A., Smith G. and Knight R. (2012) Ultra-high-throughput microbial community analysis on the Illumina HiSeq and MiSeq platforms (short communication). *ISME J.* **6**, 1621–1624.

Cleveland C. C., Neff J. C., Townsend A. R. and Hood E. (2004) Composition, dynamics, and fate of leached dissolved organic matter in terrestrial ecosystems: results from a decomposition experiment. *Ecosystems* **7**, 275–285.

Couture R. M. and Van Cappellen P. (2011) Reassessing the role of sulfur geochemistry on arsenic speciation in reducing environments. *J. Hazard. Mater.* **189**, 647–652.

Couture R. M., Rose J., Kumar N., Mitchell K., Wallschläger D. and Van Cappellen P. (2013) Sorption of arsenite, arsenate, and thioarsenates to iron oxides and iron sulfides: a kinetic and spectroscopic investigation. *Environ. Sci. Technol.* **47**, 5652–5659.

Demergasso C. S., Chong G., Escudero L., Mur J. J. P. and Alió C. P. (2007) Microbial precipitation of arsenic sulfides in Andean salt flats. *Geomicrobiol. J.* **24**, 111–123.

Di Toro D. M., Mahony J. D. and Gonzales A. M. (1996) Particle oxidation model of synthetic FeS and sediment acid-volatile sulfide. *Environ. Toxicol. Chem.* **15**, 2156–2167.

Dixit S. and Hering J. G. (2003) Comparison of arsenic(V) and arsenic(III) sorption onto iron oxide minerals: Implications for arsenic mobility. *Environ. Sci. Technol.* **37**, 4182–4189.

Douglass D. L., Shing C. and Wang G. (1992) The light-induced alteration of realgar to pararealgar. *Am. Miner.* **77**, 1266–1274.

Drahota P., Filippi M., Ettler V., Rohovec J., Mihaljevič M. and Šebek O. (2012) Natural attenuation of arsenic in soils near a highly contaminated historical mine waste dump. *Sci. Total Environ.* **414**, 546–555.

Drahota P., Falteisek L., Redlich A., Rohovec J., Matoušek T. and Čepička I. (2013) Microbial effect on the release and attenuation of arsenic in the shallow subsurface of a natural geochemical anomaly. *Environ. Pollut.* **180**, 84–91.

Drahota P., Grösslová Z. and Kindlová H. (2014) Selectivity assessment of an arsenic sequential extraction procedure for evaluating mobility in mine wastes. *Anal. Chim. Acta* **839**, 34–43.

Drahota P., Mikutta C., Falteisek L., Duchoslav V. and Klementová M. (2017) Biologically induced formation of realgar deposits in soil. *Geochim. Cosmochim. Acta* **218**, 237–256.

Drahota P., Kulakowski O., Culka A., Knappová M., Rohovec J., Veselovský F. and Racek M. (2018) Arsenic mineralogy of near-neutral soils and mining waste at the Smolotely-Líšnice historical gold district, Czech Republic. *Appl. Geochem.* **89**, 243–254.

Edgar R. C. (2013) UPARSE: Highly accurate OTU sequences from microbial amplicon reads. *Nat. Methods* **10**, 996–998.

Falteisek L., Duchoslav V. and Drahota P. (2019) Realgar (As4S4) bioprecipitation in microcosm fed by a natural groundwater and organic matter. *Environ. Sci. Pollut. Res.*. https://doi.org/10.1007/s11356-019-05237-4.

Farquhar M. L., Charnock J. M., Livens F. R. and Vaughan D. J. (2002) Mechanisms of arsenic uptake from aqueous solution by

interaction with goethite, lepidocrocite, mackinawite, and pyrite: an X-ray absorption spectroscopy study. *Environ. Sci. Technol.* **36**, 1157–1762.

Fendorf S. and Kocar B. D. (2009) *Biogeochemical processes controlling the fate and transport of arsenic: implications for South and Southeast AsiaAdvances in Agronomy*. Elsevier Academic Press Inc, San Diego, pp. 137–164.

Fuller R. D., Mitchell M. J., Krouse H. R., Wyskowski B. J. and Driscoll C. T. (1986) Stable sulfur isotope ratios as a tool for interpreting ecosystems sulfur dynamics. *Water Air Soil Pollut.* **28**, 163–171.

Gallegos T. J., Han Y. S. and Hayes K. F. (2008) Model predictions of realgar precipitation by reaction of As(III) with synthetic mackinawite. *Environ. Sci. Technol.* **42**, 9338–9343.

Gao X. and Schulze D. G. (2010) Chemical and mineralogical characterization of arsenic, lead, chromium, and cadmium in a metal-contaminated Histosol. *Geoderma* **156**, 278–286.

Gee G. W. and Bauder J. W. (1979) Particle-size analysis by hydrometer: a simplified method for routine textural analysis and a sensitivity test of measurement parameters. *Soil Sci. Soc. Am. J.* **43**, 1004–1007.

Gomes M. L. and Hurtgen M. T. (2013) Sulfur isotope systematics of a euxinic, low-sulfate lake. Evaluating the importance of the reservoir effect in modern and ancient oceans. *Geology* **41**, 663–666.

Gomes M. L. and Hurtgen M. T. (2015) Sulfur isotope fractionation in modern euxinic systems: implications for paleoenvironmentsl reconstructions of paired sulfate-sulfide isotope records. *Geochim. Cosmochim. Acta* **157**, 39–55.

Graham U. M. and Ohmoto H. (1994) Experimental study of formation mechanisms of hydrothermal pyrite. *Geochim. Cosmochim. Acta* **58**, 2187–2202.

Han Y. G., Jeong H. Y., Demond A. H. and Hayes K. F. (2011) X-ray absorption and photoelectron spectroscopic study of the association of As(III) with nanoparticulate FeS and FeS-coated sand. *Water Res.* **45**, 5727–5735.

Hoffmann M., Mikutta C. and Kretzschmar R. (2012) Bisulfide reaction with natural organic matter enhances arsenite sorption: insights from X-ray absorption spectroscopy. *Environ. Sci. Technol.* **46**, 11788–11797.

Huerta-Diaz M. A., Tessier A. and Carignan R. (1998) Geochemistry of trace metals associated with reduced sulfur in freshwater sediments. *Appl. Geochem.* **13**, 213–233.

Islam F. S., Gault A. G., Boothman C., Polya D. A., Charnock J. M., Chatterjee D. and Lloyd J. R. (2004) Role of metal-reducing bacteria in arsenic release from Bengal delta sediments. *Nature* **430**, 68–71.

Ikogou M., Ona-Nguema G., Juillot F., Le Pape P., Menguy N., Richeux N., Guigner J.-M., Noël V., Brest J., Baptiste B. and Morin G. (2017) Long-term sequestration of nickel in mackinawite formed by *Desulfovibrio capillatus* upon Fe(III)-citrate reduction in the presence of thiosulfate. *Appl. Geochem.* **80**, 143–154.

IUSS Working Group WRB (2006) *Guidelines for Soil Description*. FAO, Rome.

Johnson D. W. and Henderson G. S. (1979) Sulfate adsorption and sulfur fractions in a highly-weathered soil under a mixed deciduous forest. *Soil Sci.* **128**, 34–40.

Katoh K., Asimenos G. and Toh H. (2009) Multiple alignment of DNA sequences with MAFFT. *Methods Mol. Biol.* **537**, 39–64.

Keon N. E., Swartz C. H., Brabander D. J., Harvey C. and Hemond H. F. (2001) Validation of an arsenic sequential extraction method for evaluating mobility in sediments. *Environ. Sci. Technol.* **35**, 2778–2784.

Kerr G., Craw D., Trumm D. and Pope J. (2018) Authigenic realgar and gold in dynamic redox gradients developed on historic mine wastes, New Zealand. *Appl. Geochem.* **97**, 123–133.

Kirk M. F., Roden E. E., Crossey L. J., Brealey A. J. and Spilde M. N. (2010) Experimental analysis of arsenic precipitation during microbial sulfate and iron reduction in model aquifer sediment reactors. *Geochim. Cosmochim. Acta.* **74**, 2538–2555.

Kocar B. D., Borch T. and Fendorf S. (2010) Arsenic repartitioning during biogenic sulfidization and transformation of ferrihydrite. *Geochim. Cosmochim. Acta* **74**, 980–994.

Kolker A. (2012) Minor element distribution in iron disulfides in coal: a geochemical review. *Int. J. Coal. Geol.* **94**, 32–43.

Kostka J. E. and Luther G. W. (1994) Partitioning and speciation of solid phase iron in saltmarsh sediments. *Geochim. Cosmochim. Acta* **58**, 1701–1710.

La Force M. J., Hansel C. M. and Fendorf S. (2000) Arsenic speciation, seasonal transformations, and co-distribution with iron in a mine waste-influenced palustrine emergent wetland. *Environ. Sci. Technol.* **34**, 3937–3943.

Lafuente B., Downs R. T., Yang H. and Stone N. (2015) The power of databases: the RRUFF project. In *Highlights in Mineralogical Crystallography* (eds. D. Armbruster and R. M. Danisi). W. De Gruyter, Berlin, pp. 1–30.

Langner P., Mikutta C. and Kretzschmar R. (2012) Arsenic sequestration by organic sulphur in peat. *Nat. Geosci.* **5**, 66–73.

Langner P., Mikutta C. and Kretzschmar R. (2014) Oxidation of organosulfur-coordinated arsenic and realgar in peat: Implications for the fate of arsenic. *Environ. Sci. Technol.* **48**, 2281–2289.

Langner P., Mikutta C., Suess E., Marcus M. A. and Kretzschmar R. (2013) Spatial distribution and speciation of arsenic in peat studied with microfocused X-ray fluorescence spectrometry and X-ray absorption spectroscopy. *Environ. Sci. Technol.* **47**, 9706–9714.

Larsen O. and Postma D. (2001) Kinetics of redictive bulk dissolution of lepidocrocite, ferrihydrite and goethite. *Geochim. Cosmochim. Acta* **65**, 1367–1379.

Lee J. H., Kim M. G., Yoo B., Myung N. V., Maeng J., Lee T., Dohnalkova A. C., Fredrickson J. K., Sadowsky M. J. and Hur H. G. (2007) Biogenic formation of photoactive arsenic-sulfide nanotubes by *Shewanella* sp. strain HN-41. *Proc. Natl. Acad. Sci. U.S.A.* **104**, 20410–20415.

Lenkge M. F., Sanpawanitchakit C. and Tempel R. N. (2009) The oxidation and dissolution of arsenic-bearing sulfides. *Can. Mineral.* **47**, 593–613.

Le Pape P., Battaglia-Brunet F., Parmentier M., Joulian C., Gassaud C., Fernandez-Rojo L., Guigner J. M., Ikogou M., Stetten L., Olivi L., Casiot C. and Morin G. (2017) Complete removal of arsenic and zinc from heavily contaminated acid mine drainage *via* an indigenous SRB consortium. *J. Hazard. Mater.* **321**, 764–772.

Lizama A. K., Fletcher T. D. and Sun G. (2011) Removal processes for arsenic in constructed wetlands. *Chemosphere* **84**, 1032–1043.

Louca S. and Crowe S. A. (2017) Microscale reservoir effects on microbial sulfur isotope fractionation. *Geochim. Cosmochim. Acta* **203**, 117–139.

Lovley D. R. (2012) Electromicrobiology. *Annu. Rev. Microbiol.* **66**, 391–409.

Lowers H. A., Breit G. N., Foster A. L., Whitney J., Yount J., Uddin N. and Muneem A. (2007) Arsenic incorporation into authigenic pyrite, Bengal Basin sediment, Bangladesh. *Geochim. Cosmochim. Acta* **71**, 2699–2717.

MacLean L. C. W., Tyliszczak T., Gilbert P. U. P. A., Zhou D., Pray T. J., Onstott C. and Southam G. (2008) A high-resolution chemical and structural study of framboidal pyrite formed

within a low-temperature bacterial biofilm. *Geobiology* **6**, 471–480.

Masue-Slowey Y., Kocar B. D., Jofré S. A. B., Mayer K. U. and Fendorf S. (2011) Transport implications resulting from internal redistribution of arsenic and iron within constructed soil aggregates. *Environ. Sci. Technol.* **45**, 582–588.

Mitchell M. J., Mayer B., Bailey S. W., Hornbeck J. W., Alewell C., Driscoll C. T. and Likens G. E. (2001) Use of stable isotope ratios for evaluating sulfur sources and losses at the Hubbard Brook Experimental Forest. *Water Air Soil Pollut.* **130**, 75–86.

Mitsch W. J. and Gosselink J. G. (2007) *Wetlands*, fourth ed. John Wiley & Sons Inc, New York.

Moon E. M., Bush T. T., Gibbs D. H. M. and Mata J. P. (2017) Divergent Fe and S mineralization pathways during the oxidative transformation of greigite, $Fe_3S_4$. *Chem. Geol.* **468**, 42–48.

Morse J. W. and Arakaki T. (1993) Adsorption and coprecipitation of divalent metals with mackinawite (FeS). *Geochim. Cosmochim. Acta* **57**, 3635–3640.

Muniz-Miranda M., Sbrana G., Bonazzi P., Menchetti S. and Pratesi G. (1996) Spectroscopic investigation and normal mode analysis of $As_4S_4$ polymorphs. *Spectrochim. Acta A* **52**, 1391–1401.

Niazi N. K. and Burton E. D. (2016) Arsenic sorption to nanoparticulate mackinawite (FeS): an examination of phosphate competition. *Environ. Pollut.* **2018**, 111–117.

Nickson R. T., McArthur J. M., Ravenscroft P., Burgess W. G. and Ahmed K. M. (2000) Mechanism of arsenic release to groundwater, Bangladesh and West Bengal. *Appl. Geochem.* **15**, 403–413.

Novák M., Kirchner J. W., Fottová D., Přechová E., Jačková I., Krám P. and Hruška J. (2005) Isotopic evidence for processes of sulfur retention/release in 13 forested catchments spanning a strong pollution gradient (Czech Republic, central Europe). *Global Biogeochem. Cycles* **19**, GB4012. https://doi.org/10.1029/2004GB002396.

Novák M., Botrell S. H., Fottová D., Buzek F., Groscheová H. and Žák K. (1996) Sulfur isotope signals in forest soils of Central Europe along an air pollution gradient. *Environ. Sci. Technol.* **12**, 3473–3476.

Novák M., Wieder R. K. and Schell W. R. (1994) Sulfur during early diagenesis in Sphagnum peat: insights from $\delta^{34}S$ ratio profiles in $^{210}Pb$-dated peat cores. *Limnol. Oceanogr.* **39**, 1172–1185.

O'Day P. A., Vlassopoulos D., Root R. A. and Rivera N. A. (2004) The influence of sulphur and iron on dissolved arsenic concentrations in the shallow subsurface under changing redox conditions. *Proc. Natl. Acad. Sci. U.S.A.* **101**, 13703–13708.

Ohfuji H. and Rickard D. (2005) Experimental syntheses of framboids – a review. *Earth Sci. Rev.* **71**, 147–170.

Omoregie E. O., Couture R. M., Van Cappellen P., Corkhill C. L., Charnock J. M., Polya D. A., Vaughan D., Vanbroekhoven K. and Lloyd J. R. (2013) Arsenic bioremediation by biogenic iron oxides and sulfides. *Appl. Environ. Microbiol.* **79**, 4325–4335.

Paul C. J., Ford R. G. and Wilkin R. T. (2009) Assessing the selectivity of extractant solutions for recovering labile arsenic associated with iron (hydr)oxides and sulfides in sediments. *Geoderma* **152**, 137–144.

Poulton S. W., Krom M. D. and Raiswell R. (2004) A revised scheme for the reactivity of iron (oxyhydr)oxide minerals towards dissolved sulfide. *Geochim. Cosmochim. Acta* **68**, 3703–13415.

Raven M. R., Sessions A. L., Fischer W. W. and Adkins J. W. (2016) Sedimentary pyrite $\delta^{34}S$ differs from pore water sulfide in Santa Barbara Basin: proposed role of organic sulfur. *Geochim. Cosmochim. Acta* **203**, 120–134.

Rezanezhad F., Price J. S., Quinton W. L., Lennartz B., Milojevic T. and Van Cappelen P. (2016) Structure of peat soils and implications for water storage, flow and solute transport: a review update for geochemists. *Chem. Geol.* **429**, 75–84.

Rickard D. and Luther G. W. (2007) Chemistry of iron sulfides. *Chem. Rev.* **107**, 514–562.

Rickard D. and Morse J. W. (2005) Acid volatile sulfide (AVS). *Mar. Chem.* **97**, 141–197.

Rittle K. A., Drever J. I. and Colberg P. J. S. (1995) Precipitation of arsenic during bacterial sulphate reduction. *Geomicrobiol. J.* **13**, 1–11.

Rochette E. A., Bostick B. C., Li G. C. and Fendorf S. (2000) Kinetics of arsenate reduction by dissolved sulfide. *Environ. Sci. Technol.* **34**, 4714–4720.

Rodriguez-Freire L., Moore S. E., Sierra-Alvarez R., Root R. A., Chorover J. and Field J. A. (2015) Arsenic remediation by formation of arsenic sulfide minerals in a continuous anaerobic bioreactor. *Biotechnol. Bioeng.* **113**, 522–530.

Rodriguez-Freire L., Sierra-Alvarez R., Root R., Chorover J. and Field J. A. (2014) Biomineralization of arsenate to arsenic sulfides is greatly enhanced at mildly acidic conditions. *Water Res.* **66**, 242–253.

Roberts L. C., Hug S. J., Voegelin A., Dittmar J., Kretzschmar R., Wehrli B., Saha G. C., Badruzzaman A. B. M. and Ali M. A. (2011) Arsenic dynamics in porewater of an intermittently irrigated paddy field in Bangladesh. *Environ. Sci. Technol.* **45**, 971–976.

Root R. A., Fathordoobadi S., Alday F., Ela W. and Chorover J. (2013) Microscale speciation of arsenic and iron in ferric-based sorbents subjected to simulated landfill conditions. *Environ. Sci. Technol.* **47**, 12992–13000.

Root R. A., Vlassopoulos D., Rivera N. A., Rafferty M. T., Andrews C. and O'Day P. A. (2009) Speciation and natural attenuation of arsenic in a tidally influenced shallow aquifer. *Geochim. Cosmochim. Acta* **73**, 5528–5553.

Savage K. S., Tingle T. N., O'Day P. A., Waychunas G. A. and Bird D. K. (2000) Arsenic speciation in pyrite and secondary weathering phases, Mother Lode Gold District, Toulumne County, California. *Appl. Geochem.* **15**, 1219–1244.

Schloss P. D., Westcott S. L., Ryabin T., Hall J. R., Hartmann M., Hollister E. B., Lesniewski R. A., Oakley B. B., Parks D. H., Robinson C. J., Sahl J. W., Stres B., Thallinger G. G., Van Horn D. J. and Weber C. F. (2009) Introducing mothur: open-source, platform-independent, community-supported software for describing and comparing Microbial Communities. *Appl. Environ. Microbiol.* **75**, 7537–7541.

Schuh C. S., Jamieson H. E., Palmer M. J. and Martin A. J. (2018) Solid-phase speciation and post-depositional mobility of arsenic in lake sediments impacted by ore roasting at legacy gold mines in the Yellowknife area, Northwest Territories, Canada. *Appl. Geochem.* **91**, 208–220.

Schwertmann U. (1964) Differenzierung der eisenoxide des bodens durch extraktion mit ammoniumoxalat-lösung. *Z. Pflanzen. Bodenk.* **105**, 194–202.

Sim M. S., Bosak T. and Ono S. (2011) Large sulfur isotope fractionation does not require disproportionation. *Science* **333**, 74–77.

Smedley P. L. and Kinniburgh D. G. (2002) A review of the source, behaviour and distribution of arsenic in natural waters. *Appl. Geochem.* **17**, 517–568.

Stamatakis A. (2014) RAxML Version 8: a tool for phylogenetic analysis and post-analysis of large phylogenies. *Bioinformatics* **30**, 1312–1313.

Stams A. J. M. and Plugge C. M. (2009) Electron transfer in syntrophic communities of anaerobic bacteria and archaea. *Nat. Rev. Microbiol.* **7**, 568–577.

Stanjek H., Fassbinder J. W. E., Vali H., Wägele H. and Graf W. (1994) Evidence of biogenic greigite (ferromagnetic $Fe_3S_4$) in soil. *Eur. J. Soil Sci.* **45**, 97–103.

Stuckey J. W., Schaefer M. V., Kocar B. D., Dittmar J., Pacheco J. L., Benner S. G. and Fendorf S. (2015) Peat formation concentrates arsenic within sediment deposits of the Mekong delta. *Geochim. Cosmochim. Acta* **149**, 190–205.

Sweeney R. E. and Kaplan I. R. (1973) Pyrite framboid formation: laboratory synthesis and marine sediments. *Econ. Geol.* **68**, 618–634.

Vargas C., Quiroz W., Bravo M. and Neaman A. (2015) Stability of arsenic during soil treatment and storage. *J. Chil. Chem. Soc.* **60**, 3045–3048.

Veeramani H., Scheinost A. C., Monsegue N., Qafoku N. P., Kukkadapu R., Newville M., Lanzirotti A., Pruden A., Murayama M. and Hochella M. F. (2013) Abiotic reductive immobilization of U(VI) by biogenic mackinawite. *Environ. Sci. Technol.* **47**, 2361–2369.

Větrovský T. and Baldrian P. (2013) Analysis of soil fungal communities by amplicon pyrosequencing: current approaches to data analysis and the introduction of the pipeline SEED. *Biol. Fertil. Soils* **49**, 1027–1037.

Wallmann K., Hennies K., König I., Petersen W. and Knauth H. D. (1993) New procedure for determining reactive Fe(III) and Fe(II) minerals in sediments. *Limnol. Oceanogr.* **38**, 1803–1812.

Wang M., Chou I.-M., Lu W. and De Vivo B. (2015) Effects of $CH_4$ and $CO_2$ on the sulfidization of goethite and magnetite: an *in situ* Raman spectroscopic study in high-pressure capillary optical cells at room temperature. *Eur. J. Mineral.* **27**, 193–201.

Weber I., Böttger U., Pavlov S. G., Hübers H.-W., Hiesinger H. and Jessberger E. K. (2017) Laser alteration on iron sulfides under various environmental conditions. *J. Raman. Spectrosc.* **48**, 1509–1517.

Wilkin R. T. and Ford R. G. (2002) Use of hydrochloric acid for determining solid-phase arsenic partitioning in sulfidic sediments. *Environ. Sci. Technol.* **36**, 4921–4927.

Wilkin R. T. and Ford R. G. (2006) Arsenic solid-phase partitioning in reducing sediments of a contaminated wetland. *Chem. Geol.* **228**, 156–174.

Wolthers M., Charlet L., Van der Weijden C. H., Van der Linde P. R. and Rickard D. (2005) Arsenic mobility in the ambient sulfidic environment: sorption of arsenic(V) and arsenic(III) onto disordered mackinawite. *Geochim. Cosmochim. Acta* **69**, 3483–3492.

Yoon S. J., Yáñez C., Bruns M. A., Martínez-Villegas N. and Martínez C. E. (2012) Natural zinc enrichment in peatlands: biogeochemistry of ZnS formation. *Geochim. Cosmochim. Acta* **84**, 165–176.

Zachariáš J., Žák K., Pudilová M. and Snee L. W. (2013) Multiple fluid sources/pathways and severe thermal gradients during formation of the Jílové orogenic gold deposits, Bohemian Massif, Czech Republic. *Ore Geol. Rev.* **54**, 81–109.

Zhang S. Y., Williams P. N., Luo J. and Zhu Y. G. (2017) Microbial mediated arsenic biotransformation in wetlands. *Front. Environ. Sci. Eng.* **11**, 1–11.

*Associate editor:* Dominik Weiss

# III.

**Peřestá M.**, Drahota P., Culka A., Matoušek T., Mihaljevič M. (2022) Impact of organic matter on As sulfidation in wetlands: An in situ experiment. *Science of the Total Environment* **819**, 152008.

Science of the Total Environment 819 (2022) 152008

Contents lists available at ScienceDirect

Science of the Total Environment

journal homepage: www.elsevier.com/locate/scitotenv

# Impact of organic matter on As sulfidation in wetlands: An *in situ* experiment

Magdaléna Peřestá [a], Petr Drahota [a,*], Adam Culka [a], Tomáš Matoušek [b], Martin Mihaljevič [a]

[a] Institute of Geochemistry, Mineralogy and Mineral Resources, Faculty of Science, Charles University, Albertov 6, 128 43 Prague 2, Czech Republic
[b] Institute of Analytical Chemistry, Czech Academy of Sciences, Veveří 97, 602 00 Brno, Czech Republic

## HIGHLIGHTS

- *In situ* incubation of organic matter in As-enriched wetland soils over 15 months.
- As and Fe were observed to precipitate as biogenic sulfides.
- Realgar and bonazziite were observed as the main As-bearing sulfides.
- Reduced exchange of solutes caused oversaturation with respect to AsS minerals.

## GRAPHICAL ABSTRACT

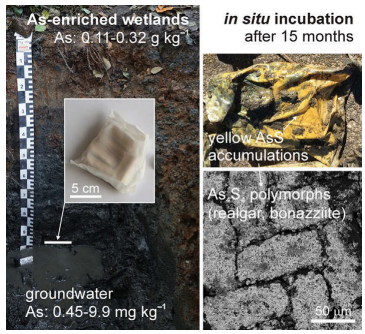


## ARTICLE INFO

*Article history:*
Received 27 September 2021
Received in revised form 17 November 2021
Accepted 23 November 2021
Available online 28 November 2021

Editor: Filip M.G. Tack

*Keywords:*
Arsenic
Organic matter
As sulfide
Fe(II) sulfide
*In situ* biomineralization
Bioremediation

## ABSTRACT

Arsenic incorporation into newly formed As sulfides has recently been identified as an important As sequestration pathway in both laboratory experiments and natural As-wetlands. Here, we used an *in situ* experimental technique with double nylon experimental bags (10-µm mesh) to study the effect of low-cost organic materials (sawdust, wood cubes and hemp shives) on As sulfidation in three naturally As-enriched wetland soils under water-saturated (~1 m depth) and neutral pH conditions. After 15 months of *in situ* incubation, all of the organic materials and their corresponding inner bags were covered by yellow-black mineral accumulations, dominantly composed of crystalline $As_4S_4$ polymorphs (realgar and bonazziite) and reactive Fe(II) sulfides (probably mackinawite); while the major fraction of As (~80%) was sequestered as AsS minerals. The amount of As accumulation in the experimental bags varied significantly (0.03–4.24 g As kg$^{-1}$) and corresponded with different levels of As (0.23–9.4 mg As L$^{-1}$) in the groundwater. Our findings suggest an authigenic formation of AsS minerals in strongly reducing conditions of experimental bags by a combination of reduced exchange of solutes through the pores of the bag and comparatively fast microbial production of dissolved sulfide. Arsenic sulfide formation, as an effective treatment mechanism for natural and human-constructed wetlands, appears to be favored for As(III)-rich waters with a low Fe(II)/As(III) molar ratio. These conditions prevent the consumption of dissolved As and sulfide by their preferential incorporation into natural organic matter, and newly-formed Fe(II) sulfides, respectively.

## 1. Introduction

A high concentration of As in groundwater is widely acknowledged as an environmental concern, due to its widespread occurrence and threat to human health (Smedley and Kinniburgh, 2002; Nordstrom, 2002). The mobility of As is closely linked to its speciation, involving both arsenate (As

* Corresponding author.
*E-mail address:* petr.drahota@natur.cuni.cz (P. Drahota).

http://dx.doi.org/10.1016/j.scitotenv.2021.152008

(V)) and the more mobile (and notably more toxic) arsenite (As(III)) species. Under well-aerated (oxic) conditions, As(V) oxyanions are dominant and tend to be sequestered by metal (oxyhydr)oxides, especially by Fe(III) (oxyhydr)oxides. Under reducing conditions, soluble arsenic mostly occurs as As(III) (*e.g.*, arsenious acid), and its high concentration in groundwater is generally acknowledged to be caused by the combination of (i) the microbial dissolution of As-bearing Fe(III) (oxyhydr)oxides, (ii) the microbial reduction of As(V) to As(III), and (iii) a lower sorption affinity of mineral surfaces for As(III) with the pH of most natural waters (Nickson et al., 2000; Dixit and Hering, 2003; Islam et al., 2004). Arsenic concentrations under reducing conditions of groundwater can be increased or lowered by microbial sulfidogenesis (Kirk et al., 2004; Eberle et al., 2021), which strongly affects As geochemistry through a variety of processes. Under sulfate-reducing conditions, the soluble As(III) may either be sequestered by co-precipitation with or adsorption on Fe sulfides such as pyrite ($FeS_2$), mackinawite (FeS), and greigite ($Fe_3S_4$) (Belzile and Lebel, 1986; Wilkin and Ford, 2006; Lowers et al., 2007; Kirk et al., 2010; Burton et al., 2014), precipitated as As-sulfides such as orpiment ($As_2S_3$), realgar ($\alpha$-$As_4S_4$) and bonazziite ($\beta$-$As_4S_4$) (Rittle et al., 1995; O'Day et al., 2004; Langner et al., 2012; Drahota et al., 2017; Kerr et al., 2018; Falteisek et al., 2020; Kumar et al., 2020), or bound *via* sulfhydryl groups to organic matter (Langner et al., 2012; Hoffmann et al., 2012; Couture et al., 2013). On the other hand, reduced S can reduce both Fe(III) and As(V), which then drives As release into the aqueous phase (Rochette et al., 2000; Poulton et al., 2004), or can play a key role in keeping As dissolved in the groundwater by the formation of the highly mobile thioarsenic species (Besold et al., 2018; Eberle et al., 2020, 2021).

A number of recent studies have proposed that precipitation of As-sulfides can lead to massive As removal (up to ~100%) from solution under a wide range of pH (3–8) (Newman et al., 1997; Demergasso et al., 2007; Ledbetter et al., 2007; Lee et al., 2007; Battaglia-Brunet et al., 2012; Rodriguez-Freire et al., 2014, 2016; Le Pape et al., 2017; Falteisek et al., 2019), suggesting a potentially effective As remediation pathway for anaerobic subsurface environments (Alam and McPhedran, 2019). Rittle et al. (1995) presented the first evidence that As-sulfides can be products of microbial sulfate reduction, and subsequently this piece of information has become the focus of research using microorganisms, instead of chemicals, to precipitate As from groundwater, and as a suitable option for low-cost and effective As treatment. For instance, Le Pape et al. (2017) incubated acid mine drainage water with the indigenous microbial consortium, for 94 days under anoxic conditions, and documented the total removal of dissolved As (67 mg $L^{-1}$) from solution in two of the triplicate batch experiments. The arsenic precipitated as realgar ($\leq$34%) and amorphous orpiment (33–73%). Similarly, Rodriguez-Freire et al. (2016) observed 91% As removal from slightly acidic contaminated water (~75 mg As/L) as a mixture of realgar and orpiment in a continuous anaerobic bioreactor. The bioreactors were inoculated with an anaerobic mixed culture, obtained from a full-scale bioreactor treating beer brewery wastewater.

Because most bioremediation studies performed under sulfate-reducing conditions were conducted in laboratory batch and column experiments (Alam and McPhedran, 2019), in this study we focused on naturally As-enriched wetlands, resembling systems of artificially constructed anaerobic wetlands, characterized by sulfate-reducing processes utilizing a passive bioremediation approach. We used a double bag technique (10 μm mesh) to simulate long-term (15 months) interaction of low-cost organic materials with indigenous sulfate-reducing microorganisms of three wetland soils with naturally elevated As levels. The objective of this study was to determine the effect of organic matter incubation on As sulfidation in a natural wetland system. The specific aims were to (i) quantitatively assess the *in situ* accumulation of As in three low-cost artificial organic materials incubated in three different natural geochemical subsurface systems, and (ii) characterize the major mechanisms of As sequestration. We took advantage of well-documented wetland sites in the Czech Republic, which serve as effective sinks for As under reducing conditions due to the formation two As sulfide polymorphs and arsenian iron sulfides (Drahota et al., 2017; Knappová et al., 2019).

## 2. Materials and methods

### 2.1. Experimental setup

We used a modified experimental bag technique (Mihaljevič et al., 2010; Ettler et al., 2012) for *in situ* incubation of (i) hemp shives, (ii) sawdust, and (iii) wooden cubes (5 × 1 × 1 cm) in the wetland soils. The sawdust and the cubes were made from partly decomposed alder trees (*Alnus* sp.), which has been documented as a suitable carbon source for microbial processes (Highley, 1995). Each of the types of organic matter (5 ± 0.005 g or 5 pieces of the wood cubes) were inserted into double experimental nylon bags (Sefar AG NITEX, Switzerland; 10 μm mesh opening; 6 × 6 cm inner bag; 8 × 8 cm outer bag), and the bags were sealed by welding. Chemical characterizations of each of these organic materials is given in Table S1.

### 2.2. Field sites and sampling

The *in situ* incubations were examined from three wetland sites with naturally elevated levels of As in the central part of the Czech Republic (Fig. S1). Sites M1 (49°44′43″N, 14°20′01″E) and M2 (49°44′10″N, 14°20′06″E) were located on the banks of a small creek at the Mokrsko geochemical anomaly (Drahota et al., 2017). Experimental site S3 (49°37′31″N, 14°09′32″E) was situated nearby an abandoned mining site located nearby the village of Smolotely (Fig. S1). Natural weathering and erosion of the arsenopyrite-bearing Au mineralization in the bedrock has caused an enrichment of As in soils ($\geq$0.2 g $kg^{-1}$) on an area of approx. 1 $km^2$ at Mokrsko and more than 3 $km^2$ at Smolotely (Drahota et al., 2009; 2018). Mineralogical and speciation analyses of As in wetland soils revealed that As was mainly present as realgar at Mokrsko (Drahota et al., 2017) or $As_4S_4$ polymorphs and arsenian Fe sulfides at Smolotely (Knappová et al., 2019). Our previous studies showed that these authigenic sulfides accumulated to a considerable extent (up to millimeter-scale deposits) in the exterior parts of the particulate organic matter, implying a key role of the particulate organic matter in As sulfidation.

Approximately one meter deep soil pits were excavated at each site and the bottom soil was sampled for geochemical and mineralogical characterization. The soils were collected using a non-steel trowel, immediately placed in Ar-purged zip-lock plastic bags, and stored at 4 °C under an inert atmosphere. The experimental bags, with different types of natural organic matter, each in three replicates, were alternately inserted at a depth of 1 m (Fig. S2), and introduced ~10 cm from the soil pit front, in order to minimize the disturbance of the overlying soil structure. Subsequently, the soil pits were filled with excavated soil matrix. After 15 months, the bags were collected and immediately placed in Ar-purged zip-lock plastic bags, and then stored at 4 °C under an inert atmosphere until their transport to the laboratory. The external nylon bag, containing traces of the soil matrix was discarded, and the internal bags (IB) with the natural organic materials (NOM) were freeze-dried and kept in anoxic conditions until their separate analyses. Groundwater samples were repeatedly collected ($n$ = 4) using tension lysimeters (SPE 20 with a double 0.2 μm nylon membrane) that were installed at a depth of 1 m, approximately 50 cm from the soil pits (Fig. S2). The lysimeters were allowed to equilibrate with the groundwater for 2 months before the first sampling.

### 2.3. Solid-phase characterization

Fresh soil samples were used for measurements of pH, Eh, and color determination using a Munsell soil color chart. The soil pH and Eh were measured in degassed, deionized water suspensions (1:2.5; *w/v*) after 1 h of agitation, using a calibrated pH electrode, Pt electrode, and WTW multimeter. The particle size distribution was determined by the hydrometer method. An aliquot sample, used for geochemical and mineralogical characterization, was freeze-dried, sieved (<2 mm), and milled to analytical fineness and then stored in anoxic conditions. Homogenized soil samples were

analyzed for total element concentrations by energy-dispersive X-ray fluorescence (XRF) spectrometry (ARL 9400 $XP^+$, Thermo ARL).

Near-total chemical composition of the solid materials were determined in three (soil, NOM) or two (IB) replicates by Lefort *aqua regia* digestion (3:1, $HNO_3$:HCl) on a hot plate. The digests were then analyzed by inductively coupled plasma optical emission spectrometry (ICP-OES; Agilent 5100) or by quadrupole-based inductively coupled plasma mass spectrometry (ICP-MS; Thermo Scientific Xseries$^{II}$). The accuracy of the analytical determinations were checked by triplicate measurements of NIST 2710a (Montana I soil - Highly Elevated Trace Element Concentrations) and NIST 2711 (Montana II soil - Moderately Elevated Trace Element Concentrations) standard reference materials; and were found to be ≤5% of the relative standard deviation (RSD) for As, and ≤12% for Fe (Table S2). Total C, N, S, and inorganic carbon (TIC) were determined in triplicate (soil, IB) or duplicate (NOM) using elemental analyzers (Thermo Flash 2000, Eltra SC 500, and CS-530). Total organic carbon (TOC) was determined by subtracting the TIC from the total amount of C present.

Three single chemical extraction procedures were carried out immediately after the freeze-drying of each of the solid materials (IB, NOM, and soil). Readily soluble As was determined by extracting samples in deoxygenated 0.05 mM $(NH_4)_2SO_4$ for 4 h (Wenzel et al., 2001), and exchangeable As was determined by extracting samples in deoxygenated 0.1 M $NaH_2PO_4$ buffered to pH 5.5 for 16 h (Keon et al., 2001). Arsenic bound to poorly crystalline Fe (oxyhydr)oxides was targeted with an extract of 0.2 M $NH_4$-oxalate (2 h in dark) (Keon et al., 2001). All extractions were conducted in triplicate (soil, NOM) or duplicate (IB). After centrifugation and filtration (0.2-μm nylon pore filter), all extracts were analyzed using ICP-OES or ICP-MS. Tests of the phosphate and oxalate solutions on nanocrystalline orpiment (synthetic $As_2S_3$; 99.9%, Alfa Aesar) and well-crystalized realgar (Mineralogical Museum of Faculty of Sciences, Charles University, Prague) revealed the utility of phosphate and oxalate for differentiating As associated with poorly crystalline Fe (oxyhydr)oxides and As sulfides. The extractions recovered <0.33% of the As from the sulfide phases, in accord with the results of Paul et al. (2009).

The mineralogical investigations of the soil and incubated materials (IB and NOM) were assessed by powder X-ray diffraction (XRD), scanning electron microscopy with an attached energy dispersive X-ray spectrometer (SEM-EDS), and analysis by Raman micro-spectroscopy (RMS). X-ray diffractograms were collected on a PANalytical X'Pert Pro diffractometer (conditions: Cu Kα radiation, 40 kV and 30 mV, 2$\theta$ range 5 to 70° or 80°, step 0.02° and 400 s (IB), (or step 0.01° and 350 s (soils)) using an X'Celerator detector). The surface of the NOM and the IB were examined by a TESCAN VEGA scanning electron microscopy equipped with an Oxford Link X-Max 50 EDS. The elemental composition of mineral phases in the NOM (prepared as polished sections) were determined using a JEOL JXA8530F electron probe microanalyser (EPMA) equipped with a field emission gun source for SEM imaging and EDS analysis (JEOL JED-2300F spectrometer). The operating conditions were 15 kV, with a beam current of 1.5 nA and 20 nA for EDS and EMPA quantitative analysis, respectively. RMS analyses of the mineral phases were performed using a Renishaw InVia Reflex Raman spectrometer coupled with a Leica microscope using a 50× objective. Excitation was either provided by the 514.5 nm or 785 nm line of a diode laser for the non-sulfide and sulfide phases, respectively. The spectrum of each mineral was recorded at 0.1–5% laser power to avoid thermal degradation over the spectral range of 100–900 $cm^{-1}$.

### 2.4. Groundwater analyses

Groundwater samples were immediately analyzed in the field for temperature, Eh, pH, dissolved $S^{2-}$, Fe(II), and total Fe using a portable WTW multimeter and DR3900 spectrophotometer (Hach Lange). Dissolved sulfides were analyzed by the methylene blue method (Hach method 8131), and Fe(II) concentrations were determined using the Hach 1,10-phenanthroline method. Total Fe was determined by the same method, following pre-reduction of dissolved Fe(III) by ascorbic acid. Samples for major cation and trace element analyses were acidified with $HNO_3$ (suprapure, Merck); a sample aliquot for aqueous As speciation analysis was preserved by adding 0.1 M EDTA-$Na_2$ solution to a concentration of 1 mM (Bednar et al., 2002). The major and minor cations as well as trace elements were determined using ICP-OES and ICP-MS. The major anions were determined using a Dionex ICS-2000 ion chromatography system. Bicarbonate was calculated from the alkalinity, and measured by microtitration (Schott TitroLine Easy automatic titrator) with 0.05 M HCl. The analyses of aqueous arsenite and arsenate were performed by anion exchange HPLC-ICP-MS (Agilent 1200 Series HPLC isocratic pump, and Agilent 7700× mass spectrometer). Recovery of the sums of As(III) and As(V) in the groundwater, compared to total As content, determined by ICP-OES, were 89–102%.

## 3. Results and discussion

### 3.1. Characteristics of wetland sites

The Eh and pH values were relatively similar, indicating the soil conditions moderately reducing (Eh between −38 and 8 mV) and near neutral (pH: 6.39 to 6.67) at all of the studied sites. The soils (classified as Dystric Gleysols) were characterized by different concentrations of As (110–3320 mg $kg^{-1}$), Fe, S, and TOC (Table 1). The highest concentrations of As, S, and TOC were detected in the M1; the lowest concentrations of these elements were documented in the S3. Concentrations of Fe displayed the exact opposite trend for As, S, and TOC, with the highest content in the S3, and the lowest in the M1. Concentrations of potentially hazardous metals (Co, Cu, Ni, Pb, Zn) were always low (≤40 mg $kg^{-1}$) (Table S3).

The soil samples were mainly composed of quartz, plagioclase, amphibole, and phyllosilicate minerals (chlorite, illite, and/or muscovite). XRD detected realgar in the M1 soil (Fig. S3), which is in accordance with the frequent visual detection of yellow sulfide accumulations in this soil, composed primarily of authigenic realgar (Drahota et al., 2017). Sporadic yellow accumulations of AsS phases were also detected in the S3 soil, but no sulfide minerals were detected in the soils using XRD (Fig. S3), indicating the abundance of AsS phases below the detection limit of the XRD (*ca.* 0.1 wt% for crystalline compounds). No sulfide minerals were identified in the M2 soil using XRD nor visually. These findings are in accordance with the oxalate extraction results, indicating that a high As fraction (~30% of the total As) in the M2 and S3 soil samples is bound to the poorly-crystalline Fe(III) (oxyhydr)oxides; in contrast, this fraction is low (7% of the total As) in the realgar-rich M1 sample (Table S4).

All groundwater samples were near-neutral and suboxic, with similar $SO_4^{2-}$ (80–159 mg $L^{-1}$) concentrations between the sites; but with different As (0.36–10.1 mg $L^{-1}$) and Fe (1.7–27.8 mg $L^{-1}$) concentrations (Table 1). Corresponding with the bulk soil contents, high As levels in the groundwater were accompanied by low Fe concentrations (M1 site), and *vice versa* (S site), documenting the variable Fe/As molar ratios between the sites: ~0.5

**Table 1**
Composition of soil and groundwater in the wetlands.

| | | M1 | M2 | S3 |
|---|---|---|---|---|
| Soil | As | 3.32 | 0.46 | 0.11 |
| (g $kg^{-1}$) | Fe | 13.0 | 17.3 | 38.2 |
| | S | 2.87 | 1.10 | 0.51 |
| | TOC | 69.6 | 12.4 | 4.86 |
| Groundwater | Eh [mV] | 136 ± 8 | 171 ± 5 | 135 ± 6 |
| $n$ = 4 (mg $L^{-1}$) | pH | 7.14 ± 0.1 | 7.05 ± 0.1 | 7.03 ± 0.1 |
| | $As_{tot}$[a] | 9.86 ± 0.1 | 1.00 ± 0.1 | 0.45 ± 0.2 |
| | $Fe_{tot}$[a] | 3.3 ± 0.9 | 7.18 ± 0.5 | 20.5 ± 4 |
| | Ca | 66.6 ± 0.6 | 74.9 ± 2 | 53.5 ± 3 |
| | Na | 32.8 ± 14 | 23.1 ± 1 | 15.0 ± 0.5 |
| | Mg | 10.2 ± 0.2 | 17.3 ± 0.3 | 17.7 ± 1 |
| | Mn | 2.2 ± 0.0 | 0.27 ± 0.01 | 3.0 ± 0.2 |
| | Cl | 25.1 ± 1 | 52.3 ± 5 | 11.5 ± 3 |
| | $HCO_3$ | 122 ± 42 | 194 ± 4 | 137 ± 20 |
| | $SO_4$ | 136 ± 10 | 84.8 ± 5 | 135 ± 14 |
| | $S^{2-}$ | 0.08 ± 0.00 | 0.03 ± 0.00 | 0.05 ± 0.00 |

[a] As and Fe predominate in their reduced forms ($As^{III}$ > 72%, $Fe^{II}$ > 95%).

in M1, ~10 in M2, and ~50 in S3. Arsenic and Fe occurred predominantly in their reducing forms (As(III) > 72%; Fe(II) > 95%), while the reducing form of S (aqueous sulfide) only occurred in a negligible fraction of the total S (<0.2%) (Table S5).

### 3.2. Chemical characteristics of incubated materials

All experimental bags collected from the soil after 15 months of incubation were covered by newly-formed yellow and black precipitates (Fig. 1), which occurred on all inner bags and locally on the surface of the NOM. During freeze-drying, the black precipitates changed to a rusty brown color (Fig. S4), indicating oxidation of the highly-reactive initial black phases to Fe(III) (oxyhydr)oxides. The yellow deposits remained intact throughout the processing of the samples.

Chemical analyses of both the NOM and IB showed that the deposits are composed of variable amounts of As, Fe, and S (Fig. 2), which chemically corresponded to the natural accumulations of authigenic As and Fe sulfides associated with NOM fragments previously documented in the wetland soils in this study (Drahota et al., 2017; Knappová et al., 2019) as well as in different mine environments (Kerr et al., 2018; Falteisek et al., 2020). Arsenic concentrations in the NOM and IB ranged from 30 mg $kg^{-1}$ in the S3 site to 4320 mg $kg^{-1}$ in the M1 site (Table S6). While the As accumulation in the NOM and IB corresponded with the different levels of As in the wetlands (M1 > M2 > S3), Fe accumulation in the incubated materials (Fig. 2) did not follow the increasing Fe levels from M1 to S3 wetlands (Table 1). In addition to these elements, Al also displayed a high content in the incubated materials (up to 2700 mg $kg^{-1}$); its accumulation was ascribed to allogenic clay minerals that were transported from the surrounding soil *via* the groundwater. The trace metals exhibited negligible or no accumulations (IB: ≤7.0 mg Cu $kg^{-1}$, ≤2.7 mg Pb $kg^{-1}$, and ≤14.5 mg Zn $kg^{-1}$).

The chemical compositions of the incubated materials indicated some trends (Fig. 2). Accumulations of As, Fe, and S were usually higher in the IB (up to 40× for As, 6× for Fe, and 22× for S) than in the corresponding NOM; with the exception of Fe and S levels in the sawdust incubation in the M2 and S3 sites, which displayed slightly higher values in the NOM (≤1.7×). The highest accumulations of As, Fe, and S in the NOM were always documented in the sawdust, while the lowest As and Fe increments were frequently found in the wood cubes (Table S6). Given the fact that the sawdust and wood cubes were prepared from the same material (*Alnus* sp.), the accumulation efficiency for As, Fe, and S is not primarily influenced by the NOM type, but rather is linked to morphological properties of the NOM such as specific surface area and porosity. Interestingly, the chemical compositions with the IB showed almost the opposite trend for As, with the lowest As concentrations in the sawdust (Fig. 2b). The highest concentrations of Fe and S were detected in the IB with the shives.


**Fig. 1.** Experimental double bags with NOM (hemp shives, wooden cubes, sawdust) after their incubation in the Mokrsko (M1) wetland. Note the characteristic yellow (AsS phases) and black (FeS phases) precipitates formed on the inner bag and on the surface of the NOM.

### 3.3. Mineralogy of incubated materials

Identification of the mineral phases in the As-Fe-S deposits using XRD analysis was hindered by high background levels caused by cellulose (NOM) and nylon (IB). The high backgrounds masked all diffraction peaks in the NOM (spectra not shown), and enabled identification of realgar and bonazziite as the major authigenic crystalline phases of the As-Fe-S deposits on the IB from the M1 and M2 sites (Fig. S5). Quartz, kaolinite, and muscovite/illite in the XRD patterns probably represent an allochtonous admixture from the surrounding soils. Occurrence of clay minerals corresponded with relatively high Al contents in the IB (Table S6).

Examination of the As-Fe-S deposits using SEM-EDS, EMPA, and RMS revealed that the mineralogical composition was similar across all samples and study sites. The deposits were composed of nearly stoichiometric As-S phases; with Fe (oxyhydr)oxides, and pure sulfur in different proportions. The yellow deposits were dominated by AsS phases, which were identified as realgar or bonazziite (Figs. 3, and 4a, b). The AsS polymorphs primarily occurred as massive aggregates of skeletal crystals (Figs. 3b, d, and S6a); suggesting their rapid formation from highly saturated conditions. Arsenic sulfides also created filamentous aggregates (Fig. S6b) that have commonly been documented in laboratory experiments (Lee et al., 2007; Le Pape et al., 2017) as well as in field sites (Knappová et al., 2019; Falteisek et al., 2020). The oxidized rusty brown precipitates that formed from initial black coatings during freeze-drying (*cf.* Figs. 1 and S4), were dominated by Fe (oxyhydr)oxide; native sulfur and realgar or bonazziite filaments occurred as minority constituents (Fig. 3e). Most of EMPA and EDS analyses of Fe (oxyhydr)oxides detected relatively high contents of S (≤5.4 wt%) and As (≤2.9 wt%). The RMS analyses of S-rich domains indicated that the S exists as native S (Fig. 4c), probably occurring in nano-sized coprecipitates with the Fe (oxyhydr)oxides. Only a few of the RMS spectra contained bands of pure Fe (oxyhydr)oxides; all of them corresponding to poorly-crystalline ferrihydrite (Fig. 4d). This finding is consistent with oxalate extraction results (Table S4), revealing poorly-crystalline Fe (oxyhydr)oxides as the major Fe phase for the NOM (60–97% of the total Fe) and IB (32–88% of the total Fe). In contrast, high sulfate- and low oxalate-extractable As fractions (Table S4) indicate that Fe (oxyhydr)oxides sequestered a relatively low As fraction ($\bar{x} \pm \sigma$: 11 ± 8%; sulfate fraction subtracted from oxalate fraction); a relatively high As fraction is mobile ($\bar{x} \pm \sigma$: 12 ± 4%), and the major As fraction ($\bar{x} \pm \sigma$: 77 ± 10%) is sequestered by As sulfides. Examination of the deposits by SEM-EDS showed that native S was also present as individual orthorhombic crystals (up to 10 μm long) embedded in a fine Fe (oxyhydr)oxide matrix (Fig. 3e). This mineralogical assemblage has repeatedly been documented as the typical oxidation product of Fe monosulfides (Burton et al., 2006) including black-colored mackinawite (Burton et al., 2009). Formation of the oxic Fe and S phases from the initial black deposits of Fe monosulfides on the bags and OM materials during the sample processing (freeze-drying) is consistent with the extremely rapid oxidation kinetics of Fe monosulfides (Di Toro et al., 1996; Burton et al., 2006, 2009). The newly-formed Fe sulfide phases also included rare equidimensional and equimorphic Fe disulfide crystals of ~1 μm in size (Fig. S6d). Other rare authigenic mineral phases identified in the deposits include CuS and $FeAs_2$ (Fig. S6c, e), probably corresponding to covellite and löllingite, the most common CuS and Fe-As phases formed in low-temperature conditions (Tazaki et al., 2003; Gramp et al., 2006; Alsina et al., 2014; Mansor et al., 2019).

### 3.4. Immobilization of As by sulfide precipitation

The NOM in the experimental bags sequestered As as $As_4S_4$ polymorphs. This is completely in line with recent studies on microbial sulfidogenesis of organic matter in soils and mine wastes; with laboratory batches and

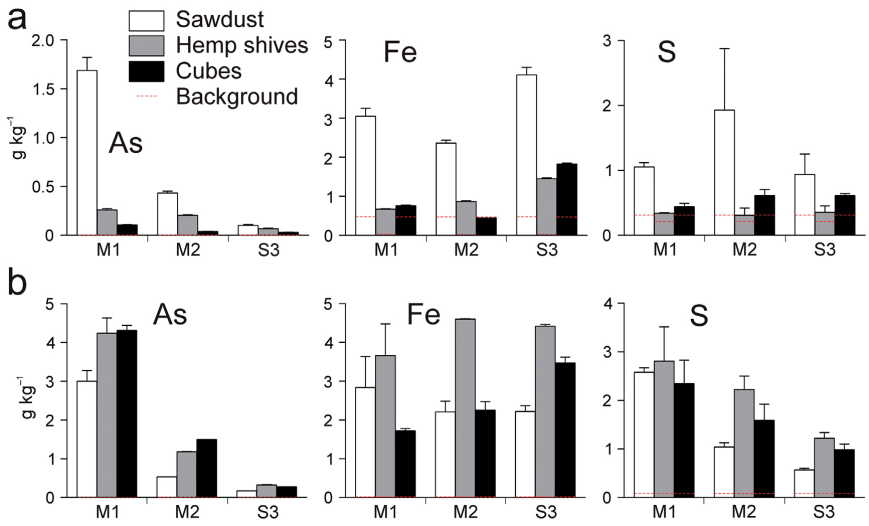


**Fig. 2.** Concentration of As, Fe, and S in the organic materials and inner bags after 15 months of incubation in the Mokrsko (M1, M2) and Smolotely (S3) wetlands: (a) natural organic materials (sawdust, hemp shives, and wooden cubes), and (b) corresponding inner bags. The dashed line represents the background concentrations in the natural organic materials (a) or inner bag (b).

columns reporting that these species are the primary end products of sulfate reduction in As-enhanced environments (Rodriguez-Freire et al., 2016; Drahota et al., 2017; Le Pape et al., 2017; Kerr et al., 2018; Falteisek et al., 2019; Knappová et al., 2019; Falteisek et al., 2020). It appears that the abundance of microbially available organic C within the experimental bags stimulated sulfate reduction within and along the IB to produce aqueous sulfide, and fermentation to amplify reducing conditions (Drahota et al., 2017; Falteisek et al., 2019; Knappová et al., 2019). The sustained sulfide supply initially drove formation of mackinawite; leading to a decrease in the aqueous Fe(II) (Rickard and Morse, 2005), and possibly to the adsorption of a small As fraction (Wolthers et al., 2005; Vega et al., 2017). The maximum pool of adsorbed As likely corresponded to the As fraction recovered from poorly-crystalline Fe (oxyhydr)oxide (mackinawite oxidation products) by oxalate ($\overline{x} \pm \sigma$: 11 ± 8%). The relative lack of aqueous Fe(II) in the presence of the relatively high aqueous sulfide and As then induced the precipitation of AsS mineral phases (O'Day et al., 2004). We

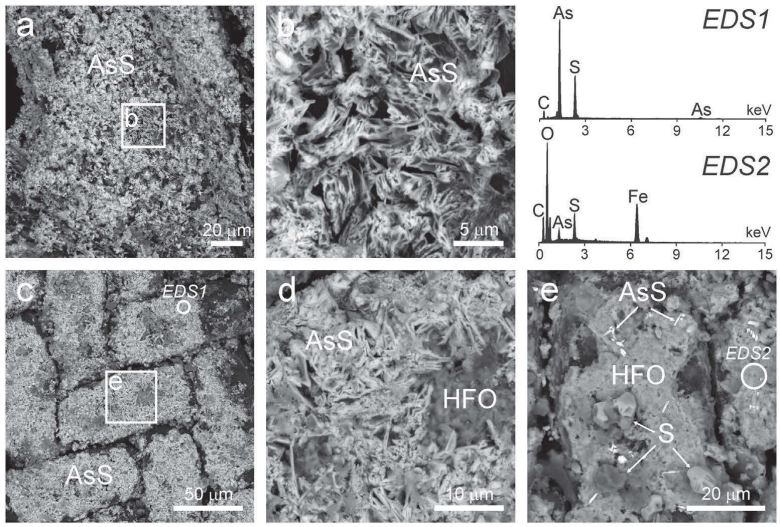


**Fig. 3.** SEM analyses of the mineral phases in As-Fe-S deposits precipitated on the surface of NOM and IB over the 15 months of incubation in the wetland soil. SEM images of a typical region with a high concentration of arsenic sulfide (AsS) on the NOM (a) and IB (c) from the M1 site. The detailed SEM images (b, d) and EDS analysis (*EDS1*) show aggregates of AsS skeletal crystals. SEM image (e) and EDS spectrum (*EDS2*) of Fe (oxyhydr)oxide (HFO) and native sulfur (S).

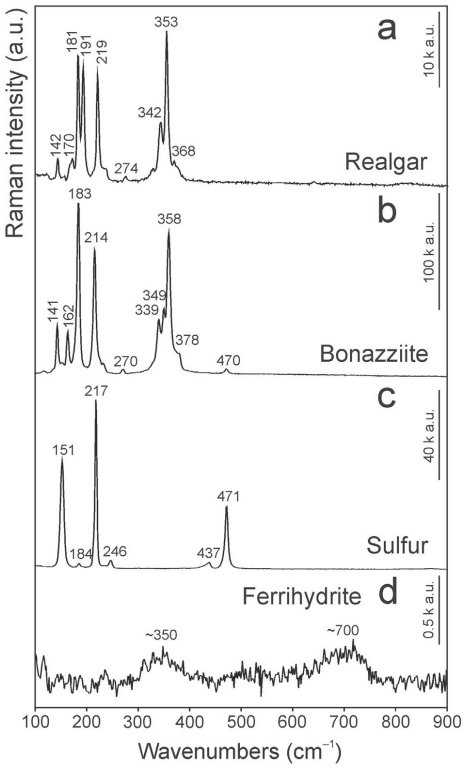


**Fig. 4.** Raman spectra of major mineral phases in the As-Fe-S deposits obtained from the NOM (a, b) or IB (c, d).

only found evidence of $As_4S_4$ mineral polymorphs (realgar and bonazziite), which is consistent with the lower solubility of realgar at neutral to alkaline pH in comparison to orpiment (Wilkin et al., 2003). Additionally, there was also evidence of low-temperature formation of $As_4S_4$ polymorphs in many natural environments (Langner et al., 2013; Drahota et al., 2017; Kerr et al., 2018; Knappová et al., 2019; Falteisek et al., 2020).

Formation of AsS mineral deposits in all experimental bags is consistent with a model for AsS mineral precipitation on the exterior parts of the NOM fragments in highly heterogeneous and complex natural systems, such as organic-rich soil and mine waste (Langner et al., 2013; Drahota et al., 2017; Kerr et al., 2018; Knappová et al., 2019). In this model, buried NOM fragments represent highly localized environments with mass-transfer limitations on solute transport, and where microbial sulfate reduction and fermentation developed the highly reducing conditions that led to sufficiently long-term oversaturation with respect to As sulfides. The fact that AsS mineral deposits formed in all of the experimental bags, including those from the M2 site (free of AsS phases in the soil) suggests that oversaturation conditions developed as a result of the reduced exchange of solutes through the bag's pores. It is likely that the exchange of solutes gradually reduced over the incubation period, as a consequence of FeS precipitation causing pore clogging (Fig. 3c). The other possible roles of the bags (*e.g.*, holder or template) in precipitation of sulfide minerals are implausible, because formation of sulfide deposits was restricted to inner bags. Outer bags that limited transport of solutes were free of sulfide minerals.

This model of AsS mineral formation is not fully consistent with the recent findings of Kumar et al. (2020), who documented the formation of realgar in aquifer sand, around the organic-rich clay lenses, which incorporated all As into NOM, probably through sulfhydryl groups. It appears that these contradictory observations are related to a combination of preferential As incorporation into the NOM, relative to AsS mineral precipitation (Langner et al., 2012; Couture et al., 2013; Besold et al., 2018) and to different As levels in the studied systems. The low concentrations of As in the column experiments ($\leq 42$ μg $L^{-1}$ in the aqueous phase) of Kumar et al. (2020) were fully complexed with NOM, while an excess of dissolved As relative to the number of its binding sites to the NOM in our experimental sites (450–9860 μg $L^{-1}$ in the aqueous phase) and several other natural systems (always $\geq 300$ μg $L^{-1}$ in the aqueous phase) led to AsS mineral precipitation (Langner et al., 2013; Drahota et al., 2017; Knappová et al., 2019). It should be noted that sorption affinity of As(III) to NOM under neutral pH conditions, such as those in the Mokrsko and Smolotely wetlands (Table 1), is low; and this affinity is additionally reduced for highly mobile thioarsenates (Besold et al., 2018; Eberle et al., 2020) that often dominate in sulfidic waters (Stauder et al., 2005; Stucker et al., 2013; Besold et al., 2018). These findings would match the surprisingly high fraction of readily soluble (sulfate-extractable) As in the incubated materials (Table S4), and very high concentrations of As(III) in the groundwater (Table 1) that even increased in the soil horizons rich in NOM (Drahota et al., 2017).

### 3.5. Implications for As remediation

With the example of our *in situ* experiment, we have been able to show that the widely investigated process of As sulfidation can specifically be applied as a passive bioremediation approach at artificially-constructed anaerobic wetlands that are often preferred option for the treatment of contaminated net acid waters with relatively low concentration of solutes (Lottermoser, 2010). The incubation of low-cost organic materials, such as wood particles, sawdust, and hemp shives, which act as suitable electron donors for microbial metabolism, and represent a redox partner for electron acceptors like sulfate (Waybrant et al., 1998; Zagury et al., 2006), caused sequestration of As through the precipitation of realgar and bonazziite on the NOM exteriors. Precipitation of crystalline As sulfides appears to be a suitable treatment process for the removal of As from contaminated anoxic waters, because (i) they contain approximately a two order greater concentration of As than of Fe sulfides, (ii) they are substantially less sensitive to oxidative dissolution than Fe sulfides are (Di Toro et al., 1996; Burton et al., 2006, 2009; Langner et al., 2014; Drahota et al., 2021), and (iii) they can completely remove aqueous As under optimal conditions (Le Pape et al., 2017). Despite these potential benefits for remediation, this treatment method has significant drawbacks limiting its extensive application in constructed wetlands. The presence of high Fe(II) concentrations in the water, which is common for anoxic or acidic As-rich waters (Smedley and Kinniburgh, 2002), is expected to efficiently remove dissolved sulfide from solution, and thereby minimize direct interactions between dissolved As and sulfide. Excess sulfide in solution is preferentially incorporated into the NOM, forming sulfhydryl groups, which provide binding sites for As, especially at low pH (Hoffmann et al., 2012; Langner et al., 2012). At neutral to alkaline pH, As is highly mobile due to formation of thioarsenates (Besold et al., 2018; Eberle et al., 2020). All of these findings indicate that AsS mineral formation in organic-rich systems is likely limited by dissolved As(III) and sulfide concentrations, or inhibited by high Fe(II) in solution. In practice, immobilization of As as AsS mineral phases in constructed wetlands would likely only be efficient for sulfide-rich waters with high As (III) concentrations and a low Fe(II)/As(III) ratio. Nevertheless, our results demonstrated that AsS minerals can precipitate in natural systems with relatively variable dissolved As(III) concentrations (0.23–9.4 mg $L^{-1}$) and Fe (II)/As(III) molar aqueous ratios (0.5–80) that correspond to many natural waters with elevated As concentrations as well as mine effluents (Williams, 2001; Smedley and Kinniburgh, 2002).

Our results also indicated that the hydraulic properties of the substrate represent another key parameter for AsS formation in wetland systems. Previous studies have documented the formation of AsS deposits on the exteriors of NOM fragments that are characterized by steep chemical and

microbial gradients due to diffusion-limited mass transfer between the mobile (soil) and immobile (NOM fragments) pore water regions (Rezanezhad et al., 2016; Drahota et al., 2017; Knappová et al., 2019). Precipitation of AsS mineral phases in the incubated materials, particularly IB, suggests that the outer bags played a similar role as immobile regions for the NOM fragments in developing and keeping the redox gradients by pore-scale mass-transfer limitations. All these findings imply that wetland systems would (at least locally) achieve oversaturation with respect to AsS minerals under a specific hydrological and biogeochemical regime, which requires sufficiently fast microbial production of dissolved sulfide compared to water flow velocity and related migration of solutes. It seems that not only the hydraulic properties, but also the organic material source, should be considered as an important parameter influencing the sulfate reduction rate in wetland systems. It has been proven by many studies that mixtures of several natural organic materials, both organic (animal manure, compost) and cellulosic (wood chips, sawdust) wastes, display better results in sulfate reduction and metal removal than a single organic source (Waybrant et al., 1998; Zagury et al., 2006), such as those used in this study.

Increasingly detailed information about low-temperature AsS formation in subsurface environments is becoming available, including the role of microbial activity, organic-rich domains, and the chemical compositions of the maternal solutions (Drahota et al., 2017; Knappová et al., 2019; Kumar et al., 2020). However, additional studies are required to predictively relate this information to effective As sequestration within newly-formed AsS phases in passive treatment systems such as constructed wetlands or peatlands. In particular, our understanding of how the spatial heterogeneity and hydraulic properties of the porous structure of soil or peat affect solute transport, sulfate reduction rate, and accompanying AsS formation remains fairly limited. Furthermore, the initial hydraulic properties of anaerobic treatment systems may decrease over time as a consequence of physical consolidation, NOM decomposition, and sulfide precipitation causing pore clogging (Rockhold et al., 2002; Rezanezhad et al., 2016). Thus, future research should focus on exploring the optimal hydraulic properties of organic-rich substrates that would provide AsS formation as an effective and long-term treatment method for As in constructed wetlands.

## 4. Conclusion

The experimental bag technique was used to simulate the interaction of natural organic matter with the indigenous sulfate-reducing microorganisms of three As-enriched wetland soils, with a special emphasis on As immobilization by the newly formed sulfide phases. A 15 months *in situ* incubation of low-cost organic materials (sawdust, wood cubes, and hemp shives) in pH-neutral soils with contrasting As and Fe concentrations (As: 0.45–9.9 mg $L^{-1}$; Fe: 3.3–21 mg $L^{-1}$) in the groundwater resulted in precipitation of As and Fe sulfides in all types of organic materials and all of the studied wetland sites. The newly-formed sulfide accumulations formed on the surface of organic matter and inner bags, and consisted mainly of crystalline realgar, bonazziite (both $As_4S_4$), and reactive Fe(II) sulfides (probably mackinawite). Rare authigenic minerals, only detected in one or two grains, included pyrite, covellite and löllingite. The fraction of As bound to AsS polymorphs was always high (~80%). The remaining As fraction was probably bound to Fe(II) monosulfides and corresponded with mobile thioarsenic species.

We propose that formation of sulfide minerals in the experimental bags was promoted by reduced exchange of solutes through the pores of the bags as well as comparatively fast microbial production of dissolved sulfide stimulated by organic matter within the bags. Although the AsS mineral formation is inhibited by aqueous Fe(II), and limited by dissolved As(III) and sulfide due to their preferential incorporation into other solid substrates (organic matter and Fe(II) sulfides), our results documented precipitation of AsS minerals in organic-rich natural environments with relatively low As(III) ($\geq$0.23 mg $L^{-1}$) and high Fe(II)/As(III) molar ratio ($\leq$80) in the groundwater. These findings indicate that a bioremediation process relying on the mechanism of AsS precipitation offers the potential to promote removal of As from many contaminated waters and effluents. However, further study of the optimal hydraulic properties of the organic-rich substrates providing the long-term AsS precipitation is important to better understand the feasibility of this process in treatment systems such as constructed wetlands.

## CRediT authorship contribution statement

**Magdaléna Peřestá:** Conceptualization, Data curation, Formal analysis, Funding acquisition, Investigation, Project administration, Resources, Visualization, Writing – original draft, Writing – review & editing. **Petr Drahota:** Conceptualization, Data curation, Formal analysis, Funding acquisition, Investigation, Methodology, Project administration, Resources, Supervision, Validation, Visualization, Writing – original draft, Writing – review & editing. **Adam Culka:** Formal analysis, Investigation, Writing – review & editing. **Tomáš Matoušek:** Formal analysis, Funding acquisition, Investigation, Writing – review & editing. **Martin Mihaljevič:** Formal analysis, Investigation, Writing – review & editing.

## Declaration of competing interest

The authors declare that they have no known competing financial interests or personal relationships that could have appeared to influence the work reported in this paper.

## Acknowledgements

This study was financially supported by the Czech Science Foundation (GACR 16-09352S) and Center for Geosphere Dynamics (UNCE/SCI/006). The contribution of TM was supported by the Institute of Analytical Chemistry of the Czech Academy of Sciences (RVO: 68081715). Part of the laboratory equipment for this study was purchased from the Operational Programme Prague - Competitiveness (Project CZ.2.16/3.1.00/21516); We gratefully acknowledge L. Jílková, L. Vondrovicová and V. Vonásková for their laboratory assistance. We also wish to thank Dr. Peter Lemkin for editing the English manuscript. The authors really appreciate all the detailed review of Prof. Dave Craw and two anonymous referees for improving the manuscript.

## Appendix A. Supplementary data

Supplementary data to this article can be found online at https://doi.org/10.1016/j.scitotenv.2021.152008.

## References

Alam, R., McPhedran, K., 2019. Applications of biological sulfate reduction for remediation of arsenic – a review. Chemosphere 222, 932–944.

Alsina, M.A., Zanella, L., Hoel, C., Pizarro, G.E., Gaillard, J.-F., Pasten, P.A., 2014. Arsenic speciation in sinter mineralization from a hydrothermal channel of El Tatio geothermal field, Chile. J. Hydrol. 518, 434–446.

Battaglia-Brunet, F., Crouzet, C., Burnol, A., Coulon, S., Morin, D., Joulian, C., 2012. Precipitation of arsenic sulphide from acidic water in a fixed-film bioreactor. Water Res. 46, 3923–3933.

Bednar, A.J., Garbarino, J.R., Ranville, J.F., Wildeman, T.R., 2002. Preserving and distributions of inorganic arsenic species in groundwater and acid mine drainage samples. Environ. Sci. Technol. 36, 2213–2218.

Belzile, N., Lebel, J., 1986. Capture of arsenic by pyrite in near-shore marine-sediments. Chem. Geol. 54, 279–281.

Besold, J., Biswas, A., Suess, E., Scheinost, A.C., Rossberg, A., Mikutta, C., Kretzschmar, R., Gustafsson, J.P., Planer-Friedrich, B., 2018. Monothioarsenate transformation kinetics determining arsenic sequestration by sulfhydryl groups of peat. Environ. Sci. Technol. 52, 7317–7326.

Burton, E.D., Bush, R.T., Sullivan, L.A., 2006. Acid-volatile sulfide oxidation in coastal flood plain drains: iron-sulfur cycling and effects on water quality. Environ. Sci. Technol. 40, 1217–1222.

Burton, E.D., Bush, R.T., Sullivan, L.A., Hocking, R.K., Johnston, S.G., Fitzpatrick, R.W., Raven, M., McClure, S., Jang, L.Y., 2009. Iron-monosulfide oxidation in natural sediments. Resolving the microbially mediated S transformations using XANES, electron microscopy, and selective extractions. Environ. Sci. Technol. 43, 3128–3134.

Burton, E.D., Johnston, S.G., Kocar, B.D., 2014. Arsenic mobility during flooding of contaminated soil: the effect of microbial sulfate reduction. Environ. Sci. Technol. 48, 13660–13667.
Couture, R.-M., Wallschläger, D., Rose, J., Van Cappellen, P., 2013. Arsenic binding to organic and inorganic sulfur species during microbial sulfate reduction: a sediment flow-through reactor experiment. Environ. Chem. 10, 285–294.
Demergasso, C.S., Chong, G., Escudero, L., Mur, J.J.P., Pedros-Alió, C., 2007. Microbial precipitation of arsenic sulfides in andean salt flats. Geomicrobiol. J. 24, 111–123.
Di Toro, D.M., Mahoney, J.D., Gonzales, A.M., 1996. Particle oxidation model of synthetic FeS and sediment acid-volatile sulfide. Environ. Toxicol. Chem. 15, 2156–2167.
Dixit, S., Hering, J.G., 2003. Comparison of arsenic(V) and arsenic(III) sorption onto iron oxide minerals: implications for arsenic mobility. Environ. Sci. Technol. 37, 4182.
Drahota, P., Rohovec, J., Filippi, M., Mihaljevič, M., Rychlovský, P., Červený, V., Pertold, Z., 2009. Mineralogical and geochemical controls of arsenic speciation and mobility under different redox conditions in soil, sediment and water at the Mokrsko-West gold deposit, Czech Republic. Sci. Total Environ. 407, 3372–3384.
Drahota, P., Mikutta, C., Falteisek, L., Duchoslav, V., Klementová, M., 2017. Biologically induced formation of realgar deposits in soil. Geochim. Cosmochim. Acta 218, 237–256.
Drahota, P., Kulakowski, O., Culka, A., Knappová, M., Rohovec, J., Veselovský, F., Racek, M., 2018. Arsenic mineralogy of near-neutral soils and mining waste at the smolotely-Líšnice historical gold district, Czech Republic. Appl. Geochem. 8, 243–254.
Drahota, P., Peřestá, M., Trubač, J., Mihaljevič, M., Vaněk, A., 2021. Arsenic fractionation and mobility in sulfidic wetland soils during experimental drying. Chemosphere 277, 130306.
Eberle, A., Besold, J., Kerl, C.F., Lezama-Pacheco, J.S., Fendorf, S., Planer-Friedrich, B., 2020. Arsenic fate in peat controlled by the pH-dependent role of reduced sulfur. Environ. Sci. Technol. 54, 6682–6692.
Eberle, A., Besold, J., León Ninin, J.M., Kerl, C.F., Kujala, K., Planer-Friedrich, B., 2021. Potential of high pH and reduced sulfur for arsenic mobilization – insights from a Finnish peatland treating mining waste water. Sci. Total Environ. 758, 143689.
Ettler, V., Mihaljevič, M., Šebek, O., Matys Grygar, T., Klementová, M., 2012. Experimental in situ transformation of Pb smelter fly ash in acidic soils. Environ. Sci. Technol. 46, 10539–10548.
Falteisek, L., Duchoslav, V., Drahota, P., 2019. Realgar (As4S4) bioprecipitation in microcosm fed by a natural groundwater and organic matter. Environ. Sci. Pollut. Res. 26, 18766–18776.
Falteisek, L., Drahota, P., Culka, A., Laufek, F., Trubač, J., 2020. Bioprecipitation of As4S4 polymorphs in an abandoned mine adit. Appl. Geochem. 113, 104511.
Gramp, J.P., Sasaki, K., Bigham, J.M., Karnachuk, O.V., Tuovinen, O.H., 2006. Formation of covellite (CuS) under biological sulfate-reducing conditions. Geomicrobiol J. 23, 613–619.
Highley, T.L., 1995. Comparative durability of untreated wood in use above ground. Int. Biodeterior. Biodegrad. 35, 409–419.
Hoffmann, M., Mikutta, C., Kretzschmar, R., 2012. Bisulfide reaction with natural organic matter enhances arsenite sorption: insights from X-ray absorption spectroscopy. Environ. Sci. Technol. 46, 11788–11797.
Islam, F.S., Gault, A.G., Boothman, C., Polya, D.A., Charnock, J.M., Chatterjee, D., Lloyd, J.R., 2004. Role of metal-reducing bacteria in arsenic release from Bengal delta sediments. Nature 430, 68–71.
Keon, N.E., Swartz, C.H., Brabander, D.J., Harvey, C., Hemond, H.F., 2001. Validation of an arsenic sequential extraction method for evaluating mobility in sediments. Environ. Sci. Technol. 35, 2778–2784.
Kerr, G., Craw, D., Trumm, D., Pope, J., 2018. Authigenic realgar and gold in dynamic redox gradients developed on historic mine wastes, New Zealand. Appl. Geochem. 97, 123–133.
Kirk, M.F., Holm, T.R., Park, J., Jin, Q.S., Sanford, R.A., Fouke, B.W., Bethke, C.M., 2004. Bacterial sulfate reduction limits natural arsenic contamination in groundwater. Geology 32, 953–956.
Kirk, M.F., Roden, E.E., Crossey, L.J., Brealey, A.J., Spilde, M.N., 2010. Experimental analysis of arsenic precipitation during microbial sulfate and iron reduction in model aquifer sediment reactors. Geochim. Cosmochim. Acta 74, 2538–2555.
Knappová, M., Drahota, P., Falteisek, L., Culka, A., Penížek, V., Trubač, J., Mihaljevič, M., Matoušek, T., 2019. Microbial sulfidogenesis of arsenic in naturally contaminated wetland soil. Geochim. Cosmochim. Acta 267, 33–50.
Kumar, N., Noël, V., Planer-Friedrich, B., Besold, J., Lezama-Pacheco, J., Bargar, J.R., Brown Jr., H.E., Fendorf, S., Boye, K., 2020. Redox heterogeneities promote thioarsenate formation and release into groundwater from low arsenic sediments. Environ. Sci. Technol. 54, 3237–3244.
Langner, P., Mikutta, C., Kretzschmar, R., 2012. Arsenic sequestration by organic Sulphur in peat. Nat. Geosci. 5, 66–73.
Langner, P., Mikutta, C., Suess, E., Marcus, M.A., Kretzschmar, R., 2013. Spatial distribution and speciation of arsenic in peat studied with microfocused X-ray fluorescence spectrometry and X-ray absorption spectroscopy. Environ. Sci. Technol. 47, 9706–9714.
Langner, P., Mikutta, C., Kretzschmar, R., 2014. Oxidation of organosulfur-coordinated arsenic and realgar in peat: implications for the fate of arsenic. Environ. Sci. Technol. 48, 2281–2289.
Le Pape, P., Battaglia-Brunet, F., Parmentier, M., Joulian, C., Gassaud, C., Fernandez-Rojo, L., Guigner, J.-M., Ikogou, M., Stetten, L., Olivi, L., Casiot, C., Morin, G., 2017. Complete removal of arsenic and zinc from a heavily contaminated acid mine drainage via an indigenous SRB consortium. J. Hazard. Mater. 321, 764–772.
Ledbetter, R.N., Connon, S.A., Neal, A.L., Dohnalkova, A., Magnuson, T.S., 2007. Biogenic mineral production by a novel arsenic-metabolizing thermophilic bacterium from the Alvord basin, Oregon. Appl. Environ. Microbiol. 73, 2936–5928.
Lee, J.H., Kim, M.G., Yoo, B., Myung, N.V., Maeng, J., Lee, T., Dohnalkova, A.C., Fredrickson, J.K., Sadowsky, M.J., Hur, H.G., 2007. Biogenic formation of photoactive arsenic-sulfide nanotubes by Shewanella sp. Strain HN-41. Proc. Natl. Acad. Sci. U. S. A. 104, 20410–20415.
Lottermoser, B.G., 2010. Mine wastes. Characterization, treatment and environmental impacts. 3rd edition. .
Lowers, H.A., Breit, G.N., Foster, A.L., Whitney, J., Yount, J., Uddin, N., Muneem, A., 2007. Arsenic incorporation into authigenic pyrite, Bengal Basin sediment, Bangladesh. Geochim. Cosmochim. Acta. 71, 2699–2717.
Mansor, M., Berti, D., Hochella Jr., M.F., Murayama, M., Xu, J., 2019. Phase, morphology, elemental composition, and formation mechanisms of biogenic and abiogenic fe-cu-sulfide nanoparticles: a comparative study on their occurrences under anoxic conditions. Am. Miner. 104, 703–717.
Mihaljevič, M., Ettler, V., Šebek, O., Drahota, P., Strnad, L., Procházka, R., Zeman, J., Sracek, O., 2010. Alteration of arsenopyrite in soils under different vegetation covers. Sci. Total Environ. 408, 1286–1294.
Newman, D.K., Beveridge, T.J., Morel, F.M.M., 1997. Precipitation of arsenic trisulfide by desulfotomaculum auripigmentum. Appl. Environ. Microbiol. 63, 2022–2028.
Nickson, R.T., McArthur, J.M., Ravenscroft, P., Burgess, W.G., Ahmed, K.M., 2000. Mechanism of arsenic release to groundwater, Bangladesh and West Bengal. Appl. Geochem. 15, 403–413.
Nordstrom, D.K., 2002. Public health – worldwide occurrences of arsenic in groundwater. Science 296, 2143–2145.
O`Day, P.A., Vlassopoulos, D., Root, R.A., Rivera, N.A., 2004. The influence of sulphur and iron on dissolved arsenic concentrations in the shallow subsurface under changing redox conditions. Proc. Natl. Acad. Sci. U. S. A. 101, 13703–13708.
Paul, C.J., Ford, R.G., Wilkin, R.T., 2009. Assessing the selectivity of extractant solutions for recovering labile arsenic associated with iron (hydr)oxides and sulfides in sediments. Geoderma 152, 137–144.
Poulton, S.W., Krom, M.D., Raiswell, R., 2004. A revised scheme for the reactivity of iron (oxyhydr)oxide minerals towards dissolved sulfide. Geochim. Cosmochim. Acta 68, 3703–3715.
Rezanezhad, F., Price, J.S., Quinton, W.L., Lennartz, B., Milojevic, T., Van Cappellen, P., 2016. Structure of peat soils and implications for water storage, flow and solute transport: a review update for geochemists. Chem. Geol. 429, 75–84.
Rickard, D., Morse, J.W., 2005. Acid volatile sulfide (AVS). Mar. Chem. 97, 141–197.
Rittle, K.A., Drever, J.I., Colberg, P.J.S., 1995. Precipitation of arsenic during bacterial sulphate reduction. Geomicrobiol J. 13, 1–11.
Rochette, E.A., Bostick, B.C., Li, G.C., Fendorf, S., 2000. Kinetics of arsenate reduction by dissolved sulfide. Environ. Sci. Technol. 34, 4714–4720.
Rockhold, M.L., Yarwood, R.R., Niemet, M.R., Bottomley, P.J., Selker, J.S., 2002. Considerations for modeling bacterial-induced changes in hydraulic properties of variably saturated porous media. Adv. Water Res. 25, 477–495.
Rodriguez-Freire, L., Sierra-Alvarez, R., Root, R., Chorover, J., Field, J.A., 2014. Biomineralization of arsenate to arsenic sulfides is greatly enhanced at mildly acidic conditions. Water Res. 66, 242–253.
Rodríguez-Freire, L., Moore, S.E., Sierra-Alvarez, R., Root, R.A., Chorover, J., Field, J.A., 2016. Arsenic remediation by formation of arsenic sulfide minerals in a continuous anaerobic bioreactor. Biotechnol. Bioeng. 113, 522–530.
Smedley, P.L., Kinniburgh, D.G., 2002. A review of the source, behaviour and distribution of arsenic in natural waters. Appl. Geochem. 17, 517–568.
Stauder, S., Raue, B., Sacher, F., 2005. Thioarsenates in sulfidic waters. Environ. Sci. Technol. 39, 5933–5939.
Stucker, V.K., Williams, K.H., Robbins, M.J., Ranville, J.F., 2013. Arsenic geochemistry in a biostimulated aquifer: an aqueous speciation study. Environ. Toxicol. Chem. 32, 1216–1223.
Tazaki, K., Rafiqul, I.A.B.M., Nagal, K., Kurihara, T., 2003. FeAs2 biomineralization on encrusted bacteria in hot springs: an ecological role in symbiotic bacteria. Can. J. Earth Sci. 40, 1725–1738.
Vega, A.S., Planer-Friedrich, B., Pastén, P.A., 2017. Arsenite and arsenate immobilization by preformed and concurrently formed disordered mackinawite (FeS). Chem. Geol. 475, 62–75.
Waybrant, K.R., Blowes, D.W., Ptacek, C.J., 1998. Selection of reactive mixtures for use in permeable reactive walls for treatment of mine drainage. Environ. Sci. Technol. 32, 1972–1979.
Wenzel, W.W., Kirchbaumer, N., Prohaska, T., Stingeder, G., Lombi, E., Adriano, D.C., 2001. Arsenic fractionation in soils using an improved sequential extraction procedure. Anal. Chim. Acta 436, 309–323.
Wilkin, R.T., Ford, R.G., 2006. Arsenic solid-phase partitioning in reducing sediments of a contaminated wetland. Chem. Geol. 228, 156–174.
Wilkin, R.T., Wallschläger, D., Ford, R.G., 2003. Speciation of arsenic in sulfidic waters. Geochem. Trans. 4, 1–7.
Williams, M., 2001. Arsenic in mine waters: an international study. Environ. Geol. 40, 267–278.
Wolthers, M., Charlet, L., Van der Linde, P.R., Rickard, D., 2005. Arsenic mobility in the ambient sulfidic environment: sorption of arsenic(V) and arsenic(III) onto disordered mackinawite. Geochim. Cosmochim. Acta 69, 3483–3492.
Zagury, G.J., Kulnieks, V.I., Neculita, C.M., 2006. Characterization and reactivity assessment of organic substrates for sulphate-reducing bacteria in acid mine drainage treatment. Chemosphere 64, 944–954.

# IV.

Drahota P., **Peřestá M.**, Trubač J., Mihaljevič M., Vaněk A. (2021) Arsenic fractionation and mobility in sulfidic wetland soils during experimental drying. *Chemosphere* **277**, 130306.

Chemosphere 277 (2021) 130306

Contents lists available at ScienceDirect

Chemosphere

journal homepage: www.elsevier.com/locate/chemosphere

# Arsenic fractionation and mobility in sulfidic wetland soils during experimental drying

Petr Drahota [a, *], Magdaléna Peřestá [a], Jakub Trubač [a], Martin Mihaljevič [a], Aleš Vaněk [b]

[a] Institute of Geochemistry, Mineralogy and Mineral Resources, Faculty of Science, Charles University, Albertov 6, 128 43, Prague 2, Czech Republic
[b] Department of Soil Science and Soil Protection, Faculty of Agrobiology, Food and Natural Resources, Czech University of Life Sciences Prague, Kamýcká 129, 165 00, Praha 6, Czech Republic

## HIGHLIGHTS

- Sulfidic wetland soils were flooded and dried for three months.
- Arsenic is preferentially released from arsenian Fe sulfides.
- Fe(III) (oxyhydr)oxides sequestered most of the released As, Co, Cu, Ni.
- Acidification of soils resulted in the pH-dependent release of the metal(-loid)s.

## GRAPHICAL ABSTRACT

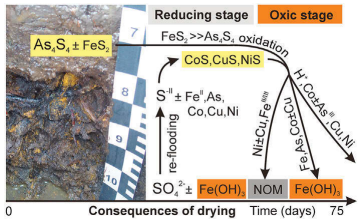


## ARTICLE INFO

*Article history:*
Received 18 December 2020
Received in revised form
11 March 2021
Accepted 14 March 2021
Available online 17 March 2021

Handling Editor: X. Cao

*Keywords:*
Wetland soil
Arsenic
Realgar
Oxidation
Mobility

## ABSTRACT

In this study, two Czech wetland soils enriched in authigenic sulfide minerals (especially realgar) were collected from the saturated zone (60–100 cm), flooded with local groundwater and allowed to dry for up to 98 days. The objective was to examine the mobility of As, Fe, S and trace metals using selective chemical extractions, S isotopes and X-ray diffraction through the drying process. During the initial stage of incubation (~20 days), the re-flooding of the soils triggered a microbially-mediated $SO_4^{2-}$ reduction, which immobilized the Co, Cu and Ni. The reductive dissolution of As-bearing Fe (oxyhydr)oxides and the release of As were documented only in the Fe-rich/organic-low soil. Over the next stage of incubation (~75 days), the exposure and drying of the soils led to the oxidation of the Fe and As sulfides. The arsenic and trace metals released via oxidation of the sulfide phases (particularly Fe sulfides) were almost entirely sequestered by the Fe(III) (oxyhydr)oxides, but acidification during the oxidation stage of the incubation resulted in the pH-dependent release of the As and trace metals (Co, Cu, Ni) (especially in the Fe-rich/organic-low soil). These findings suggest that sulfidic soils in wetlands can be considered as long-term sources of As during major drought events.



## 1. Introduction

Wetland soils are sensitive biogeochemical systems that are characterized by highly variable soil redox conditions that sustain a complex pattern of biogeochemical cycling of redox-sensitive, potentially hazardous metal(loid)s like As (Wilkin and Ford, 2006; Root et al., 2009; Langner et al., 2013; Drahota et al., 2017). The environmental fate and transport of As in these soils is primarily linked to the redox cycling of iron and sulfur (Edenborn et al., 1986; La Force et al., 2000; Blodau et al., 2008; Weber et al.,

* Corresponding author.
*E-mail address:* petr.drahota@natur.cuni.cz (P. Drahota).

https://doi.org/10.1016/j.chemosphere.2021.130306
0045-6535/

2010; Yamaguchi et al., 2011; Parsons et al., 2013; Langner et al., 2014; Huang et al., 2016). In oxic soils, As predominates in its +5 oxidation state, As(V), in the form of arsenate oxyanions ($H_2AsO_4^-$, $HAsO_4^{2-}$). The high affinity of As(V) for Fe(III) (oxyhydr)oxides may effectively immobilize aqueous As. When flooding occurs or a rise in groundwater table happens, soils become anoxic and aqueous As concentrations commonly reveal a drastic increase (Hess and Blanchar, 1977; Blodau et al., 2008; Burton et al., 2008; Weber et al., 2010). The arsenic behavior here may be also affected by the microbial $SO_4^{2-}$ reduction. Aqueous sulfide can promote the mobilization of As through the formation of thioarsenicals (Stucker et al., 2014). Aqueous sulfide can also immobilize the As by facilitating the precipitation of the As sulfide and Fe sulfide minerals (Belzile and Lebel, 1986; Rittle et al., 1995; O'Day et al., 2004) or its binding to the sulfhydryl groups of organic matter (Hoffmann et al., 2012; Langner et al., 2012).

We recently investigated the solid phase speciation of As in two naturally As-enriched wetlands (3600–21000 mg As $kg^{-1}$ at Mokrsko and 110–1160 mg As $kg^{-1}$ at Smolotely) in central Czech Republic (Drahota et al., 2017; Knappová et al., 2019). The bulk X-ray absorption spectroscopy (XAS) revealed that the As at Mokrsko was dominantly (≥71%) sequestered by authigenic realgar ($\alpha$-$As_4S_4$) (Drahota et al., 2017), locally forming monomineralic deposits on the fragments of natural organic matter (NOM). Authigenic AsS polymorphs (realgar and bonazziite ($\beta$-$As_4S_4$)) and arsenian Fe sulfides (pyrite ($FeS_2$) and greigite ($Fe_3S_4$)) were also identified as the dominant As mineral phases associated with the NOM fragments at the Smolotely wetland (Knappová et al., 2019). Besides the verification of As sulfides in the soil of the wetlands, microscopic and spectroscopic analyses revealed the presence of As(III/V) sorbed and/or coprecipitated to Fe(III) (oxyhydr)oxides (Drahota et al., 2013, 2017, 2018; Knappová et al., 2019). The coexistence of these As phases was attributed to the authigenic formation of sulfides in strongly reducing microenvironments, and nonequilibrium conditions induced by a fluctuating water table (Drahota et al., 2017; Knappová et al., 2019).

Summer droughts and associated low water tables in freshwater wetlands lead to strong changes in the redox conditions (Seybold et al., 2002; Mansfeldt, 2003; Vorenhout et al., 2004). These periodic soil drainages may cause the oxidation of the sulfide mineral phases (Burton et al., 2006; Langner et al., 2014), providing wetlands with As-bearing sulfides potential sources for As. The major objective was to test whether the medium-term oxidizing conditions in the As sulfide-bearing Mokrsko and Smolotely wetland soils contribute to mobilization of As, as was shown for a high-As (≥280 mg As $kg^{-1}$) peatland (Langner et al., 2014), or conversely, if metal (oxyhydr)oxides cause an As immobilization, as was documented for a peat soil with low As (≤25 mg As $kg^{-1}$) (Blodau et al., 2008). The specific aims of this study were to (i) elucidate the short-term temporal dynamics of the As and trace metals fractions and their coupling to other redox processes in the soils (ii) assess the influence of the soil variables (e.g., organic matter content, total As content, different proportion of Fe sulfides), on the dynamics of the As and trace metals, and (iii) identify the potential importance of the sulfide oxidation for the S, Fe and As dynamics.

## 2. Materials and methods

### 2.1. Soil sampling

Wetland soils were collected from two naturally contaminated geochemical anomalies in Czech Republic (Mokrsko: 49°44′43"N, 14°20′01"E; Smolotely: 49°37′31"N, 14°9′32"E) known to contain high levels of As bound in biogenic sulfides (Drahota et al., 2013, 2017; Knappová et al., 2019).

In May 2018, 1 m deep soil pits were excavated in both wetland sites (Fig. S1) to obtain soil samples from the saturated zone (60–100 cm) affected by the water table fluctuation. Approximately 17 kg of wet soil from this depth interval was sieved (<2 mm) and moved to an experimental container (40 cm length, 34 cm width and 17 cm height), where the samples were thoroughly homogenized by mixing with a plastic spatula. The soils were saturated and covered with groundwater (water depth 0.5 cm) collected at the same time by near suction lysimeters (~3 m distance from the pit and 1 m depth). All these processing operations were performed in the field immediately after the collection of the samples (within 90 min). The containers were then transported to the laboratory and kept in the open air at a laboratory temperature (25.5 ± 1.2 °C).

### 2.2. Laboratory procedures

To examine the As and metal fractionations during gradual drying of flooded soils, every 3 days of the first month and then once after the second (day 64) and third month (day 96), 10–20 g of the triplicate soil sample was collected using a clean 50-mL plastic tube. The samples were collected throughout the soil depth (~7.5 cm) in the container in order to include both the oxic and reduced species in the respective surface and bottom zone of the soil layer, and split into three subsamples. The first subsample was dried under a stream of Ar in anaerobic glove box and immediately analyzed for the reactive solid-phase Fe(II), inorganic $SO_4^{2-}$, and chemical fractions of the metals. The soil pH and Eh were measured in the suspension of 'fresh' soil subsample and degassed deionized water, using a combined pH electrode, a Pt electrode and a WTW multimeter. The Eh values obtained, therefore, do not represent the real redox potentials in the undisturbed soil, but should be considered only as the relative indicators for the evolution of the soil redox conditions. The water content of another 'fresh' subsample was estimated as the weight loss after heating the sample for at least 8 h at 105 °C.

To assess the reactivity of the dominant biogenic As sulfide under the oxic conditions of the wetland soil, a small amount (ca. 3 μg) of nanocrystalline realgar was deposited on a silicon single-crystal zero-background sample holder and placed for one month into a desiccator with stable relative humidity (97%) maintained by a saturated $K_2SO_4$ solution. The nanocrystalline realgar sample was scraped from the NOM particles buried in the wetland soil at Mokrsko. The sample was analyzed by powder X-ray diffraction (XRD) analysis at the start, and after 15, 33, 64 and 96 days exposure to the oxic atmosphere.

### 2.3. Analytical methods

The particle size distribution was estimated by a combination of a sieving and hydrometer method (Gee and Bauder, 1979). The mineralogy was investigated by powder XRD analysis (PANalytical X'Pert Pro diffractometer, Cu K$\alpha$ radiation, 40 keV, 30 mA), and the total sulfur, organic carbon (TOC), and inorganic carbon (TIC) contents were measured using an Eltra CS 530 and Eltra CS 500 TIC analyzers (ELTRA, Germany). The selected metals (Co, Cu, Fe, Mn, and Ni) were quantified after digestion in mineral acids using ICP OES (Agilent 5100) or ICP MS (Thermo Scientific Xseries$^{II}$) as described previously (Drahota et al., 2018). A reactive solid-phase Fe(II) was determined following the method of Kostka and Luther (1994). The inorganic $SO_4^{2-}$ was determined by shaking the samples in deoxygenated 15 mM $NaH_2PO_4$ (Johnson and Henderson, 1979). After centrifugation and filtration, the supernatant solution was analyzed for $SO_4^{2-}$ by ion chromatography (HPLC; Dionex ICS-

2000, USA).

### 2.4. Arsenic determinations and fractionation

The As concentration was determined in triplicate in the pseudo-total Lefort *aqua-regia* digests using ICP MS. Arsenic partitioning was quantified using three chemical extractions outlined by Keon et al. (2001) and Wenzel et al. (2001). A deoxygenated 0.05 M $(NH_4)_2SO_4$ (4 h) was used to remove the readily mobile As and other metals, which may potentially be used for estimating their aqueous concentrations in the soil solutions (Wenzel et al., 2002). The average relative standard deviations (RSDs) of the triplicate extractions were 9% for the As (max. 24%) and always lower than 7% for the metals analyzed (Co, Cu, Fe, Mn, Ni). The exchangeable As was determined (average RSD 6%; max. 17%) by deoxygenated 0.1 M $NaH_2PO_4 \cdot 2H_2O$ buffered to pH 5.5 for 16 h (Keon et al., 2001; Paul et al., 2009). The As and metals bound to poorly crystalline Fe (oxyhydr)oxides were targeted by a 0.2 M $NH_4$-oxalate extract (2 h in the dark) (Drahota et al., 2014) at the start and after 9, 21, 33, 64 and 96 days of drying. The average RSDs were 5% for the As (max. 10%) and less than 8% for the metals. The relatively high RSDs of some wetland sample extractions could be solely ascribed to the wetland soil heterogeneity, which seems to increase during the incubation experiment (graphs below). This finding has been inferred from the investigation of the single extraction reproducibility in the NIST 2710a soil standard, which revealed high precision (RSD≤3.1%) for all the extraction procedures (Table S1).

### 2.5. Sulfur isotope analysis

The authigenic sulfide phases in the wetland soils are significantly depleted by $^{34}S$ (Drahota et al., 2017; Knappová et al., 2019). Sulfur isotope analysis can be therefore used as an indicator of a sulfide oxidation progress. For the $\delta^{34}S$ analyses, soil samples from the start and after 9, 21, 33, 64 and 96 days were pooled to produce a composite sample. Fifty grams of dry soil were extracted with a deoxygenated 200 mL solution of 15 mM $NaH_2PO_4 \cdot 2H_2O$, and the fraction of inorganic $SO_4^{2-}$ was precipitated as $BaSO_4$ (Révész et al., 2012). The $BaSO_4$ was analyzed measuring the $^{34}S/^{32}S$ ratio with a Thermo Delta V Advantage coupled with a Thermo Flash 2000 Elemental Analyzer at the Laboratory for Stable and Radiogenic Isotopes of the Faculty of Science, Charles University.

## 3. Results and discussion

### 3.1. Initial properties of the soils

The soils collected from the Mokrsko and Smolotely wetlands were described as Dystric Gleysols (IUSS Working Group WRB, 2006). The measured Eh and pH values were almost similar, indicating moderately reducing (Mokrsko: 3±8 mV; Smolotely: 8±5 mV) and near neutral (Mokrsko: pH 6.60 ± 0.07; Smolotely: pH 6.41 ± 0.05) conditions at both wetland sites. The soils contained very high As levels at 5890 mg $kg^{-1}$ (Mokrsko) and 433 mg $kg^{-1}$ (Smolotely) (Table 1). There were also large differences in the Fe, S, TOC as well as the particle size distribution and water content between the soils (Table 1). The concentration of other potentially hazardous metals (Co, Cu, Ni) were low (≤30 mg $kg^{-1}$), with the oxalate extraction results suggesting their minor association (10–40%) with Fe (oxyhydr)oxides.

In a previous study, we found that 65% of the total As in the depth range of 60–100 cm in the identical site of the Mokrsko wetland soil was sequestered by nanocrystalline realgar and 35% of the total As was bound to Fe(III) (oxyhydr)oxides (Drahota et al., 2017). The fact that nanocrystalline realgar was identified in the XRD pattern of the bulk soil (Fig. S2) indicates that its content should be relatively high, because the lowest detection limits of the XRD for crystalline compounds has been set at approx. 0.1% (Sanchez and Gunter, 2006).

**Table 1**
The selected initial properties of the soils used in the drying experiment.

| | Mokrsko | Smolotely |
|---|---|---|
| water content (w $w^{-1}$) | 63.0 ± 0.5 | 35.1 ± 0.3 |
| Sand | 39 | 64 |
| Silt | 54 | 26 |
| Clay | 7 | 7 |
| TOC (g $kg^{-1}$) | 79.7 ± 0.2 | 11.0 ± 0.1 |
| total S (g $kg^{-1}$) | 5.83 ± 0.06 | 1.62 ± 0.15 |
| total Fe (g $kg^{-1}$) | 24.1 ± 0.1 | 43.4 ± 0.5 |
| total Mn (mg $kg^{-1}$) | 632 ± 45 | 688 ± 5 |
| total As (mg $kg^{-1}$) | 5890 ± 370 | 433 ± 7 |
| total Co (mg $kg^{-1}$) | 6.8 ± 0.1 | 14.1 ± 0.1 |
| total Cu (mg $kg^{-1}$) | 29.0 ± 0.1 | 21.5 ± 1.1 |
| total Ni (mg $kg^{-1}$) | 12.4 ± 0.3 | 13.6 ± 0.1 |
| sulfate As (mg $kg^{-1}$) | 124 ± 11 (2.1) | 6.0 ± 0.6 (1.5) |
| phosphate As (mg $kg^{-1}$) | 440 ± 23 (7.5) | 33 ± 3 (7.7) |
| oxalate As (mg $kg^{-1}$) | 1630 ± 23 (28) | 206 ± 26 (48) |
| oxalate Fe (g $kg^{-1}$) | 11.7 ± 0.9 (49) | 19.6 ± 1.2 (45) |
| HCl Fe (mg $kg^{-1}$) | 6.0 ± 0.3 (0.02) | 8.0 ± 0.6 (0.02) |

The data are the mean ± standard deviation of the triplicate determinations; the extractability values in parentheses are calculated as a percentage of the total concentration.

Yellow accumulations of As sulfides associated with the NOM fragments were also visually identified in the sample of the Smolotely wetland soil (Fig. S1), but no sulfide mineral was identified in the bulk sample using the XRD (Fig. S2). The results of the oxalate extraction indicated that ~48% of the total As was sorbed and/or coprecipitated with the Fe (oxyhydr)oxides (Table 1).

It should be noted that the concentrations of Fe(II) extracted in HCl, which is a proxy for nanocrystalline mackinawite (FeS) (Cornwell and Morse, 1987; Wallmann et al., 1993), were very low and comprised less than 0.03% of the total Fe in both wetland soils (Table 1). These low values are in accordance with our previous mineralogical observations (Drahota et al., 2017; Knappová et al., 2019), which were not able to detect the reactive Fe(II) minerals (mackinawite or green rust) and suggested their negligible content in the wetland soils under study.

### 3.2. Changes in the major geochemical parameters during drying

Fig. 1 shows the evolution of the moisture content, pH and redox potential (Eh) over time. During the first 6 days of incubation, the moisture contents remained almost constant because the soils were fully saturated due to the excess groundwater in the containers. Then the moisture contents decreased gradually in both samples. After 33 days of incubation, the Smolotely sample displayed the complete loss of the soil water while the Mokrsko soil lost approximately 80% of the total soil water. This difference cannot be ascribed to different rates of drying, but may be attributed to the almost twice as much water holding capacity of the Mokrsko wetland soil, which is due to finer texture and significantly higher content of organic matter compared to the Smolotely soil (Table 1). The changes in the pH and Eh were negligible within the first 18 days of incubation in both samples. After 18 days of incubation, the pH and Eh in the Mokrsko soil changed rather slowly and gradually (by 0.9 units pH and 410 mV Eh) over 15 days, while the Smolotely soil displayed a rapid decrease in the pH (by 1.5 units) and increase in the Eh (by 490 mV) over 6–9 days. The

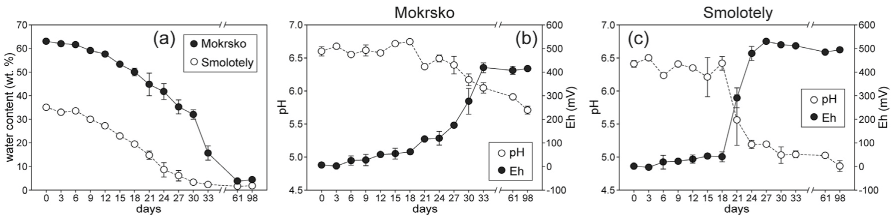


**Fig. 1.** The changes to the soil quality during the drying experiment: (a) the content of the water, pH and Eh in (b) the Mokrsko soil and (c) the Smolotely soil. The data are the mean ± standard deviation of the triplicate samples. Note that Eh values should be considered as the relative indicators for the progress of the oxidation.

periods of intensive oxidation were caused by a loss of 23–80% of the water in the Mokrsko soil (days 18–33) and a 47–79% loss of the water in the Smolotely soil (days 18–24).

### 3.2.1. Sulfate and S isotopes

The phosphate-extractable $SO_4^{2-}$ dropped by 26 mg $kg^{-1}$ of S (29% of the total soluble $SO_4^{2-}$) and 15 mg $kg^{-1}$ of S (35% of the total soluble $SO_4^{2-}$) within 6 days of the incubation in the Mokrsko and Smolotely soil (Fig. 2), respectively. The removal of the soluble $SO_4^{2-}$ was accompanied by a significant increase in the $\delta^{34}S$ values in the phosphate-extractable $SO_4^{2-}$ (Fig. 2). These data indicate that around a third of the soluble $SO_4^{2-}$, which was immobilized within the first 6 days of the incubation, was depleted in $^{34}S$ by 18.3‰ in the Mokrsko soil and 24.9‰ in the Smolotely soil relative to initial isotopic composition of the phosphate-extractable $SO_4^{2-}$; thus implying a dissimilatory $SO_4^{2-}$ reduction (Canfield, 2001) during the initial stage of incubation.

The concentrations of the phosphate-extractable $SO_4^{2-}$ in the Mokrsko and Smolotely soil began to gradually increase after 6 days and 24 days of incubation, respectively, and coincided with the decrease in the $\delta^{34}S$ values indicating the oxidation of the microbially-reduced sulfide depleted by $^{34}S$ (Fig. 2). The increments of the phosphate-extractable $SO_4^{2-}$ values over the full experiment duration corresponded to 49 mg $kg^{-1}$ of S (55%) in the Mokrsko soil and 40 mg $kg^{-1}$ of S (96%) in the Smolotely soil; the respective depletions in the $^{34}S$ isotope corresponded to 4.5‰ and 1.8‰. The $\delta^{34}S$ values of the phosphate-extractable $SO_4^{2-}$ increments, estimated from the mass balance approach, correspond to −10.9‰ in the Mokrsko soil and −6.6‰ in the Smolotely soil. These values almost fit the range of the isotopic composition of the authigenic sulfide minerals (between −8.3 and −4.5‰) in the wetland soils of both sites (Drahota et al., 2017; Knappová et al., 2019), indicating the release of $SO_4^{2-}$ from the oxidation of the authigenic As and Fe sulfides. This is in agreement with the findings of Rigby et al. (2006), who found that soluble $SO_4^{2-}$ concentrations in organic-rich soils are not affected by side reactions or precipitation and could be successfully used as an indicator of a sulfide oxidation progress.

### 3.2.2. Iron

The sulfate-extractable Fe, which likely involves dissolved Fe(II) and perhaps organic Fe complexes, was very low and remained almost constant (6–10 mg $kg^{-1}$) for the full experiment duration in the Mokrsko soil (Fig. 2). These values are in accordance with the low concentration of Fe in the porewater of the reducing wetland (Drahota et al., 2017) as well as in the oxic environments at the site (Drahota et al., 2009). The reasons for low soluble Fe concentrations in the Mokrsko wetland are not clear but very low Fe/TOC ratio (~0.07) in the soil may suggest formation of Fe complexes bound to organic matter (Mikutta and Kretzschmar, 2011; Bhattacharyya et al., 2018; Vantelon et al., 2019). The initial concentration of the soluble Fe in the Smolotely soil was more than an order higher (100 mg $kg^{-1}$) and began to increase substantially (up to 237 mg $kg^{-1}$) during the initial reducing stage of incubation. This is

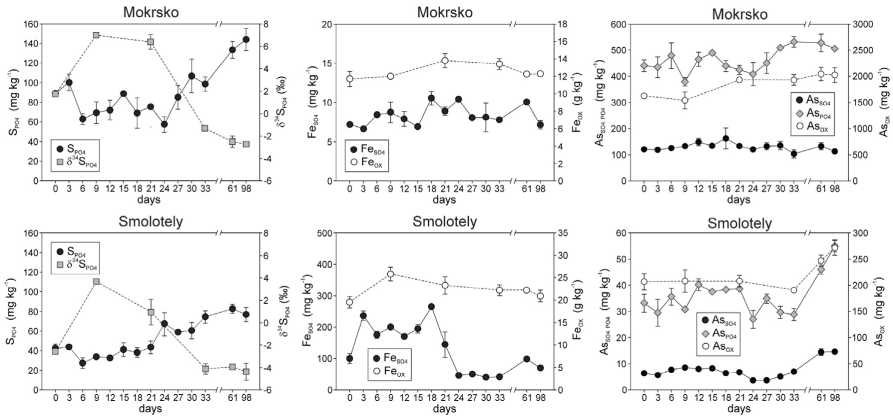


**Fig. 2.** The changes to the S, Fe and As concentrations and the sulfur isotope compositions ($\delta^{34}S_{PO4}$) of the operationally defined phosphate ($S_{PO4}$, $As_{PO4}$), sulfate ($Fe_{SO4}$, $As_{SO4}$) and oxalate ($Fe_{ox}$, $As_{ox}$) fractions during the drying experiment. The data points are the mean of the triplicate samples and the error bars are ± the standard deviation.

attributable to the microbial reductive dissolution of the relatively abundant Fe(III) (oxyhydr)oxides present in the soil. In contrast to Mokrsko soil, the soluble Fe concentrations were not controlled by the organic matter due to substantially higher Fe/TOC ratio (~0.85) in the Smolotely soil (Vantelon et al., 2019).

The decrease of the sulfate-extractable Fe in the Smolotely soil during the oxic stage of incubation (between days 18 and 21) coincided with a notable change in the soil color from greenish gray to rusty-brown and a marked decrease in the pH and an increase in the Eh (Fig. 1), indicating the oxidation of Fe(II) and hydrolysis of Fe(III). Consequently, the Fe(II) oxidation is likely a primary driver of the acidification in the Smolotely soil. It should be noted that the corresponding formation of the Fe(III) precipitates is not notably reflected in the oxalate-extracted Fe concentrations (Fig. 2). The increments of the final oxalate-extractable Fe values were estimated at 0.5 g $kg^{-1}$ in the Mokrsko and 1.5 g $kg^{-1}$ in the Smolotely samples. The contribution of newly-precipitated phases to the pool of pre-existing Fe(III) (oxyhydr)oxides is therefore low and corresponds to 2% and 3.5% in the Mokrsko and Smolotely samples, respectively.

### 3.3. Changes in the arsenic fractionation

Similarly to sulfate-extractable Fe, mobile As concentrations remained relatively constant (2.3 ± 0.4% of the total As) over the full experiment duration in the Mokrsko soil (Fig. 2), implying that the change in the redox conditions and associated variations in the pH values have a negligible effect on the mobility of As. The phosphate- and oxalate-extractable As concentrations displayed increasing trends with the time of the oxic stage of the incubation (after 24 days of incubation) and corresponded to the increase of the phosphate-extractable $SO_4^{2-}$ (Fig. 2). In contrast, oxalate-extractable Fe during the oxic stage of incubation revealed the imperceptible, rather decreasing, trend. These findings indicate that the As released during the As sulfide oxidation is more likely sequestered by the pre-existing Fe(III) (oxyhydr)oxides. They sequestered approximately 400 mg $kg^{-1}$ of As, which roughly correspond to 570 mg $kg^{-1}$ of realgar. This value is higher than the amount of oxidized As sulfide (160 mg $kg^{-1}$ of realgar) that has been estimated from the phosphate-extractable $SO_4^{2-}$ concentrations, implying that all the As released from the oxidation of realgar is effectively sequestered in the Fe(III) (oxyhydr)oxides. These conclusions are in accordance with the findings of Langner et al. (2014), who documented complete sequestration of the As released during the oxidation of realgar and As(III)-NOM complexes by Fe (oxyhydr)oxides in the contaminated peatland.

In the Smolotely soil, the initial sulfate-extractable As of 6.0 mg $kg^{-1}$ (1.4% of the total As) increased by 50% and peaked between 9 and 15 days. The increased concentrations of the soluble As during the initial reducing stage of the incubation (the first 15 days) may be attributed to the reduction of As(V) to As(III) which is more mobile compared to As(V) (Burton et al., 2008). In addition, the reductive dissolution of the Fe(III) (oxyhydr)oxides can release the co-associated As and decrease the mineral surface area and, thus, its ability to retain As (Pedersen et al., 2006). During the reducing stage of the incubation, the sulfate-extractable As positively correlated to the sulfate-extractable Fe(II) ($r = 0.52$, $P < 0.05$). Although the soluble As and Fe correlated well overall, they indicated the decoupling during the initial 9 days and at day 18 (Fig. S3). Mobilization of As was delayed by 9 days relative to Fe(II) (Fig. 2) suggesting changes in As speciation and sorption affinity (Islam et al., 2004; Pedersen et al., 2006; Burton et al., 2008) or precipitation of As and/or Fe phases (O'Day et al., 2004; Burton et al., 2013). The latter explanation is unlikely, because AsS phases precipitate after the formation of FeS phases (Gallegos et al., 2008; Han et al., 2011) and FeS precipitation was not supported by low and relatively constant HCl-extractable Fe(II) for the full incubation duration (Fig. S4).

A significant increase in the sulfate-extractable As up to 14.5 mg $kg^{-1}$ (3.5% of the total As) during the oxic stage of the Smolotely soil incubation was associated with the marked increase in the phosphate- and oxalate-extractable As concentrations as well as with phosphate extractable $SO_4^{2-}$ (Fig. 2). These findings indicate that after the 24 days of the incubation, the As was released from the sulfide mineral phases and subsequently immobilized with the Fe(III) (oxyhydr)oxides via adsorption and coprecipitation. The increasing trend in the soluble As is not consistent with the adsorption of As(V) as a function of the pH, because a decrease in the pH (here from 5.19 to 4.86) is related to the higher adsorption of the As(V) species (Manning and Goldberg, 1997; Dixit and Hering, 2003; Goh and Lim, 2004; Kim, 2010). Arsenic(III) has a less negative charge characteristic than As(V) and conversely its adsorption decreases with a decreasing pH (Manning and Goldberg, 1997; Dixit and Hering, 2003; Goh and Lim, 2004). The high sulfate-extractable As concentrations in the Smolotely soil during the oxic stage of incubation thus likely correspond to the As(III) that is released from the reactive sulfide phases. These phases do not primarily include authigenic AsS phases, because their complete oxidation in the similar conditions is expected within 4–7 years (Langner et al., 2014). In contrast, Moon et al. (2017) found that after 4 days, 20–85% of greigite oxidized, and about 20% of the sedimentary pyrite typically oxidizes during the first week (Morse, 1991). Highly reactive sulfide phases in the Smolotely wetland thus likely include Fe sulfides such as greigite and framboidal pyrite, which are abundant here and contain up to 2.7 wt% As (Knappová et al., 2019).

### 3.4. Changes in the trace metal fractionation

The observed decrease from the start to day 24 in the Mokrsko sample or day 18 in the Smolotely sample (reducing stage of incubation) in the soluble Co, Cu, and Ni (except for the Cu in the Mokrsko sample) occurred at the same time as the onset of the microbial $SO_4^{2-}$ reduction (cf. Figs. 2 and 3). It may indicate that the microbial $SO_4^{2-}$ reduction resulted in the immobilization of a portion of the Co, Cu, and Ni in spite of the fact that relatively large fraction of Cu and Co (only in Mokrsko sample) was solubilized from the reductive dissolution of the Fe(III) (oxyhydr)oxides as demonstrated by their concentrations in the oxalate extracts (Fig. 3). This is consistent with trace metal speciation in sulfate-reducing environments, where $S^{-II}_{(aq)}$ plays an important role in controlling metal mobility through a several reactions (Huerta-Diaz et al., 1998; Morse and Luther, 1999; Burton et al., 2008). The interactions of Co, Cu and Ni with $S^{-II}_{(aq)}$ can include the sorption to, or the coprecipitation with, the Fe sulfide or can include the formation of the discrete nonferrous sulfide phases (Huerta-Diaz et al., 1998; Morse and Luther, 1999). CoS (linnaeite), CuS (covellite and chalcotite) and NiS (millerite) are less soluble than the Fe sulfides (Huerta-Diaz et al., 1998). Hence, the soluble Co, Cu and Ni can precipitate with $S^{-II}_{(aq)}$ preferably to Fe and, thereby, be immobilized as linnaeite, covellite/chalcotite and millerite, respectively.

Increasing the concentrations of the oxalate-extractable Co, Cu and Ni during the oxic stage of the incubation (Fig. 3) indicate the sequestration of these metals in the Fe(III) (oxyhydr)oxides. The soluble concentrations of the trace metals also begin to increase (except Cu and Ni in the Mokrsko soil) suggesting the noneffective sorption of the metals. The increasing trends in the soluble trace metals are consistent with their desorption as a function of the pH, because a decrease in the pH is related to the higher desorption of

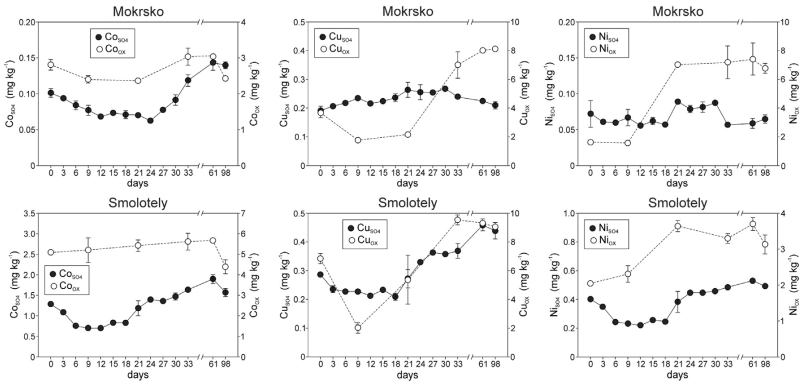


**Fig. 3.** The changes to the Co, Cu and Ni concentrations of the operationally defined sulfate ($Co_{SO4}$, $Cu_{SO4}$, $Ni_{SO4}$) and oxalate ($Co_{ox}$, $Cu_{ox}$, $Ni_{ox}$) fractions during the drying experiment. The data points are the mean of the triplicate samples and the error bars are ± the standard deviation.

Co, Cu and Ni (Kinniburgh and Jackson, 1981; Bibak, 1994). The imperceptible trends in the soluble Cu and Ni during the reductive dissolution and subsequent oxidative precipitation of the Fe(III) (oxyhydr)oxides in the Mokrsko soil sample demonstrate their different behavior in the organic-rich system. These results are in agreement with findings of Grybos et al. (2007), who found that the Co in wetland soils is solely bound to the Fe(III) oxyhydroxides, while the Cu and Ni could be bound to both the organic matter and Fe(III) (oxyhydr)oxides. This may suggest that organic matter can retard the Cu and Ni mobility in the organic-rich Mokrsko wetland soil during all remobilization processes (Fe(III) (oxyhydr)oxide reduction or pH-dependant desorption).

### 3.5. Oxidation of the realgar

The XRD data for the nanocrystalline realgar exposed to the oxic conditions over 96 days did not reveal a notable change in the diffraction intensity of the realgar with respect to the minor admixture of quartz (Fig. S5a), supporting the presumption the high realgar stability and its resistance towards oxidative dissolution (Lengke and Tempel, 2003). Moreover, Langner et al. (2014) found that the oxidation kinetics of nanocrystalline realgar in an environmental system characterized by stagnant groundwater were several orders of magnitude slower compared to systems with an advective flow. This suggests that the oxidation kinetics of the As sulfide in the wetland soil are very slow and controlled by the diffusion of $O_2$ to the arsenic sulfide surface and/or the removal of the oxidation products.

The XRD data did not identify the presence of realgar oxidation products, which always include well-crystalline arsenolite ($As_2O_3$) with intensive diffraction peaks at 13.9° and 27.9° 2θ along with small quantity of X-ray amorphous As–S phase (Ballirano and Maras, 2006; Pratesi and Zoppi, 2015). The first tiny arsenolite peaks in the XRD pattern of the nanocrystalline realgar-rich concentrate were confirmed after 180 days of the exposure to air (data not shown). The only oxidation product of the sulfide oxidation already identified after 15 days of realgar exposure to air was gypsum (Fig. S5b). Gypsum is a typical initial weathering product of Fe sulfide weathering (Hayes et al., 2014) and can be, thus, attributed to oxidation of pyrite that has been detected as a rare component of the realgar-rich NOM fragments from Mokrsko wetland (Drahota et al., 2017). This supports our presumption that As is preferentially released from the oxidation of the reactive arsenian Fe sulfides (especially in the Smolotely soil). These findings imply that short-term declines in the water table in wetlands will probably not cause the oxidation of authigenic realgar in soil, but can potentially lead to the oxidation-induced loss of the As bound to the Fe sulfides.

### 3.6. Implications regarding As mobility in wetlands

Groundwater-re-flooded wetland soil subjected to drought simulation showed changes in the rate and magnitude of As, Fe and trace metal fractionation during the incubation. The results revealed differential behavior among the soils that can be attributed to different contents of Fe and NOM as well as solid phase speciation of As. In agreement with other studies (e.g., Hess and Blanchar, 1977; Blodau et al., 2008; Burton et al., 2008), re-flooding of Fe-rich and NOM-low Smolotely soil caused the onset of microbially-mediated Fe(III)-reduction, which released Fe(II) and was associated with mobilization of As. In contrast, the reducing stage of incubation of NOM-rich and Fe-low Mokrsko soil had low effect on As and Fe mobility. It is likely that As-bearing Fe(III) (oxyhydr)oxides in the Mokrsko soil are substantially protected from the reductive dissolution as a result of NOM chemical protection via sorption onto the mineral surface and by the formation of Fe coprecipitates with organic molecules (Kaiser and Guggenberger, 2003). Physical protection from reductive dissolution might also occur if Fe(III) (oxyhydr)oxides are embedded within the organic matrix. Furthermore, low concentrations of sulfate-extractable Fe (i.e., ≤0.04% of total Fe) over the full incubation duration are probably controlled by formation of both Fe(II)- and Fe(III)-NOM complexes, which have been shown as a predominant Fe species in Fe-low peats and organic-rich soil (Bhattacharyya et al., 2018). Mobility of Fe in the oxic stage of Smolotely soil incubation was also low, but was likely controlled by Fe(II) oxidation and precipitation of Fe(III) (oxyhydr)oxides. Oxalate extractions indicated formation of only low amounts of newly-formed Fe(III) species (≤3.5% of the oxalate-extractable Fe). However, these values might be underestimated due to enhanced soluble Fe(II) in the initial soil samples that significantly catalyze the oxalate extraction of highly crystalline Fe(III) oxides such as

goethite and hematite (Suter et al., 1988; Phillips et al., 1993). This explanation is plausible especially for Smolotely wetland soil, which contains high concentration of Fe(II) (20.5 ± 3.5 mg $L^{-1}$) in the groundwater (Knappová et al., 2017). In accordance with previous studies (Burton et al., 2006; Langner et al., 2014), As released by oxidation of sulfide phases is almost completely sequestered by these newly-formed and/or pre-existing Fe(III) species. It is likely that As is preferentially released from arsenian Fe sulfides, because of their significantly higher oxidation kinetics in comparison to realgar (Morse, 1991; Lengke and Tempel, 2003; Langner et al., 2014; Moon et al., 2017).

## 4. Conclusions

In the present study, we studied the partitioning of As, Co, Cu, Fe, Ni and S between the different chemical fractions during the experimental drying of two naturally As-enriched wetland soils (Mokrsko and Smolotely) containing authigenic As and Fe sulfide minerals. The results revealed the different behavior between the wetland soils containing variable concentration of Fe (Mokrsko: 24 g $kg^{-1}$, Smolotely: 43 g $kg^{-1}$) and organic matter (Mokrsko: 80 g $kg^{-1}$, Smolotely: 11 g $kg^{-1}$). The initial re-flooding (first ~20 days) triggered the microbially-induced $SO_4^{2-}$ reduction in both wetland soil samples, while the reductive dissolution of the Fe (oxyhydr)oxides and As mobilization was documented only in the Fe-rich system of the Smolotely soil. During the oxic stage of the incubation (next 74 days), most of the As and trace metals (Co, Cu, Ni) released from the sulfide (primarily reactive Fe sulfides) oxidation was sequestered by the Fe(III) (oxyhydr)oxides. However, the sulfate-extractable As concentrations remained relatively high and constant (~130 mg $kg^{-1}$ at the organic-rich Mokrsko soil) over the full experiment duration or even increased substantially in the oxic stage of the Smolotely soil incubation. The increase in the soluble As as well as trace metal concentrations during the acidification in the Smolotely soil was ascribed to the pH-dependent release of the As(III) and trace metal cations. In contrast, low and almost constant concentrations of soluble Fe, Cu and Ni in the organic-rich Mokrsko soil seem to be controlled by their affinity to organic matter. Although our results document the relatively low As mobilization potential under relatively short droughts (several weeks), the preservation of the anoxic conditions must be regarded as a fundamental management strategy of these and other sulfidic wetlands enriched in As.

## Credit author statement

Petr Drahota, Conceptualization, Supervision, Methodology, Investigation, Writing – original draft, Funding acquisition. Magdaléna Peřestá; , Investigation, Methodology, Writing – review & editing. Jakub Trubač; , Investigation, Writing – review & editing. Martin Mihaljevič; , Investigation, Writing – review & editing. Aleš Vaněk, Investigation, Writing – review & editing

## Declaration of competing interest

The authors declare that they have no known competing financial interests or personal relationships that could have appeared to influence the work reported in this paper.

## Acknowledgements

This study was financially supported by the Czech Science Foundation (GACR 16-09352S) and Center for Geosphere Dynamics (UNCE/SCI/006). Part of the laboratory equipment for this study was purchased from the Operational Programme Prague - Competitiveness (Project CZ.2.16/3.1.00/21516). We gratefully acknowledge L. Jílková, L. Vondrovicová and V. Vonásková for laboratory assistance. We also wish to thank Alan Harvey Cook for editing the English manuscript.

## Appendix A. Supplementary data

Supplementary data to this article can be found online at https://doi.org/10.1016/j.chemosphere.2021.130306.

## References

Ballirano, P., Maras, A., 2006. In-situ X-ray transmission powder diffraction study of the kinetics of the light-induced alteration of realgar ($\alpha$-$As_4S_4$). Eur. J. Mineral 18, 589–599.
Belzile, N., Lebel, J., 1986. Capture of arsenic by pyrite in near-shore marine-sediments. Chem. Geol. 54, 279–281.
Bhattacharyya, A., Schmidt, M.P., Stavitski, E., Martínez, C.E., 2018. Iron speciation in peats: chemical and spectroscopic evidence for the co-occurrence of ferric and ferrous iron in organic complexes and mineral precipitates. Org. Geochem. 115, 124–137.
Bibak, A., 1994. Cobalt, copper, and manganese adsorption by aluminium and iron oxides and humic acid. Commun. Soil Sci. Plant Anal. 25, 3229–3239.
Blodau, C., Fulda, B., Bauer, M., Knorr, K.-H., 2008. Arsenic speciation and turnover in intact organic soil mesocosms during experimental drought and rewetting. Geochem. Cosmochim. Acta 72, 3991–4007.
Burton, E.D., Bush, R.T., Sullivan, L.A., 2006. Acid-volatile sulfide oxidation in coastal flood plain drains: iron-sulfur cycling and effects on water quality. Environ. Sci. Technol. 40, 1217–1222.
Burton, E.D., Bush, R.T., Sullivan, L.A., Johnston, S.G., Hocking, R.K., 2008. Mobility of arsenic and selected metals during re-flooding of iron- and organic-rich acid-sulfate soil. Chem. Geol. 253, 64–73.
Burton, E.D., Johnston, S.G., Kraal, P., Bush, R.T., Claff, S., 2013. Sulfate availability drives divergent evolution of arsenic speciation during microbially mediated reductive transformation of schwertmannite. Environ. Sci. Technol. 47, 2221–2229.
Canfield, D.E., 2001. Isotope fractionation by natural populations of sulfate-reducing bacteria. Geochem. Cosmochim. Acta 65, 1117–1124.
Cornwell, J.C., Morse, J.W., 1987. The characterization of iron sulfide minerals in anoxic marine sediments. Mar. Chem. 22, 193–206.
Dixit, S., Hering, J.G., 2003. Comparison of arsenic(V) and arsenic(III) sorption onto iron oxide minerals: implications for arsenic mobility. Environ. Sci. Technol. 37, 4182–4189.
Drahota, P., Falteisek, L., Redlich, A., Rohovec, J., Matoušek, T., Čepička, I., 2013. Microbial effect on the release and attenuation of arsenic in the shallow subsurface of a natural geochemical anomaly. Environ. Pollut. 180, 84–91.
Drahota, P., Grösslová, Z., Kindlová, H., 2014. Selectivity assessment of an arsenic sequential extraction procedure for evaluating mobility in mine wastes. Anal. Chim. Acta 839, 34–43.
Drahota, P., Kulakowski, O., Culka, A., Knappová, M., Rohovec, J., Veselovský, F., Racek, M., 2018. Arsenic mineralogy of near-neutral soils and mining waste at the Smolotely-Líšnice historical gold district, Czech Republic. Appl. Geochem. 89, 243–254.
Drahota, P., Mikutta, C., Falteisek, L., Duchoslav, V., Klementová, M., 2017. Biologically induced formation of realgar deposits in soil. Geochem. Cosmochim. Acta 218, 237–256.
Drahota, P., Rohovec, J., Filippi, M., Mihaljevič, M., Rychlovský, P., Červený, V., Pertold, Z., 2009. Mineralogical and geochemical controls of arsenic speciation and mobility under different redox conditions in soil, sediment and water at the Mokrsko-West gold deposit, Czech Republic. Sci. Total Environ. 407, 3372–3384.
Edenborn, H.M., Belzile, N., Mucci, A., Lebel, J., Silverberg, N., 1986. Observations on the diagenetic behavior of arsenic in a deep coastal sediment. Biogeochemistry 2, 359–376.
Gallegos, T.J., Han, Y.S., Hayes, K.F., 2008. Model predictions of realgar precipitation by reaction of As(III) with synthetic mackinawite. Environ. Sci. Technol. 42, 9338–9343.
Gee, G.W., Bauder, J.W., 1979. Particle-size analysis by hydrometer: a simplified method for routine textural analysis and a sensitivity test of measurement parameters. Soil Sci. Soc. Am. J. 43, 1004–1007.
Goh, K.H., Lim, T.T., 2004. Geochemistry of inorganic arsenic and selenium in a tropical soil: effect of reaction time, pH, and competitive anions on arsenic and selenium adsorption. Chemosphere 55, 849–859.
Grybos, M., Davranche, M., Gruau, G., Petitjean, P., 2007. Is trace metal release in wetland soils controlled by organic matter mobility od Fe-oxyhydroxides reduction? J. Colloid Interface Sci. 314, 490–501.
Han, Y.G., Jeong, H.Y., Demond, A.H., Hayes, K.F., 2011. X-ray absorption and photoelectron spectroscopic study of the association of As(III) with nanoparticulate FeS and FeS-coated sand. Water Res. 45, 5727–5735.
Hayes, S.M., Root, R.A., Perdrial, N., Chorover, J., 2014. Surficial weathering of iron sulfide mine tailings under semi-arid climate. Geochem. Cosmochim. Acta 141,

240–257.
Hess, R.E., Blanchar, R.W., 1977. Dissolution of arsenic from waterlogged and aerated soil. Soil Sci. Soc. Am. J. 41, 861–865.
Hoffmann, M., Mikutta, C., Kretzschmar, R., 2012. Bisulfide reaction with natural organic matter enhances arsenite sorption: insights from X-ray absorption spectroscopy. Environ. Sci. Technol. 46, 11788–11797.
Huang, G., Chen, Z., Zhang, Y., Liu, F., Wang, J., Hou, Q., 2016. Changes of arsenic fractionation and bioaccessibility in wastewater-irrigated soils as a function of aging: influence of redox conditions and arsenic load. Geoderma 280, 1–7.
Huerta-Diaz, M.A., Tessier, A., Carignan, R., 1998. Geochemistry of trace metals associated with reduced sulfur in freshwater sediments. Appl. Geochem. 13, 213–233.
Islam, F.S., Gault, A.G., Boothman, C., Polya, D.A., Charnock, J.M., Chatterjee, D., Lloyd, J.R., 2004. Role of metal-reducing bacteria in arsenic release from Bengal delta sediments. Nature 430, 68–71.
IUSS Working Group WRB, 2006. Guidelines for Soil Description. FAO, Rome.
Johnson, D.W., Henderson, G.S., 1979. Sulfate adsorption and sulfur fractions in a highly-weathered soil under a mixed deciduous forest. Soil Sci. 128, 34–40.
Kaiser, K., Guggenberger, G., 2003. Mineral surfaces and soil organic matter. Eur. J. Soil Sci. 54, 219–236.
Keon, N.E., Swartz, C.H., Brabander, D.J., Harvey, C., Hemond, H.F., 2001. Validation of an arsenic sequential extraction method for evaluating mobility in sediments. Environ. Sci. Technol. 35, 2778–2784.
Kim, M.J., 2010. Effects of pH, adsorbate/adsorbent ratio, temperature and ionic strength on the adsorption of arsenate onto soil. Geochem. Explor. Environ. Anal. 10, 407–412.
Kinniburgh, D.G., Jackson, M.L., 1981. Cation adsorption by hydrous metal oxides and clay. In: Anderson, M.A., Rubin, A.J. (Eds.), Adsorption of Inorganics at Solid: liquid Interfaces. Ann. Arbor. Science, Ann. Arbor, pp. 91–160.
Knappová, M., Drahota, P., Falteisek, L., Culka, A., Penížek, V., Trubač, J., Mihaljevič, M., Matoušek, T., 2019. Microbial sulfidogenesis of arsenic in naturally contaminated wetland soil. Geochem. Cosmochim. Acta 267, 33–50.
Kostka, J.E., Luther, G.W., 1994. Partitioning and speciation of solid phase iron in saltmarsh sediments. Geochem. Cosmochim. Acta 58, 1701–1710.
La Force, M.J., Hansel, C.M., Fendorf, S., 2000. Arsenic speciation, seasonal transformations, and co-distribution with iron in a mine waste-influenced palustrine emergent wetland. Environ. Sci. Technol. 34, 3937–3943.
Langner, P., Mikutta, C., Kretzschmar, R., 2012. Arsenic sequestration by organic sulphur in peat. Nat. Geosci. 5, 66–73.
Langner, P., Mikutta, C., Kretzschmar, R., 2014. Oxidation of organosulfur-coordinated arsenic and realgar in peat: implications for the fate of arsenic. Environ. Sci. Technol. 48, 2281–2289.
Langner, P., Mikutta, C., Suess, E., Marcus, M.A., Kretzschmar, R., 2013. Spatial distribution and speciation of arsenic in peat studied with microfocused X-ray fluorescence spectrometry and X-ray absorption spectroscopy. Environ. Sci. Technol. 47, 9706–9714.
Lengke, M.F., Tempel, R.N., 2003. Natural realgar and amorphous AsS oxidation kinetics. Geochem. Cosmochim. Acta 67, 859–871.
Manning, B.A., Goldberg, S., 1997. Arsenic(III) and arsenic(V) adsorption on three California soils. Soil Sci. 162, 886–895.
Mansfeldt, T., 2003. In situ long-term redox potential measurements in a dyked marsh soil. J. Plant Nutr. Soil Sci. 166, 210–219.
Mikutta, C., Kretzschmar, R., 2011. Spectroscopic evidence for ternary complex formation between arsenate and ferric iron complexes of humic substances. Environ. Sci. Technol. 45, 9550–9557.
Moon, E.M., Buh, T.T., Gibbs, D.H.M., Mata, J.P., 2017. Divergent Fe and S mineralization pathways during the oxidative transformation of greigite, $Fe_3S_4$. Chem. Geol. 468, 42–48.
Morse, J.W., 1991. Oxidation-kinetics of sedimentary pyrite in seawater. Geochem. Cosmochim. Acta 55, 3665–3667.
Morse, J.W., Luther, G.W., 1999. Chemical influences on trace metal-sulfide interactions in anoxic sediments. Geochem. Cosmochim. Acta 63, 3373–3378.
O'Day, P.A., Vlassopoulos, D., Root, R.A., Rivera, N.A., 2004. The influence of sulphur and iron on dissolved arsenic concentrations in the shallow subsurface under changing redox conditions. Proc. Natl. Acad. Sci. U.S.A. 101, 13703–13708.
Parsons, C.T., Couture, R.-M., Omoregie, E.O., Bardelli, F., Greneche, J.-M., Roman-Ross, G., Charlet, L., 2013. The impact of oscillating redox conditions: arsenic immobilization in contaminated calcareous floodplain soils. Environ. Pollut. 178, 254–263.
Paul, C.J., Ford, R.G., Wilkin, R.T., 2009. Assessing the selectivity of extractant solutions for recovering labile arsenic associated with iron (hydr)oxides and sulfides in sediments. Geoderma 152, 137–144.
Pedersen, H.D., Postma, D., Jakobsen, R., 2006. Release of arsenic associated with the reduction and transformation of iron oxides. Geochem. Cosmochim. Acta 70, 4116–4129.
Phillips, E.J.P., Lovley, D.R., Roden, E.E., 1993. Composition of non-microbially reducible Fe(III) in aquatic sediments. Appl. Environ. Microbiol. 59, 2727–2729.
Pratesi, G., Zoppi, M., 2015. An insight into the inverse transformation of realgar altered by light. Am. Mineral. 100, 1222–1229.
Révész, K., Qi, H., Coplen, T.B., 2012. Determination of the $\delta^{34}S$ of sulfate in water; RSIL lab code 1951. In: Révész, K., Coplen, T.B. (Eds.), In Chap. Methods of the Reston Stable Isotope Laboratory. U.S. Geological Survey Techniques and Methods, 10-C10, p. 33. Available from: http://pubs.usgs.gov/tm/2006/tm10c10/tm10c10/.
Rigby, P.A., Dobos, S.K., Cook, F.J., Goonetilleke, A., 2006. Role of organic matter in framboidal pyrite oxidation. Sci. Total Environ. 367, 847–854.
Rittle, K.A., Drever, J.I., Colberg, P.J.S., 1995. Precipitation of arsenic during bacterial sulphate reduction. Geomicrobiol. J. 13, 1–11.
Root, R.A., Vlassopoulos, D., Rivera, N.A., Rafferty, M.T., Andrews, C., O'Day, P.A., 2009. Speciation and natural attenuation of arsenic in a tidally influenced shallow aquifer. Geochem. Cosmochim. Acta 73, 5528–5553.
Sanchez, M.S., Gunter, M.E., 2006. Quantification of amphibole content in expanded vermiculite products from Libby, Montana USA using powder X-ray diffraction. Am. Mineral. 91, 1448–1451.
Seybold, C.A., Mersle, W., Juany, J.Y., McNamee, C., 2002. Soil redox, pH, temperature, and water-table patterns of a freshwater tidal wetland. Wetlands 22, 149–158.
Stucker, V.K., Silverman, D.R., Williams, K.H., Sharp, J.O., Ranville, J.F., 2014. Thioarsenic species associated with increased arsenic release during biostimulated subsurface sulfate reduction. Environ. Sci. Technol. 48, 13367–13375.
Suter, D., Siffert, C., Sulzberger, B., Stumm, W., 1988. Catalytic dissolution of iron(III) (hydr)oxides by oxalic acid in the presence of Fe(II). Naturwissenschaften 75, 571–573.
Vorenhout, M., van der Geest, H.G., van Marum, D., Wattel, K., Wijsackers, H.J.P., 2004. Automated and continuous redox potential measurements in soil. J. Environ. Qual. 33, 1562–1567.
Vantelon, D., Davranche, M., Marsac, R., La Fontaine, C., Guénet, H., Jestin, J., Campaore, G., Beauvois, A., Briois, V., 2019. Iron speciation in iron-organic matter nanoaggregates : a kinetic approach coupling Quick-EXAFS and MCR-ALS chemometrics. Environ. Sci.: Nano 6, 2641–2651.
Wallmann, K., Hennies, K., König, I., Petersen, W., Knauth, H.D., 1993. New procedure for determining reactive Fe(III) and Fe(II) minerals in sediments. Limnol. Oceanogr. 38, 1803–1812.
Weber, F.-A., Hofacker, A.F., Voegelin, A., Kretzschmar, R., 2010. Temperature dependence and coupling of iron and arsenic reduction and release during flooding of a contaminated soil. Environ. Sci. Technol. 44, 116–122.
Wenzel, W.W., Kirchbaumer, N., Prohaska, T., Stingeder, G., Lombi, E., Adriano, D.C., 2001. Arsenic fractionation in soils using an improved sequential extraction procedure. Anal. Chim. Acta 436, 309–323.
Wenzel, W.W., Brandstetter, A., Wutte, H., Lombi, E., Prohaska, T., Stingeder, G., Adriano, D.C., 2002. Arsenic in field-collected soil solutions and extracts of contaminated soils and its implication to soil standards. J. Plant Nutr. Soil Sci. 165, 221–228.
Wilkin, R.T., Ford, R.G., 2006. Arsenic solid-phase partitioning in reducing sediments of a contaminated wetland. Chem. Geol. 228, 156–174.
Yamaguchi, N., Nakamura, T., Dong, D., Takahashi, Y., Amachi, S., Makino, T., 2011. Arsenic release from flooded paddy soils is influenced by speciation, Eh, pH, and iron dissolution. Chemosphere 83, 925–932.